ANNUAL REPORT 1988

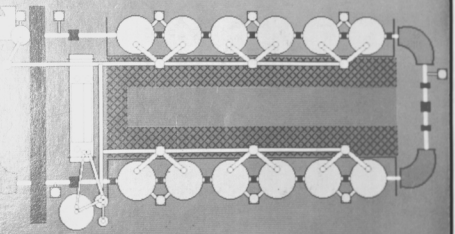

NUCLEAR PHYSICS LABORATORY
UNIVERSITY OF WASHINGTON

ANNUAL REPORT

Nuclear Physics Laboratory
University of Washington
May, 1988

Supported in part by the United States Department of Energy
under contract DE-AC06-81ER40048

Cover Photo

Our cover photo this year is a monochrome montage of two touch-screen color displays that are part of the control system for our new booster. When the cover is opened one sees on the upper left of the back cover the injector deck where two of the ion sources are now located. Also indicated below the tandem injection line is the new polarized ion source. On the front cover the booster itself is seen. The beam completes a loop starting at upper left and eventually exiting to the experimental areas (not shown) above the crossover. Touching any of the elements seen, such as cryostats, magnets, pumping stations or diagnostic elements, calls up new display pages which enable one to check the status of or change the parameters of the elements involved.

The display was generated by Mark Howe and photographed by Mary Levine. The cover was designed by Michael Strong of the Office of University Publications.

Introduction

The highlight of this past year's activity has been the completion and successful operation of our new superconducting booster. Beam was first fully accelerated and delivered to one of the experimental areas late last summer. During the fall and winter we have used the booster for several experiments, including elastic scattering of ^{7}Li ions to test Glauber model predictions, and a study of heavy ion subbarrier fusion spin distributions using ^{28}Si as the projectile. We have also been performing beam diagnostic experiments and detector calibration experiments in preparation for new studies of pre-equilibrium particle and photon emission at the higher bombarding energies obtainable with this new facility. Our initial operating experience has been very encouraging.

This past year has also seen the successful completion of an electrostatic deflector for separation of evaporation residues emitted near zero degrees from beam particles. A large-area Breskin-type gas-filled detector is used to detect the residues and produce a time signal for mass identification by time-of-flight. The shakedown of this device proceeded rapidly and it has been used successfully with both tandem and booster beams. In the tandem experiment we were able to measure the gamma ray multiplicity in the ^{16}O+^{154}Sm reaction to lower bombarding energies than possible with our earlier approach requiring detection of a discrete gamma ray associated with the de-excitation of the evaporation residue. The latter procedure is channel dependent, and can lead to a biased spin distribution as we have demonstrated in a separate study this past year. A study of the mean spin for the 3n and 4n channels has shown an appreciably higher mean spin for the former channel. The channel-weighted mean spin is found to exceed theoretical expectations at the lowest bombarding energies.

We have been pursuing information of the shape of highly excited nuclei from studies of the statistical decay of the giant dipole resonance. In hot nuclei near mass 40, observation of substantial angular anisotropies together with a large spin-dependent broadening of the giant dipole resonance provides evidence for oblate nuclear shapes due to rapid rotation. Calculations of the angular anistropies expected in both spherical and deformed nuclei at finite temperature and spin, including effects of fluctuations, show very similar patterns for oblate noncollective and prolate collective rotation, and demonstrate how anistropy measurements as a function of temperature and spin may be helpful in understanding nuclear shapes.

Our investigation into possible composition-dependent interactions manifested on a macroscopic scale continues to provide interesting results. Although our earlier results ruled out the original "fifth force" hypothesis of an intermediate-range interaction coupling to baryon number, recent theoretical speculations have raised the possibility of feeble interactions arising in a wide variety of models. We have rebuilt our apparatus and obtained a six-fold increase in sensitivity. We have examined and eliminated the possibility of reconciling our results with those of Thieberger in terms of an interaction coupling to any linear combination of baryon and lepton number with ranges $\leq$ 500 m. In particular we recently augmented our hillside source with a 1 ton Pb mass in order to investigate possible interactions coupled to nuclear isospin.

The new polarized ion source longevity and stability have been steadily improving, and modifications of the control software and remote control via the linac and new data acquisition control computers have been implemented. In December and January the source was used in an experiment to study the low energy structure of ^{14}N by elastic scattering

of polarized protons by ^{13}C. A number of experiments in the planning stages will make use of polarized beams which have not been available to us now for several years. Future emphasis of the polarized source development will be in modifications of the source as well as the low energy beam transport to improve the beam intensity and transmission through the tandem.

Radiocarbon measurements in the accelerator mass spectrometry (AMS) program have focused largely upon the determination of $^{14}CH_4$ concentrations in methane released from northern wetland environments (Alaskan tundra, Minnesota peat bogs). Methane is a very important "greenhouse" gas, and the current measurements are a part of a global study of methane sources and sinks. Our preliminary results indicate a rapid cycling (perhaps 30 years or less) of carbon through the photosynthesis–methanogenesis cycle in wetlands, a primary source of atmospheric methane. We have also participated in a world–wide interlaboratory collaborative study of ^{14}C determinations and are pleased that our AMS results for the unknown samples circulated are consistently within one standard deviation of the value established by an international comparison of results.

As in past years, we continue to perform experiments at other facilities as well as at our own. These cover a broad range of topics. We have continued our studies of pion and photonuclear interactions. In connection with the latter study, the fore–aft asymmetry data in the distribution of high energy photoneutrons in our runs on Ca and Pb have been analyzed. For both targets, the asymmetry rises sharply in the range of photon energies where the E2 isovector giant resonance is expected to lie. The experimental results raise a number interesting questions about the relative amounts of odd and even parity photoabsorption in this energy range and about the validity of the standard direct/semi–direct treatments of the absorption process.

Last year we reported on our participation in the successful trapping of antiprotons at LEAR. This is being followed up by a combined effort here, at Harvard and at CERN to develop a precision apparatus developed to measure the inertial mass of the antiproton relative to the proton to an accuracy of 10^{-8}–10^{-9}. Most items have been tested and we should be ready for the first available beam time in September.

We have embarked on a new nuclear physics effort at the PEP ring at SLAC. The phenomenon of x–scaling in deep inelastic electron scattering suggests that the virtual photon emitted by the electron is absorbed by an asymptotically–free quark. The recoiling quark (and the nuclear spectator) hadronize into physical particles on a length scale larger than the 1 fm size of individual hadrons. The PEGASYS project at PEP is aimed at measuring this length scale by using nuclear targets from hydrogen to xenon. PEGASYS will also try to determine if the hadronization length scale is significantly different in the nuclear medium than in the vacuum.

We close this introduction with a reminder that the articles in this report describe work in progress and are not to be regarded as publications or quoted without permission of the investigators. In each article the names of the investigators have been listed alphabetically, but where appropriate the names of those primarily responsible for the report have been underlined.

As always, we welcome applications from outsiders for the use of our facilities. As a convenient reference for potential users, the table on the following page lists the vital statistics of our accelerator. For further information please write or telephone

Dr. W.G. Weitkamp, Technical Director, Nuclear Physics Laboratory, University of Washington, Seattle, WA 98195; (206) 543-4080.

We are grateful to Maria Ramirez and Ida Tess for their contributions to the design and production of this report.

Robert Vandenbosch
Editor

TANDEM VAN DE GRAAFF ACCELERATOR

A High Voltage Engineering Corp. Model FN purchased in 1966 with NSF funds; operation funded primarily by the U.S. Department of Energy. See W.G. Weitkamp and F.H. Schmidt, "The University of Washington Three Stage Van de Graaff Accelerator," Nucl. Instrum. Meth. 122, 65 (1974).

Available Energy Analyzed Beams:

Ion	Max. Current (pμA)	Max. Practical Energy (MeV)
p,d	20	18
He	1.5	27
Li	0.2	36
C	1.8	63
N	0.2	62
O	1	72
Si	0.1	90
Cl	0.2	90
Ni	0.005	99
Br	0.05	108
Ag	0.001	108

BOOSTER ACCELERATOR

Our new linac Booster accelerator has become operational during the past year. We have successfully accelerated p, ^{4}He, ^{7}Li, ^{12}C, ^{16}O and ^{28}Si. We give in the following table maximum beam energies and expected intensities for these and several other representative ions.

Available Energy Analyzed Beams:

Ion	Max. Current (pμA)	Max. Energy (MeV)
p	>1	35
d	>1	37
He	0.2	65
Li	0.1	94
C	0.6	170
N	0.03	198
O	0.2	196
O	0.1	217
Si	0.1	302
Cl	0.02	393
Ni*	0.001	314

* requires stripper before dogleg

TABLE OF CONTENTS

1. ASTROPHYSICS

1.1 Search for a γ-Branch of the Unbound 5.17 MeV Level in ^{14}O

E.G. Adelberger, P.B. Fernandez, and A. Garcia

The γ width of the unbound first excited state in ^{14}O has astrophysical significance: it plays a major role in the determination of stellar environments where the hot CNO cycle can occur.[1] We are attempting to measure the γ branching ratio for this state by using the $^{12}C(^3He,n\gamma)$ reaction and searching for 5.17 MeV γ-rays in coincidence with neutrons populating the first excited state in ^{14}O.[2]

Our main concern was to find the source of the exponential background in the coincidence γ-ray spectrum.[3] One speculation was that it was due to secondary reactions in the Au backing, i.e. $^{197}Au(p,n\gamma)$ with the high energy protons being produced in the $^{12}C(^3He,p)$ reaction. We performed experimental tests that ruled out this hypothesis.

The answer to the background question came when we studied the $^{12}C(d,n\gamma)$ reaction, using the same target and set-up as for our previous $^{12}C+^3He$ runs. There are no bound excited states in ^{13}N, so the n-γ coincidence yield should be negligible. Even when we ran at E_d=2.5 MeV, below the threshold for making the first excited state in ^{13}N, the γ-ray spectrum in coincidence with neutrons showed the same exponential feature that we had observed in $^{12}C+^3He$. We then discovered that neutrons populating the ground state in ^{13}N were causing this exponential background by inelastically scattering in the γ-ray detector and then being observed in the neutron detector.

To reduce this scattered-neutron background, we increased the distance from the γ-ray detectors to the target and installed neutron attenuating material (high density polyethylene) to shield the neutron detector from the NaI's. This change in geometry reduced the exponential background in the γ-ray coincidence spectra from $^{12}C(^3He,n\gamma)$ by a factor of 6.

We made a ^{12}C target by ion implantation, $\approx$ 400 $\mu g/cm^2$ thick, using the model 860 sputter ion source. The use of electrostatic steerers driven by waveform generators enabled us to wiggle the beam from the source, resulting in better target thickness uniformity. We had two runs using this target and the new apparatus configuration. Each of these runs yielded approximately 100 hours of $^{12}C(^3He,n\gamma)$ coincidence data. From our preliminary analysis we obtain $\Gamma_\gamma/\Gamma = (3.3 \pm 2.1)\times10^{-5}$; the range of expected values from theoretical calculations is $\Gamma_\gamma/\Gamma=(3.1-6.4)\times10^{-5}$.[1]

1. C. Funck and K. Langanke, Nucl. Phys. A 464, 90(1987).
2. Nuclear Physics Laboratory Annual Report, University of Washington (1986) p. 1.
3. Nuclear Physics Laboratory Annual Report, University of Washington (1987) p. 1.

1.2 ^{37}Ca Production via ^{3}He(^{36}Ar,^{37}Ca)2n

E. Adelberger, S. Gil, A. Garcia, J. Gundlach, D. Mikolas,* T. Murakami,* W. Oliver,* and W.F. Rogers

An exploratory run was performed in order to study the feasibility of using the reaction ^{3}He(^{36}Ar,^{37}Ca)2n for producing ^{37}Ca. Our objective was to determine the B(GT) distribution for the ^{37}Ca β^+ decay by the measurement of the ^{37}K delayed proton spectrum. The motivation for this study was discussed in last year's Annual Report.[1,2]

In this first experiment we operated at $E_{lab} \simeq 11.4$ Mev/A and attempted to separate the ^{37}Ca isotope using the Recoil Product Mass Separator (RPMS) facility at MSU. This reaction is the kinematically reversed reaction used by Sextro et al.[1] at about the same energy in the center of mass system.

Our experimental setup consisted of a 15 cm long target gas cell filled with ^{3}He, which was operated with target thicknesses between 2.5 and 3.5 mg/cm^2 of ^{3}He. The gas was contained by 2 mg/cm^2 Havar window foils. The detector arrangement consisted of a three element telescope for particle identification located in vacuum at the focal plane of the RPMS, and several NaI detectors together with an intrinsic Ge detector just behind the chamber that contained the telescope. The gamma detectors were used for identification of the radioactive recoil products by their delayed gamma emissions.

We studied the recoil velocity region between 83% and 94% of the transported beam velocity, which broadly encompassed the ^{37}Ca recoil products. The particle spectrum was strongly dominated by inelastically scattered Ar particles and a few other ion species occurring close to zero degrees. The second most abundant element present was K. The high counting rate of these particles ($\approx$ 3–5 KHz) prevented us from increasing the beam current ($< \approx$ 10 pna). We found no indication of ^{37}Ca at the focal plane, presumably due to its very low production cross section, and to the restrictive circumstances in which we were forced to run.

We concluded that the target gas cell windows were responsible for the overwhelming background we observed. This background did not change when we substituted the havar with nickel windows or when we replaced the gas with ^{4}He and ^{14}N. The reaction mechanism which most likely was responsible for our observations is some type of quasi-elastic scattering from nuclei in the gas cell windows, which at near zero degrees produces beam-like particles with Z close to or equal to that of the beam, and with velocities that broadly span the region encompassing the fusion products of interest.

* National Superconducting Cyclotron Lab, Michigan State University, East Lansing, MI 48824

1. Nuclear Physics Laboratory Annual Report, University of Washington (1987) p. 2.
2. E.G. Adelberger and W.C. Haxton, Phys. Rev. C36, 879 (1987).

1.3 Measurement of the Angular Momentum of States in ^{127}Xe

E.G. Adelberger, A. Charlop, A. Garcia, S. Gil, and J.H. Gundlach

Recently Haxton[1] has pointed out that the ^{127}I(ν,e)^{127}Xe ($\tau_{1/2}$ = 35.0 d) reaction could be used in a solar neutrino detector, with a ν-capture rate being estimated roughly an order of magnitude higher per unit detector volume as compared to the Homestake mine experiment. This reaction would also be sensitive to higher energy ^{8}B-neutrinos. Haxton points out that the cross section for capturing ^{7}Be neutrinos (E_ν = 862 keV) should depend only on the strength of the Gamow-Teller 5/2 → 3/2 transition to the 125 keV state, which could be determined by a (p,n) measurement if sufficient resolution can be achieved. Two neighboring states are known to lie at 321 keV and 412 keV with $J^\pi = (1/2,3/2)^+$. The resolution critically depends on which of the two possible assignments is correct, making it important to determine the spin of those states experimentally.

We have performed a γ-γ angular correlation experiment in ^{127}Xe. The γ-rays from Xe were produced by β^+-decays of ^{127}Cs ($\tau_{1/2}$ = 6.2 h). The ^{127}Cs was produced via the ^{127}I(α,4n)^{127}Cs reaction. Samples of CaI were irradiated in air for several hours with a 20 pnA 60 MeV α-particle beam delivered from the booster. The Cs was chemically separated and concentrated.

We used three GeLi detectors 7.5 cm away from the source. One of the detectors was held fixed with respect to the source while the other two were mounted on movable arms allowing us to vary the angles with respect to the first detector from 90° to 180° and from 55° to 180° between each other.

Coincidence and singles spectra were recorded simultaneously. We were able to identify γ-ray transitions from ^{127}Xe up to 1.3 MeV in the singles spectra.

Our data analysis is still in progress but we present below one of the spectra in one detector gated by a γ-ray in the other.

1. W.C. Haxton, Phys. Rev. Lett. 60, 768 (1988)

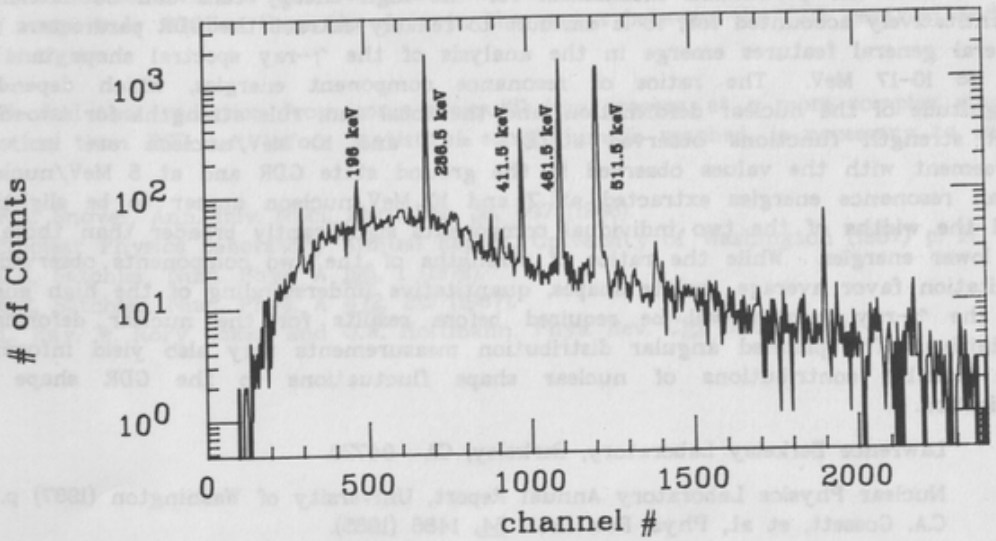

Fig. 1.3-1. GeLi-1 spectrum gated by events of 125 keV in the GeLi-2 spectrum. These data correspond to one run out of 20 taken at different angles.

2. GIANT RESONANCES

2.1 Search for Nuclear Shape Changes at Elevated Temperature

J.A. Behr, C.A. Gossett, J.H. Gundlach, K.T. Lesko,* E.B. Norman,* and K.A. Snover

We have continued the analysis of the spectral shapes of high energy γ rays emitted in the $^{12}C + ^{154}Sm$ reaction at E/A = 7 and 10 MeV/nucleon (see Ref. 1). Our goal in this work is to investigate possible nuclear shape changes at high excitation and moderate spin by extracting the shape of the giant dipole resonance (GDR) built on excited nuclear states. From the detailed shape of the GDR we may infer the average deformation of the ensemble of nuclear states populated by the high energy γ decay.

From our preliminary analysis reported last year we found that the GDR shape[2] which was used to fit the high energy γ-ray spectral shape in the $^{12}C + ^{154}Sm$ reaction at 5 Mev/nucleon was inadequate to reproduce the spectral shapes at 7 and 10 MeV/nucleon. In addition we observed high energy tails to the γ-ray spectra which cannot be accounted for by statistical decay of the compound system. Although recent work[3] has suggested that the very high energy γ yield in the $^{92}Mo + ^{92}Mo$ reaction at 19.5 MeV/nucleon can be accounted for by including a "quasideuteron" term in the inverse photoabsorption cross section used in the statistical model calculation, this mechanism does not account for the high energy tails we observe.

The high energy spectrum shape measured at E/A = 10 MeV/nucleon can be well reproduced by including a statistical decay component from the GDR built on excited states and a "nonstatistical" component with an exponential form, $K \exp(-E_\gamma/E_0)$, with parameters K and E_0 in reasonably good agreement with an extrapolation of the values observed for hard photon production observed in heavy ion collisions at intermediate energies. This result however, is insufficient to demonstrate that the high energy tails in the γ-emission spectra are produced by the so-called nuclear bremsstrahlung mechanism, and measurements of the γ-ray angular distributions are planned in order to clarify this issue.

Until the production mechanism for the high energy tails can be determined and quantitatively accounted for, it is difficult to reliably extract the GDR parameters. However several general features emerge in the analysis of the γ-ray spectral shape in the region $E_\gamma \approx$ 10–17 MeV. The ratios of resonance component energies, which depend on the magnitude of the nuclear deformation, and the total sum rule strengths for two-component GDR strength functions observed at E/A = 7 and 10 MeV/nucleon are in very good agreement with the values observed in the ground state GDR and at 5 MeV/nucleon. The mean resonance energies extracted at 7 and 10 MeV/nucleon appear to be slightly higher and the widths of the two individual components significantly broader than those observed at lower energies. While the ratios of strengths of the two components observed at high excitation favor average prolate shapes, quantitative understanding of the high energy tails in the γ-ray spectra will be required before results for the nuclear deformation are definitive. The planned angular distribution measurements may also yield information on the possible contributions of nuclear shape fluctuations to the GDR shape at high excitation.

* Lawrence Berkeley Laboratory, Berkeley, CA 94720.

1. Nuclear Physics Laboratory Annual Report, University of Washington (1987) p. 14.
2. C.A. Gossett, et al., Phys. Rev. Lett. 54, 1486 (1985).
3. N. Herrmann, et al., Phys. Rev. Lett. 60 1630 (1988).

2.2 High Energy γ Rays from ^{3}He- and α-Induced Nonstatistical Reactions

J.A. Behr, G. Feldman, H.K. Glatzel, C.A. Gossett, J.H. Gundlach, M. Kicinska-Habior, and K.A. Snover

We have continued our studies of high-energy γ rays from ^{3}He- and α-induced nonstatistical reactions. We have previously measured inclusive γ-ray spectra from ^{3}He- and α-induced reactions on a variety of targets ($61 \leq A \leq 181$) at 27 MeV bombarding energy. In all cases large structureless γ yields were observed in and above the giant dipole resonance (GDR) region (14 MeV$\leq E_{\gamma} \leq$30 MeV). The magnitude of these yields and their strong front-back asymmetry cannot be explained by a statistical emission process.[1,2]

In our continuing attempts to find reaction mechanisms to explain the data, we have calculated more carefully the radiation from semidirect (SD) excitation of the GDR in the target by the α. This reaction is isospin forbidden. It can occur through the Coulomb interaction, or through the isoscalar nuclear interaction if the ratio of neutron to proton densities is not uniformly equal to N/Z throughout the target. We have included the Coulomb interaction in our Steinwedel-Jensen model SD calculation according to a simple prescription given by Satchler[3]. We have included the isoscalar interaction in our model by adapting an ansatz for the difference in neutron and proton densities given by Satchler[4]. The resulting isoscalar cross-section depends on the square of ΔR, the difference between the neutron and proton rms radii. Taking data for ΔR from 1 GeV proton scattering data as a guide, we choose ΔR=0.13fm for ^{148}Sm[5].

For 27 MeV α + ^{148}Sm, the Coulomb and isoscalar SD radiative amplitudes are roughly equal, and are about 1/3 of the amplitude for direct radiative capture. The interference is constructive in the region of the GDR. The total direct-semidirect (DSD) cross-section is large enough to account for the data at the highest γ-ray energies, but its dependence on E_{γ} is too flat to explain the data. Our total calculation, the sum of the total DSD cross-section and the statistical emission cross-section, is still as much as an order of magnitude smaller than the data in the region between the GDR centroid and the highest energies.

We feel that radiation from some preequilibrium process, at a more complex stage of the reaction than DSD but before statistical equilibrium is reached, is necessary to explain the data.

1. K.A. Snover, Ann. Rev. Nucl. Part. Sci., 36, 597 (1986).
2. Nuclear Physics Laboratory Annual Report, University of Washington (1987) p. 17.
3. G.R. Satchler, Nucl. Phys. A 195, 1 (1972).
4. G.R. Satchler, Nucl. Phys. A 472, 215 (1987).
5. L. Ray, W. Rory Coker, and G.W. Hoffmann, Phys. Rev. C18, 2641 (1978).

2.3 GDR Shapes and Angular Distributions in Hot Nuclei

J.H. Gundlach and K.A. Snover

As a continuation of our work begun last year[1] in collaboration with J. Dudek of Strasbourg, we have extended our calculations of GDR shapes in heated Er isotopes to include angular distribution anisotropies. Representative results are shown in the figures for ^{164}Er and ^{150}Er, which are typical rare earth nuclei that are strongly (prolate) deformed and spherical, respectively, at T = I = 0. At T = 1.3 MeV, I = 30$\hbar$ (Fig. 2.3–1) ^{164}Er is still prolate deformed while ^{150}Er is slightly oblate. Both potential energy minima are, however, rather shallow, so that shape fluctuations are large. The a_2 coefficient versus gamma ray energy shows, for each case, the characteristic negative/positive dispersion shape expected for both prolate collective and oblate noncollective rotation. For nonoverlapping split–GDR components, one expects a_2(min) = –0.25 and a_2(max) = +0.125 for prolate collective rotation, and –0.25 and +0.50, respectively, for oblate noncollective rotation, for the case where the deformation is static and the shape is fully aligned with respect to the angular momentum. For realistic situations the anisotropy is reduced due to overlapping of the 2 GDR components and due to fluctuations both in the intrinsic deformation and in the orientation of the deformed shape. The calculated results for a_2 including all these effects (Fig. 2.3–1) are remarkably similar for these two different cases.

In fact, all of the calculated a_2 shapes for T = 0 to 1.9 MeV and I=0 to 60$\hbar$ are similar, differing primarily in their magnitude and to a lesser degree in their width. Figure 2.3–2 shows how the magnitude [$-a_2$(min)] varies with I for three different temperatures. The ^{150}Er* results don't depend much on T, while higher I produces larger oblate deformation and hence larger anisotropies. ^{164}Er* stays prolate at T = 0.7 MeV; the variation of [$-a_2$(min)] with I is due primarily to the onset of alignment of the (prolate) deformed shape with respect to the spin axis, which becomes complete at I $\approx$30$\hbar$. For higher T the anisotropy is reduced for all but the highest I, due to fluctuations and to the decrease in the deformation at the minimum. Thus precision angular distribution measurements may help distinguish between stiff (static) prolate shapes and soft prolate/oblate shapes. It is clear that the role of shape fluctuations is very important in general, and must be accounted for in interpreting angular distribution anisotropies.

1. Nuclear Physics Laboratory Annual Report, University of Washington (1987) p. 16.
2. ibid (1986), p. 14.

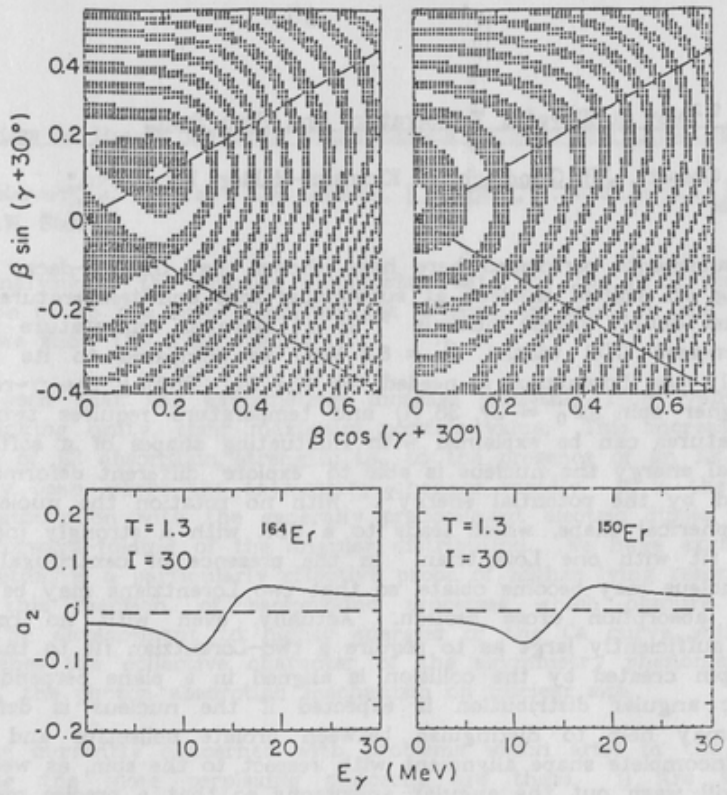

Fig. 2.3–1. Potential energy (free energy) surfaces (top) calculated at T = 1.3 MeV and I = 30$\hbar$ for ^{164}Er* (left) and for ^{150}Er* (right). The origin on the left vertical axis represents $\beta = 0$ and the axis sloping upward to the right has $\gamma = 0^{\circ}$. At this spin and temperature, ^{164}Er* is still prolate while the potential energy surface for ^{150}Er* has a minimum which is slightly oblate (noncollective). Bottom: the a_2 coefficient versus gamma ray energy.

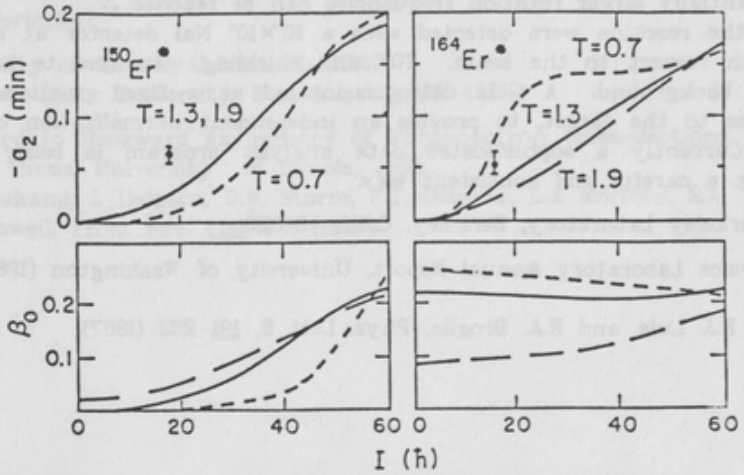

Fig. 2.3–2. The minimum a_2 [$-a_2$(min)], and the deformation β_0 at the free energy minimum, versus spin I for three different temperatures, for ^{150}Er* and ^{164}Er*. The data points are from Fig. 2.7 of ref. 2, with the result for ^{115}Sb* shown on the ^{150}Er* graph and the ^{166}Er* result shown on the ^{164}Er* graph.

2.4 The Shape of ^{92}Mo* at Elevated Temperature and High Spin

J.A. Behr, C.A. Gossett, J.H. Gundlach, M. Kicinska-Habior, K.T. Lesko,* and K.A. Snover

Previous measurements performed here have shown that GDR γ-decay can be used as a tool for probing an excited nucleus at substantial spin and temperatures. We found earlier that the quasi doubly magic nucleus ^{90}Zr at elevated temperature but low spin shows a largely increased GDR width[1] (Γ = 8.8 MeV) as compared to its ground state (Γ = 4 MeV), but only one Lorentzian is needed for the fit. Fitting the γ-ray absorption cross section at higher spin ($\ell_0 \cong 27, 36\ \hbar$) and temperature requires two Lorentzians. Qualitatively both features can be explained with fluctuating shapes of a softened nucleus. Given internal thermal energy the nucleus is able to "explore" different deformations with a probability determined by the potential energy[2]. With no rotation the nuclear shape will flucuate around a spherical shape, which leads to a GDR with a strongly increased width which may be best fit with one Lorentzian. In the presence of centrifugal and Coriolis forces the excited nucleus may become oblate, so that two Lorentzians may be necessary to describe the γ-ray absorption cross section. Actually, even with no rotation shape fluctuations may be sufficiently large as to require a two-Lorentzian fit to the GDR. Since the initial nuclear spin created by the collision is aligned in a plane perpendicular to the beam, a nonisotropic angular distribution is expected if the nucleus is deformed. This angular anisotropy may help to distinguish between prolate collective and oblate non-collective rotation. Incomplete shape alignment with respect to the spin, as well as intrinsic shape fluctuations, will wash out the angular anisotropy so that a precise measurement is required.

We performed a measurement using a 140 MeV ^{28}Si beam from the LBL-88" cyclotron onto a 1 mg/cm^2 self supporting ^{64}Ni foil to form the compound nucleus ^{92}Mo*. This measurement was chosen to allow us to look at very high spins $\ell_0 \cong 50\ \hbar$. Since the moment of inertia of this nucleus is smaller than the much-investigated rare earth nuclei, substantially larger rotation frequencies can be reached.
The γ-rays from the reaction were detected with a 10"×10" NaI detector at angles between 35° and 145° with respect to the beam. TOF and shielding was used to reduce the fast and slow neutron background. A GeLi detector located at a fixed position was used to monitor γ-rays due to the target, to provide an independent normalization of the rate of reaction events. Currently a sophisticated data analysis program is being developed to analyze the data in a careful and consistent way.

* Lawrence Berkeley Laboratory, Berkeley, Calif. 94720

1. Nuclear Physics Laboratory Annual Report, University of Washington (1987) p. 12, see also p. 10.
2. M. Gallardo, F.J. Luis, and R.A. Broglia, Phys. Lett B, 191 222 (1987).

2.5 Properties of the E2 Isovector Giant Resonance Seen in (γ,n) Studies

P.T. Debevec*, A. Freytag*, C.A. Gossett, I. Halpern, T. Murakami †, D.P. Rosenzweig, and D.W. Storm.

The analysis of the angular asymmetry data for the (γ,n) reaction in Ca and at higher energies in Pb has been completed. It is given in detail in the thesis of A. Freytag.[1] In Fig. 2.5–1 we show the main results.

It is seen that the asymmetries increase smoothly from values close to zero to values approaching unity, their maximum possible value. This increase is attributed to a concentration of E2 absorption strength; i.e., to the presence of an E2 resonance which lies in the energy span where the asymmetry changes rapidly.[2] It is the interference of this even parity absorption with the generally predominant electric dipole strength which gives rise to the forward–folding of the angular distribution.[2] We have explained elsewhere why the (γ,n) reaction is a particularly effective probe of higher lying resonances because of the absence, in this reaction, of background processes which obscure the effects of the resonance. The displacement to higher energies of the Ca curve with respect to the Pb curve establishes the collective character of the asymmetry phenomenon. It reflects the dependence of the photon absorption mechanism on nuclear size.

We are currently concerned with problems which arise in the intepretation of the data. Among the more perplexing concerns are these: i) Are we to interpret the significantly smaller slope of the asymmetry curve in Ca than in Pb as due to a much greater width of the E2 resonance in Ca? What would cause a greater width? ii) Why does the 90° yield in Pb drop so sharply compared to the average yield as the photon energy increases (Fig. 2.5–2))? Is the implied strong increase in even parity absorption consistent with the observed asymmetries? and iii) Why have we been unable to find a consistent treatment of our data and related data with the standard direct/semi–direct model for nucleon radiative capture? Are there some significant degrees of freedom which this model overlooks?

* University of Illinois, Urbana, IL 61801
† Michigan State University, East Lansing, MI 48824

1. "Forward to Backward Asymmetry of Photoneutron Cross–Sections" – Asmus Freytag, Ph. D. thesis, University of Illinois, 1988.
2. T. Murakami, I. Halpern, D.W. Storm, P.T. Debevec, L.J. Morford, S.A. Wender and D.H. Dowell, Phys. Rev. C35 479 (1987).

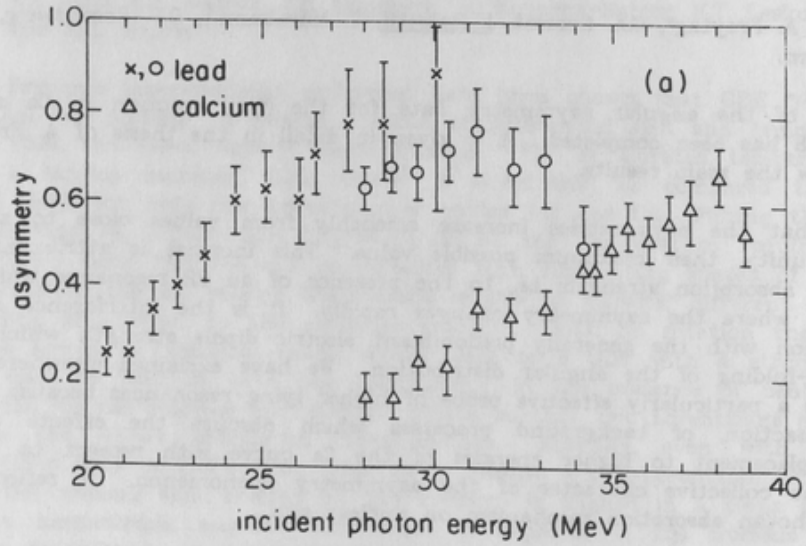

Fig. 2.5–1. The measured asymmetry; i.e., the difference in measured cross–sections at 55° and 125° divided by the sum of these cross–sections, plotted as a function of photon energy for both lead and calcium. The crosses for lead refer to our earlier run and the circles to the later one. The calcium data were all obtained in the later run. The emitted neutron energies in all cases correspond to a band of excitations at the lowest 4 MeV in the residual nuclei.

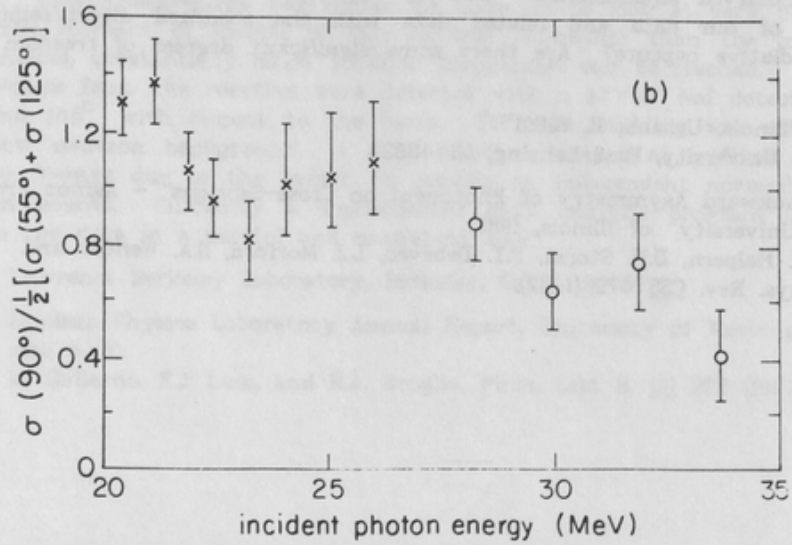

Fig. 2.5–2. The ratio of the 90° cross–section in the (γ,n) reaction on Pb for the lowest 4 MeV of excitation to the corresponding average cross–section at 55° and 125°. The crosses refer to points taken in our earlier low energy run. The circles give the data for the more recent higher energy run.

2.6 Statistical Decay of the Giant Dipole Resonance in Light A=39–45 Nuclei

J. Behr, C. Gossett, J. Gundlach, G. Feldman, M. Kicinska-Habior, and K. Snover

In last year's Annual Report[1] we described GDR decay studies in excited ^{39}K, ^{40}K, ^{42}Ca and ^{45}Sc nuclei formed in the fusion of ^{12}C, ^{13}N, ^{15}N and ^{18}O with ^{27}Al, respectively. For such near mass-symmetric fusion reactions, measurements at different bombarding energies correspond to different spin and nearly constant temperatures, since raising the bombarding energy to a good approximation simply raises the rotational energy. The measured GDR shapes, which were reasonably well-fitted by a single Lorentzian, were found to broaden considerably over the spin range studied.[1] The most likely explanation for the broadening is oblate noncollective rotation which gives rise to deformation splitting of the GDR that is unresolved in the spectrum shape.

In order to pursue this hypothesis further, we have measured angular distributions of the emitted gamma rays for 63 MeV ^{12}C+^{27}Al and 45 and 73 MeV ^{18}O+^{27}Al. All three angular distributions show negative a_2 coefficients in the range $E_\gamma \sim$ 11–20 MeV, and zero or perhaps positive a_2 values at higher E_γ, as is characteristic of either oblate noncollective or prolate collective rotation. Although the absolute anisotropies are small ($|a_2| \leq 0.15$), they are sizeable compared to the anisotropy expected due to deformation splitting (see Sec. 2.3). Since in this mass region, substantial prolate deformation (due to shell effects) is unlikely, especially at these temperatures (1.7 – 1.8 MeV), an interpretation in terms of oblate noncollective rotation is strongly favored.

1. Nuclear Physics Laboratory Annual Report, University of Washington (1987) p. 5.

3. HEAVY ION INDUCED REACTIONS

3.1 Hard Photon Production in Heavy Ion Collisions

J.A. Behr, C.A. Gossett, J.H. Gundlach, M. Kicinska-Habior, K.T. Lesko*, and K.A. Snover

Hard photon production in intermediate energy heavy ion collisions has recently been an extremely active area of both theoretical and experimental research. As reported earlier[1] we have used a large shielded NaI spectrometer at the Lawrence Berkeley Laboratory 88" Cyclotron to measure absolute production cross sections and angular distributions of γ rays from heavy ion collisions in the energy range E/A $\leq$ 20 MeV/nucleon. In the past year the emphasis of our work has been concentrated on the analysis of the angular distribution of high energy γ emission in the $^{19}F + ^{100}Mo$ and $^{19}F + ^{181}Ta$ reactions at 19 MeV/nucleon and on the calculation of the contribution to these spectra from statistical decay of a thermally equilibrated compound nucleus, the dominant production mechanism for γ rays with E_γ < 30 MeV.

While recent work[2] suggests the the high energy γ yield measured in coincidence with binary fragments in the $^{92}Mo + ^{92}Mo$ reaction at 19.5 MeV/nucleon can be accounted for by statistical emission from the highly excited fragments when a "quasideuteron" term is included in the inverse γ absorption cross section, this production mechanism does not account for our measured high energy γ yields. Furthermore, the γ-ray angular distributions observed in our work are clearly inconsistent with statistical γ emission from the compound system.

We have fitted the measured γ-ray spectra above E_γ = 35 MeV as a function of angle and γ-ray energy assuming an exponential form, $K^{\gamma}\exp(-E_\gamma/E_0)$, for the spectral shape and isotropic emission from a source moving with velocity β_s. This form for the cross section is transformed to the laboratory frame and the data for $^{19}F + ^{100}Mo$ (see Fig. 3.1-1) and $^{19}F + ^{181}Ta$ at 19 MeV/nucleon are quite well reproduced with same source velocity β_s = 0.08, and with slopes, E_0 = 7.0 and 7.3 MeV, respectively. These results are consistent with a hard photon production mechanism in which high energy γ rays are emitted primarily from individual energetic n-p collisions at an early stage of the collision process, for which one would expect β_s = 0.10 in both cases. As illustrated in Fig. 3.1-2, our data are clearly inconsistent with isotropic emission from sources moving with the velocity of the compound systems for which β_s = 0.03 and 0.02 for the Mo and Ta targets, respectively.

* Lawrence Berkeley Laboratory, Berkeley, CA 94720.

1. Nuclear Physics Laboratory Annual Report, University of Washington (1987) p. 21.
2. N. Herrmann, et al., Phys. Rev. Lett. 60 1630 (1988).

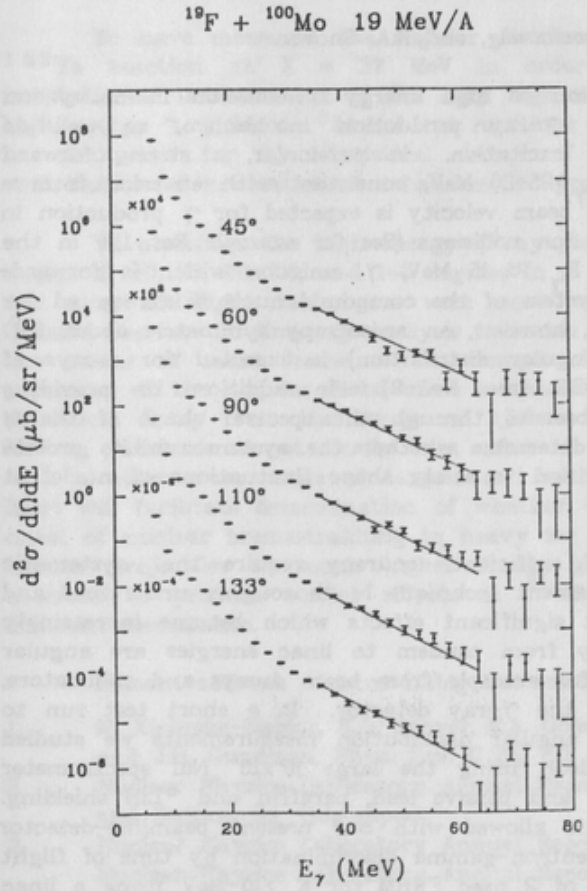

Fig. 3.1–1. High energy γ–ray spectra from the ^{19}F + ^{100}Mo reaction at 19 MeV/nucleon as a function of laboratory angle. The solid curves are described in the text.

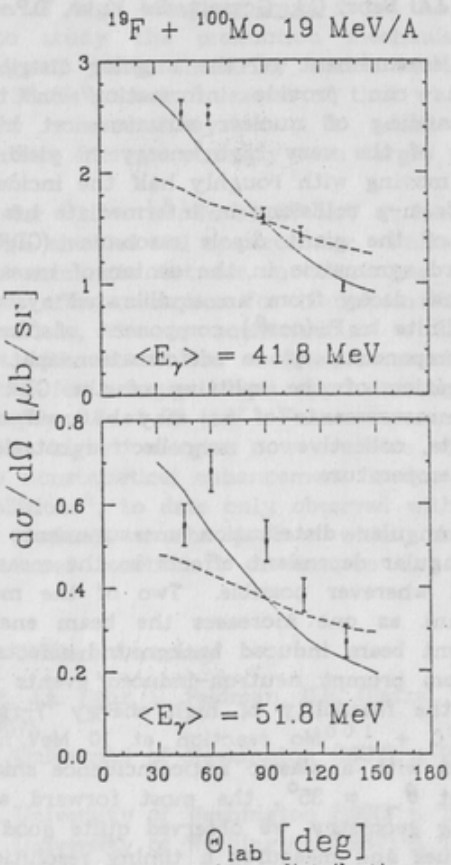

3.1–2. Angular distributions of high energy γ rays energy averaged over 10 MeV bins with $\langle E_\gamma \rangle$ = 41.8 and 51.8 MeV. The solid curves, described in the text and shown in Fig. 3.1–1, are for isotropic emission from a source moving with β_s = 0.08. The dashed curves are calculated for isotropic emission from a source with β_s = 0.03 and are normalized to the solid curves at θ=90°.

3.2 Angular Distribution Measurements of High Energy Gamma Emission Following Heavy Ion Collisions at Linac Energies

J.A. Behr, C.A. Gossett, S.J Luke, D.P. Rosenzweig, and K.A. Snover

Measurement of the angular distribution of high energy γ emission in heavy ion collisions can provide information on the γ-ray production mechanism, as well as understanding of nuclear structure at high excitation. In particular, a strong forward peaking of the very high energy γ yield, E_γ >25-30 MeV, consistent with emission from a source moving with roughly half the incident beam velocity is expected for γ production in energetic n-p collisions in intermediate heavy ion collisions (See for example Ref. 1). In the region of the giant dipole resonance (GDR), $E_\gamma \approx$ 15 MeV, γ emission which is forward-backward symmetric in the center of mass system of the compound nucleus is required for statistical decay from an equilibrated system, however, an anisotropy symmetric about 90° (i.e. a finite $a_2P_2(\cos\theta)$ component of the angular distribution) is expected for decays of the components of a deformation-split GDR (see Ref. 2). In addition to providing confirmation of the splitting of the GDR observed through the spectral shape of the γ yield, measurements of a_2 may be used to determine whether the system exhibits prolate or oblate, collective or noncollective rotation and to study shape fluctuations of nuclei at finite temperature.

Angular distribution measurements of sufficient accuracy require that systematic false angular dependent effects in the measurement technique be thoroughly understood and reduced wherever possible. Two of the most significant effects which become increasingly important as one increases the beam energy from tandem to linac energies are angular dependent beam induced background effects, for example from beam dumps and collimators, and from prompt neutron-induced events in the γ-ray detector. In a short test run to study the feasibility of high energy γ-ray angular distribution measurements we studied the ^{12}C + ^{100}Mo reaction at 10 MeV/nucleon using the large 10"x15" NaI spectrometer equipped with a plastic anticoincidence shield and passive lead, paraffin and ^6LiH shielding. Even at θ_γ = 35°, the most forward angle allowed with our present beamline-detector shielding geometry, we observed quite good neutron-gamma discrimination by time of flight techniques and measured a timing resolution of 2 nsec FWHM for E_γ >10 MeV using a linac time structure reference. We did not observe any structure in the time of flight spectrum originating from the well-shielded beam dump although there appeared to be a large random component from thermal neutron induced events. After improvements in the collimation of the beam are achieved and after the new low-energy low-frequency buncher[3] is installed we plan to begin measurements of the angular distribution of gammas produced in the ^{12}C + ^{154}Sm reaction at 10 MeV/nucleon in order to investigate the origin of the high energy tails in the 90° spectrum measured at Berkeley[1] and to look for possible signatures of shape fluctuations effects in the region of the GDR.

1. Section 2.1 and 3.1, this report.
2. Nuclear Physics Laboratory Annual Report, University of Washington (1986) p. 14, Nuclear Physics Laboratory Annual Report, University of Washington (1985) p. 9.
3. Section 10.3, this report.

3.3 High Energy Gamma Rays From ^{6}Li-Induced Reactions

J.A. Behr, C.A. Gossett, M. Kicinska-Habior, and T. Schaefer*

We have measured the angular distribution of high energy γ-rays from the ^{6}Li + ^{181}Ta reaction at E = 37 MeV in order to study the production mechanism for nonstatistical enhancement of the very high energy γ yield. In earlier work[1] we observed high energy γ yields in ^{6}Li-induced reactions at 36 MeV much in excess of that which can be accounted for by statistical decay of the compound system. In addition, the contribution of nonstatistical enhancement appeared to increase strongly with target mass.

We measured the high energy γ-ray yield for ^{6}Li + ^{181}Ta at 37 MeV at laboratory angles of 40, 65, 90, 115, and 140 degrees in a large, shielded NaI spectrometer. Pulsed beam and time of flight techniques were used to discriminate between neutron and gamma induced events. Preliminary analysis indicates that after correction for transformation into the center of mass frame of the compound nucleus, the a_1 coefficient of a Legendre expansion of the angular distribution is consistent with zero at low energies, as required for statistical decay from the compound system, while for energies above approximately 13-14 MeV a_1 increases monotonically to a value of roughly 0.8 at 25 MeV. Future measurements with a wider mass range of targets and with the higher energies now available with the linac will facilitate determination of whether the nonstatistical enhancement is due to the onset of nuclear bremsstrahlung in heavy ion collisions[2], to date only observed with much heavier projectiles at much higher energy per nucleon, or the process which has been observed to produce similar effects in ^{3,4}He-induced reactions[3], or due to an entirely different mechanism.

* Present address: Justus-Liebig-Universitat, Giessen, Germany

1. M. Kicinska-Habior, K.A. Snover, C.A. Gossett, J.A. Behr, G. Feldman, H.K. Glatzel and J.H. Gundlach, Phys. Rev. C 36, 612 (1987).
2. Nuclear Physics Laboratory Annual Report, University of Washington (1987) p. 21 and Section 3.1, this report.
3. Nuclear Physics Laboratory Annual Report, University of Washington (1985) p. 15, Nuclear Physics Laboratory Annual Report, University of Washington (1987) p. 17; Section 2.2, this report.

3.4 Bremsstrahlung Production from a Heavy Ion Transport Model

J. Randrup* and R. Vandenbosch

We have extended a previously developed model[1] for pre-equilibrium nucleon emission following stochastic exchange of nucleons to include photon production as a perturbative process. The photons arise from bremsstrahlung radiation associated with np scattering of the transferred nucleons as they propagate through the receptor nucleus. No new parameters are introduced in this extension of our model to include photon emission.

The formalism for calculating photon emission from p-n collisions in nucleus matter was tested against the only relevant photon yield data for nucleon-nucleus reactions, the data of Edgington and Rose for 140 MeV protons. The agreement is moderately good. Similar data at a lower bombarding energy would be very valuable. We have calculated inclusive energy spectra and angular distributions for all nucleus-nucleus collisions which have been studied at bombarding energies below 50 MeV/A. The agreement is generally good; for several studies with Ar and Kr projectiles the agreement is remarkably quantitative. An example of a comparison is shown in Fig. 3.4-1. The comparisons of the energy spectra and angular distributions with experiment suggest that bremsstrahlung production is the dominant mechanism for producing photons with energies in excess of approximately 30 MeV. We have also performed calculations of multiplicities for specific reaction channels, using the Nucleon-Exchange Transport Model underlying our calculations to define impact parameter ranges for central and peripheral reactions. These calculations give a near-quantitative reproduction of a number of experimental results.

Furthermore, we have shown that the high-energy photons originate from collisions induced by nucleon exchange at an early stage of the nucleus-nucleus collision. First collisions are the dominant source of hard photons, particularly those with the highest energy.

* Nuclear Science Division, Lawrence Berkeley Laboratory, Berkeley, CA 94720.

1. J. Randrup and R. Vandenbosch, Nucl. Phys. A 474, 219 (1987).
2. R. Berthelot et al., Nucl. Phys. A 474, 541 (1987).

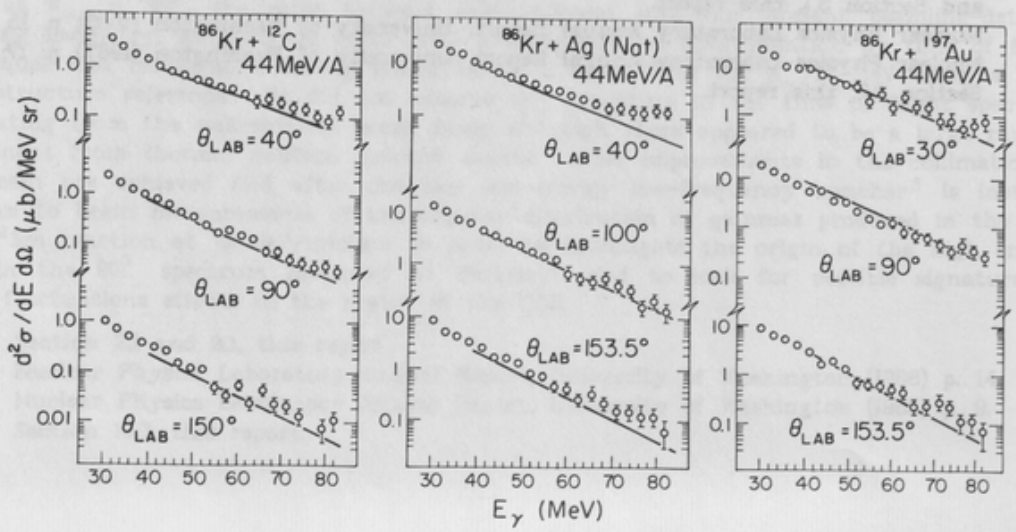

Fig. 3.4-1 Comparison of calculated differential cross sections for three angles for each of three targets with the experimental data of Berthelot et al.[2]

3.5 Spin Distributions at Near-Barrier Energies in $^{16}O+^{154}Sm$

A. Charlop, S. Gil, A. Garcia, D.D. Leach, S.J. Luke, and R. Vandenbosch.

Several experiments at near-barrier energies have found spin distributions of the compound nucleus which are broader than those expected from theoretical models, even when these models seem to successfully reproduce the excitation functions for the fusion cross sections, σ_{fus}.[1,2] In a previous γ-ray multiplicity (M_γ) study of the first moment of the spin distribution ($<\ell>$) in the system $^{16}O+^{154}Sm$ at near barrier energies, we found that σ_{fus} and $<\ell>$ could be accounted for by using a one-dimensional penetration model including the target deformation.[3] The technique used in the determination of M_γ relied upon tagging evaporation residues by the detection of discrete γ-rays emitted by the different evaporation residues. Due to light element contamination in the target and to the complex character of the gamma decay of even-odd nuclei, we were able to obtain the contribution to M_γ from the 4n channel (^{166}Yb) only. Near and below the barrier the 3n channel begins to make a contribution and its inclusion may significantly modify the conclusions reached before.

This year we have attempted to investigate this issue by using a new self-supporting ^{154}Sm target which was produced by the Oak Ridge National Laboratory using a special technique that minimizes oxygen and other low-Z contaminates. We have been able to clearly identify the gamma-rays arising from the 3n channel (^{167}Yb). In particular, we were able to observe the transitions originating in the decay through the yrast band (based on the state $5/2^+[642]$). The E_γ=221.7 keV ($17/2^+$ to $13/2^+$) transition of this band was used to tag the 3n channel.

The technique used for obtaining the contribution of the 3n channel ($M_\gamma(3n)$) to M_γ selectively samples those states in the compound nucleus that feed the state $J=17/2^+$ in ^{167}Yb. Similarly the contribution from the 4n channel, tagged by the $4^+ \rightarrow 2^+$ transition, samples those states which feed this transition. In order to eliminate the bias produced by this effect, corrections were made using results from statistical decay models. In order to eliminate the bias produced by this effect, corrections were made using results from statistical decay models. The parameters of this code were adjusted so as to reproduce the relatives yield in the same system as measured in Ref. 4.

Preliminary results for $<\ell>$ are shown in Fig. 3.5-1, where we have also plotted the contribution of the 4n channel alone. The heavy curve is based on a one-dimensional penetration model, whose parameters were adjusted so as to reproduce the fusion cross section excitation function. From this plot we can see the importance of including the 3n channel in the estimation of $<\ell>$. The larger mean spin associated with the 3n as compared to the 4n channel is readily understood as high-spin compound nuclei tend to emit fewer neutrons. We also see what appears to be a general tendency in subbarrier fusion, namely the mean spins are larger than the expectation of theoretical models that successfully reproduce the fusion cross sections, in disagreement with the expectation suggested by several authors.[5,6]

1. R. Vandenbosch et al., Phys. Rev. Lett. 56, 1234 (1986), and Phys. Rev. Lett. 57, 1499 (1987).
2. M.L. Halbert, J.R. Beene, D.C. Hensley, K. Honkanen, T.M. Semkow, V. Abenaute, D.G. Sarantites, and Z. Li, Paper presented at 6th Adriatic International Conference on Nuclear Physics, Dubrovnik, Yugoslavia, June, 1987.

3. S. Gil, R. Vandenbosch, A. Lazzarini, and A. Ray, Phys. Rev. C 31, 1752 (1985).
4. R.G. Stokstad et al. Phys. Rev. C 21, 2427 (1980).
5. H. Esbensen and S. Landowne. Nucl. Phys. A 467, 136 (1987).
6. C.H. Dasso, H. Esbensen, and S. Landowne Phys. Rev. Lett. 57, 1498 (1986).

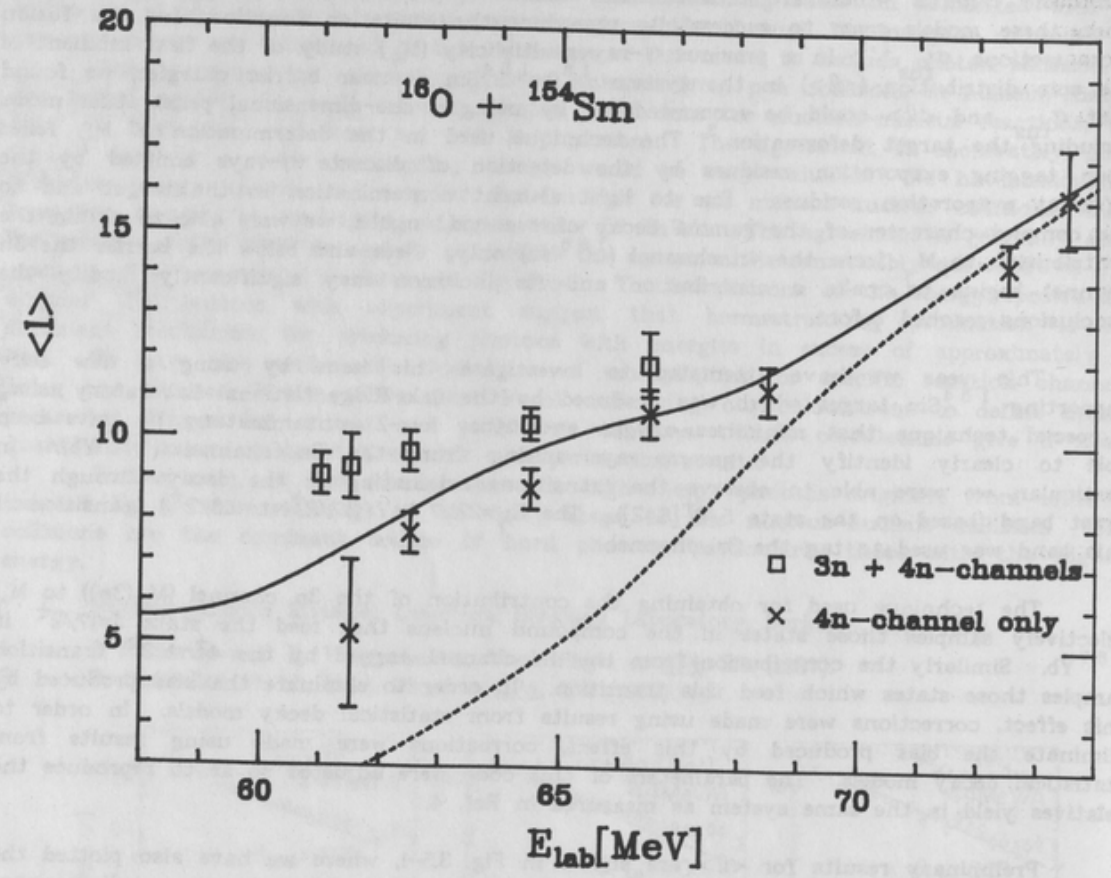

Fig. 3.5–1. Average values of the spin distribution in the compound system produced in the reaction $^{16}O+^{154}Sm$. Circles represent the contribution to $\langle \ell \rangle$ from the 4n channel only, whereas diamonds give values including both the 3n and 4n channels. The solid curve is the prediction of the Wong model as discussed in Ref. 3. The dashed curve represents the expectation of $\langle \ell \rangle$ according to the sharp cutoff model.

3.6 Heavy Ion Elastic Scattering at 10–50 MeV/Nucleon

J.G. Cramer, S. Gil, D.D. Leach, S.J. Luke, and B.T. Mclain

We are continuing our studies of elastic scattering and are planning to use the booster and the 860 source to obtain beams of various ions in the range of 10 to 15 MeV/nucleon. In September 1987 we did the first experiment with the booster, using a beam of 84 MeV ^{7}Li to bombard a ^{12}C target. With 150 to 300 nA on target we were able to obtain data out to 47° in the lab where the cross section had decreased by 3x10^{5} from its value at 3°. We were quite pleased with the performance of the booster and are confident that we will be able to study many beam–target combinations over a large angular range.

We have analyzed the ^{7}Li data and are completing analysis of our data from experiments at Michigan State in January 1987, which used 35 and 50 MeV/nucleon beams of ^{12}C on targets of ^{12}C, ^{40}Ca, ^{90}Zr, and ^{208}Pb. We plan to perform optical model fits to all our elastic cross section data and have begun to do so for the ^{7}Li on ^{12}C data. Fits to previous data for ^{12}C on ^{12}C, ^{40}Ca, ^{90}Zr, and ^{208}Pb were considerably worse at 35 MeV/nucleon than at lower energies and we plan to investigate this further with our new data at 35 and 50 MeV/nucleon. In particular, we were unable to adequately fit the earlier 35 MeV data using the M3Y double–folding model for the real part of the nuclear potential and we hope to understand this. Our initial fits to the ^{7}Li data haven't succeeded in giving the cross sections over the whole range of angles from 3° to 72° in the center of mass. Using Woods–Saxon forms for the real and imaginary parts of the nuclear potential we can fit the data out to 30° but beyond that the fit is much poorer. The data at the larger angles will constrain the potential more than our previous data and may allow us to determine its value at smaller radii.

We will also calculate total reaction cross sections, using the scattering S–matrix generated by our optical model fits, and compare these values to those calculated by the Glauber model. As described in last year's Annual Report,[1] this model has had unexpected success in predicting all measured nucleus–nucleus total reaction cross sections at energies from 5 to 200 MeV/nucleon. Our 50 MeV/nucleon ^{12}C cross sections will add to the data and our cross section for the loosely bound ^{7}Li should be a more severe test of the model.

1. Nuclear Physics Laboratory Annual Report, University of Washington (1987) p. 23.

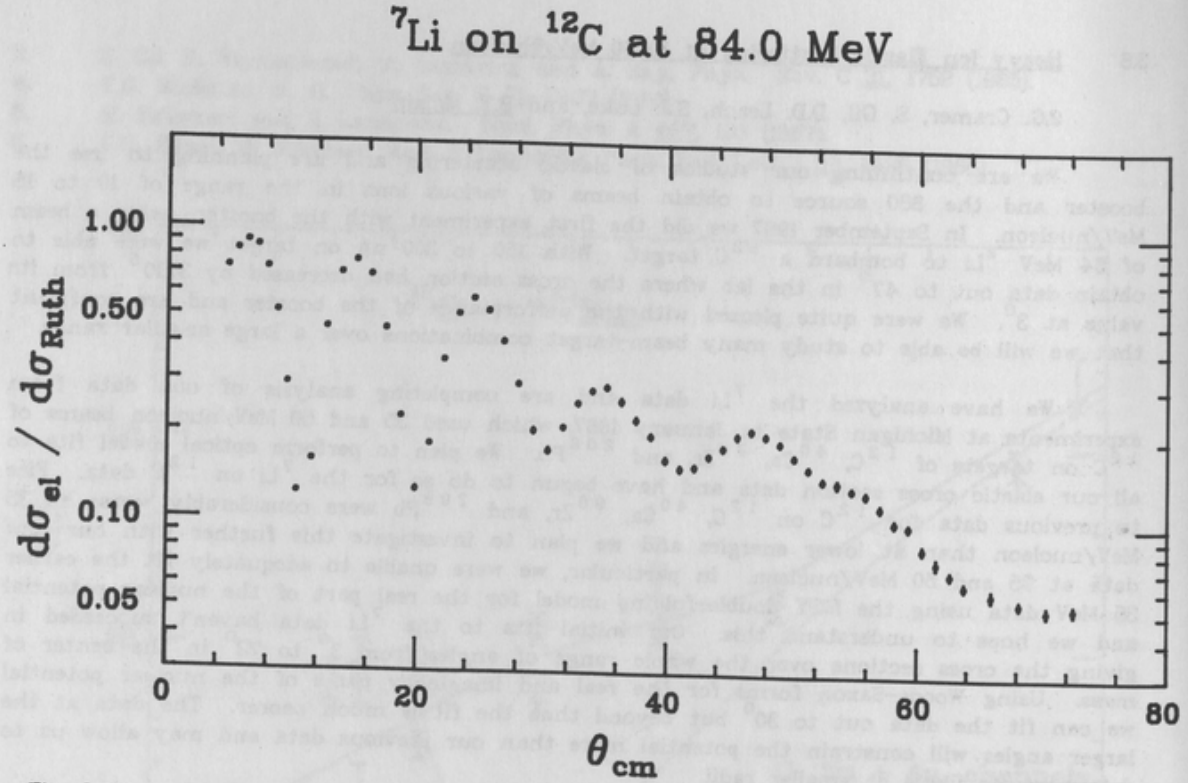

Fig. 3.6–1. Results from the first experiment using a beam from the booster. Elastic scattering angular distribution for ^{7}Li on ^{12}C at 84.0 MeV.

4. FUNDAMENTAL SYMMETRIES

4.1 Survey of Nuclei for Time-Reversal Invariance Test

E.G. Adelberger, A. Garcia, G. Loechelt, and W.F. Rogers

Nuclei in the range of A=6-33 were examined for their appropriateness for one of two time-reversal experiments involving γ-ray emission from polarized excited nuclear states. In one experiment, the angular correlation of two coincident γ-rays is observed. The second experiment involves the simultaneous observation of a single γ-ray and its linear polarization. Both of these experiments yield information about observables which are odd under time-reversal. The time-odd part of the angular correlation has the form[1]

$$W_{T-odd} = B_1 U_1 f_1(k_1,k_2,J) + B_3 U_3 f_3(k_1,k_2,J)$$

where f_1 and f_2 depend on the angles between k_1, k_2 and J, for the coincidence experiment, and

$$W_{T-odd} = (B_3 V_3)(J \cdot k)(J \cdot E)(J \cdot k \times E)$$

for the linear polarization experiment. The parameters U_1, U_3, and V_3 are intrinsic quantities which depend solely upon the spins of the nuclear states and the mixing ratios of the γ-ray transitions. The T-odd effect is enhanced by large U or V factors and by a favorable transition. We then included the branching ratios and defined the following effective factors:

$$G_1 = U_1(r_1 r_2)^{1/2} \qquad G_3 = U_3(r_1 r_2)^{1/2} \qquad G_p = V_3(r)^{1/2}$$

The larger these G-factors are, the more favorable the candidate is for the time-reversal invariance test in an ideal experiment.

A table of G-factors was compiled for nuclei with mass numbers ranging from A=6 to A=33. Below is a list of the more favorable candidates found in the search.

Nucleus	E_1(MeV)	E_2(MeV)	E_3(MeV)	G_1	G_3	G_p
^{16}O	8.87	6.13	0.00	0.158	0.013	
^{18}F	2.52	0.94	0.00	0.071	0.093	
^{19}O	2.78		0.00			0.077
^{29}Si	2.43		0.00			0.070
^{30}Si	4.83	2.24	0.00	0.086	0.185	0.074
^{31}P	1.27		0.00			0.071
^{31}S	1.25		0.00			0.081
^{32}P	1.75	0.08	0.00	0.065	0.091	0.081
^{33}P	1.43		0.00			0.114
^{33}S	1.97		0.00			0.079
^{57}Fe (a)	0.1365		0.0144			0.021
^{110}Cd (a)	2.16	0.66	0.00	0.035	0.076	

(a) Probes from which the lowest upper bounds for time-reversal violation have been obtained for experiments involving γ-ray emission from nuclei.

1. K.S. Krane, Lawrence Berkeley Laboratory report LBL-1686.

4.2 0^+–0^- Isoscalar Parity Mixing in ^{14}N

E.G. Adelberger, A. Garcia, C.A. Gossett, W. Haeberli,* P.A. Quin,* J. Sromicki,*†
H.E. Swanson, V.J. Zeps

In the last annual report[1] we presented preliminary results of the longitudinal analyzing power measurements (A_L) across the narrow $^{13}C+p$ $J^\pi=0^+$ resonance at E_p =1.15 MeV. Our results were inconsistent with the theoretical expectation by more than four standard deviations. In the past year, we have completed a third data taking run at the University of Wisconsin tandem facility. The results are consistent with our previous measurements, improving the statistical uncertainty by ~ 23%. Our final corrected results are $A_L(\Theta_2)-A_L(\Theta_1) = 8.6\pm5.9(2.4)\times10^{-6}$, where $\Theta_1=35°$ and $\Theta_2=155°$ are the mean angles of our detector (see Fig. 4.2–1).

Several associated measurements have also been improved. The measurement of a beam energy shift correlated with beam helicity has been remeasured with results consistent with zero. Strict upper limits of $\Delta E \leq 0.6$ eV have been set. We have also improved measurements of the energy dependence of the detector sensitivity to transverse polarization components (see Fig. 4.1–1 of ref. 1) improving the confidence in our modelling of the detector response. We have therefore shown that the dominant uncertainty of this experiment is due to statistical error.

Several avenues are being pursued to understand the discrepancy between our A_L measurement and theory, described in (Sec. 4.3 and Ref. 1). Plans are underway to have the apparatus brought back to Seattle to continue the measurements with the prospect of the high intensity polarized source.

* University of Wisconsin, Madison, WI 53706.
† Present address: Eidgenossische Technische Hochschule, Zurich, Switzerland.

1. Nuclear Physics Laboratory Annual Report, University of Washington (1987) p. 29 and references therein.

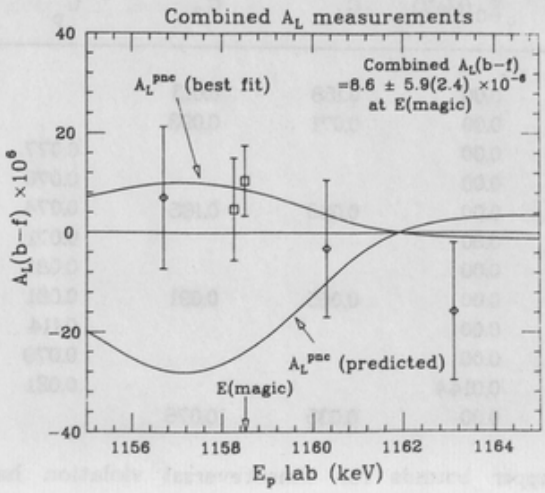

Fig. 4.2–1. Final A_L measurements (with 1σ statistical error bars) are plotted vs. energy, along with the predicted and "best fit" A_L curves. We expect systematic effects as large as $\sim 15\times10^{-6}$ for the three data points (diamond) away from E(magic). At E(magic), "worst case" systematic effects are $\leq 2\times10^{-6}$. A_L^{pnc} (best fit) was determined from the two points at E(magic). Inclusion of the other data in the analysis, however, does not significantly alter our results.

4.3 Interpretation of the Parity Violating Effect in ^{14}N

E.G. Adelberger, W.C. Haxton, C. Johnson, and V.J. Zeps

We have undertaken a program to solidify the theoretical foundation for the expected parity-mixing matrix element between the $0^+;T=1$ and $0^-;T=1$ levels at $E_x \sim 8.6$ MeV in ^{14}N. Most important is producing reliable ^{14}N wavefunctions for these levels. In previous calculations, the weak matrix element was evaluated in the usual fashion using harmonic oscillator (HO) wavefunctions as basis states. The unbound character of the 0^+ and 0^- levels (open to proton decay) suggests that the harmonic oscillator potential may not be suited for an accurate description of these levels. In the simple model,

$$|0^-> \approx |1p_{1/2}^{-3} x 2s_{1/2}>,$$

$$|0^+> \approx \alpha|1p_{1/2}^{-2}> + \beta|1p_{1/2}^{-4} x 2s_{1/2}^{2}> + \gamma|1p_{1/2}^{-4} x 1d_{5/2}^{2}>,$$

with respect to an ^{16}O core, where shell model calculations and spectroscopic factor measurements determine that $\alpha,\gamma << \beta$. Comparisons of the radial component of the $2s_{1/2}$ for HO vs. more realistic Woods-Saxon (WS) wavefunctions indicates that convergence in a harmonic oscillator basis would require excitations $>8\hbar\omega$. The one-body reduction of the two-body parity-violating operator is $\propto \vec{\sigma}\cdot\vec{p}$.[1] In this simplification, the parity mixing matrix element $<0^-|H_{weak}|0^+> \propto \alpha<2s_{1/2}|\vec{\sigma}\cdot\vec{p}|1p_{1/2}> + \beta<1p_{1/2}|\vec{\sigma}\cdot\vec{p}|2s_{1/2}>$. A comparison using WS vs. HO wavefunctions indicates a reduction of nearly 40% of the weak matrix element! We have therefore written code to calculate the two-body weak matrix element using WS wavefunctions. Once good single particle wavefunctions have been established, the results should give a more reliable calculation.

The central nuclear theory issue is the validity of the shell model basis truncation schemes in the region around A=16, and our ability to predict reliably the matrix elements of axial charge and associated E1 operators, both of which are inordinately sensitive to pairing correlations. Our prejudice is that the failure of past calculations to correlate PNC data is not due to an inadequate understanding of the shell model Hamiltonian, but rather to the technical difficulty of the calculations. We argue the the proper treatment of the $2\hbar\omega$ interaction, essential to understanding of ^{14}N and ^{16}O, requires the inclusion of $4\hbar\omega$ states in the shell model space. It appears that a first-principles $4\hbar\omega$ calculation of the spectrum of ^{16}O is extraordinarily successful: using the best available interactions and experimental single-particle energies (so that no free parameters exist) the energies of low-lying levels in ^{16}O are reproduced to better than 100keV. Our calculations were performed on the San Diego and MFE Crays.

In our view these calculations are the first that include the degrees of freedom known to be important to the structure of nuclei near A=16. Our intent is to thoroughly study PNC, axial charge β-decay, and various electromagnetic observables to assess the quality of the wavefunctions. A demonstration that theory could account for the axial charge β-decay rates in ^{16}O, ^{18}F, and ^{19}F would provide a convincing argument that the shell model can predict pseudoscalar observables. Alternatively, if large discrepancies remain, this would suggest that additional theoretical ideas are required before one can extract reliable information about the PNC NN interaction from systems which cannot be "calibrated" from β-decay measurements.

1. E.G. Adelberger and W.C. Haxton, Ann. Rev. Nucl. Part. Sci. 35, 501 (1985).

4.4 Search for Composition-Dependent Interactions Weaker than Gravity

E.G. Adelberger, S. Gil, J.H. Gundlach, B.R. Heckel, F.J. Raab, W.F. Rogers, C.W. Stubbs, H.E. Swanson, and R. Watanabe

Are there forces weaker than gravity that produce effects at macroscopic ranges? We have been conducting a torsion balance experiment to investigate this possibility since early 1986, when the "fifth force" conjecture of Fischbach et al.[1] brought this question to our attention. Our first results[2] ruled out the "fifth force" hypothesis of a Yukawa coupling to baryon number with a range 10 m $< \lambda <$ 1400 m. We obtained a limit on the dimensionless "fifth force" coupling constant of $\alpha_5 < 4\times10^{-4}$ for λ = 100 m which is to be compared with the predicted value of $\alpha_5 \simeq 10^{-2}$. This constraint was obtained by comparing the horizontal accelerations of Be and Cu test objects. However, our results were in apparent conflict with the positive result from an experiment conducted by Thieberger[3] using a detector composed of Cu and H_2O. We considered[4] a possible reconciliation scenario where the "charge" of the new Yukawa interaction would be generalized to a linear combination of baryon and lepton number, $q_5 = B\cdot\cos(\theta_5) + L\cdot\sin(\theta_5)$, where θ_5 is a mixing angle. In this picture our Be–Cu data could be consistent with Thieberger's observation for $\theta_5 = -11^\circ$, where the q_5 content of Be and Cu is equal. We explored this possibility by conducting a Be–Al comparison, and again obtained a null result, $\alpha_5(\theta_5 = -11^\circ, \lambda = 100\text{ m}) = (-7.2 \pm 19.2)\times10^{-5}$. We also pointed out[4] that near $\theta_5 = -63^\circ$ the charge (which corresponds to $q_5 = (N-Z)$) of the terrestrial sources used in the two experiments vanishes. Small differences in source composition could then conceivably account for the disagreement with Thieberger, but could not accommodate the geophysical anomalies reported by Stacey[5].

In September of last year, Boynton et al.[6] reported a new positive result from a Be/Al torsion balance operated at an impressive cliff at Index, WA. They claimed that their result was consistent with both our data and Thieberger's for $\theta_5 \simeq -63^\circ$. We are conducting an experiment with an improved apparatus (see following article) using a laboratory-scale Pb source to test this possibility, and to generally improve experimental constraints. The use of a laboratory-scale source has the following advantages: the composition, shape, size, and amount of source mass is under control and well known; the source mass can be moved and removed, and signals that appropriately follow it can be discriminated from sources of systematic error. Pb has an (N–Z)/volume that is 120 times greater than that of the Index cliff source of Boynton et al.; this and the ability to place the "fifth force" charge very close to the apparatus makes our source nearly as effective as the Index cliff for an intermediate-range coupling to isospin. We have chosen a configuration of the Pb that minimizes gravity gradient couplings to our detector. Our preliminary data show no indication of any anomalous differential coupling between the Be and Al test objects and the Pb. At the 1σ level our results disallow agreement between the various experiments[3,4,6] in terms of a coupling to isospin for any range 1 m $< \lambda <$ 1000 m. We rule out an agreement at the 2σ level to ranges of 500 m.

1. E. Fischbach et al., Phys. Rev. Lett. 56, 3 (1986).
2. C. W. Stubbs et al., Phys. Rev. Lett. 58, 1070 (1987).
3. P. Thieberger, Phys. Rev. Lett. 58, 1066 (1987).
4. E.G. Adelberger et al., Phys. Rev. Lett. 59, 849, 59, 1790 (E) (1987).
5. F.D. Stacey et al., Rev. Mod. Phys. 59, 157 (1987).
6. P.E. Boynton et al., Phys. Rev. Lett. 59, 1385 (1987).

4.5 Search for Composition-Dependent Interactions Weaker than Gravity – Apparatus Upgrade

E.G. Adelberger, S. Gil, J.H. Gundlach, B.R. Heckel, F.J. Raab, W.F. Rogers, C.W. Stubbs, H.E. Swanson, and R. Watanabe

We have rebuilt our apparatus to obtain higher sensitivity to possible feeble substance-dependent interactions, and to reduce the effect of systematic errors, especially those caused by thermal and gravitational gradients. Our detector consists of a newly designed pendulum suspended on a 20 μm diameter W fiber, whose torsional constant $\kappa \approx$ 0.30 erg/rad is determined by the moment of inertia of the pendulum and test bodies, and by the measured free oscillation period of 715 sec. Our new torsion pendulum, constructed with higher symmetry and tighter geometric tolerances, consists of a thin circular aluminum tray which constrains the centers of the test bodies to lie on the vertices of a square of side length 3.90 cm. The Be and Al test bodies ($m = 10.0364 \pm 0.0013$ g) which are identical in essentially all respects except for their chemical composition, are cylinders whose dimensions were chosen so that their individual gravitational quadrupole moments vanish. The more dense Al test bodies are hollow cylinders fitted with endcaps. Four right-angle mirrors are mounted on the tray in between the test bodies and are used by the torque monitoring system. A thin pole with cylindrical balance weights at the top and bottom ends is mounted along the axis of the pendulum tray in order to render the entire quadrupole moment of the tray + mirror + test body system zero. The mass of the entire pendulum is 67 g, making the passive-to-active-mass ratio $\approx$ 0.67, and its moment of inertia is $\approx$ 1.18 that of the mounted test bodies alone. The center-of-mass of the pendulum with and without the test bodies remains fixed at the geometric center of the test bodies. The pendulum, test bodies, supporting torsion fiber, and the inside of the surrounding electrostatic shield are all coated with a thin layer of Au.

We constructed a new vacuum can with a more rigid fiber column, and a new brass bearing on which the can rotates, resulting in greater overall mechanical rigidity of the entire apparatus. The temperature stability of the laboratory room has been improved and thermal gradients at the apparatus were reduced with passive shielding. The can is surrounded by a circular aluminum table on which machined lead bricks can be mounted above and below the plane of the pendulum at any angle ϕ in order to compensate the gravitational Q_{21} moment of the hillside or alternatively to function as an external q_5 source. The method of fiber attachment at the top suspension point has been improved, reducing feedthrough of "tilt" of the apparatus to equilibrium position shift of the pendulum. New superior fiber tilt monitors were constructed which operate on the same principle as the former. Finally, we improved the signal to noise through changes in the electronics. Compared with our former arrangement, we gain a factor of approximately 6 in overall sensitivity to substance-dependent interactions as a result of these apparatus changes.

4.6 First Operation of H-Atom Experiment with New Solenoid

T.A. Trainor and P. Wong

During the past year we have successfully integrated the major systems of the H-atom apparatus and returned the experiment to an operational condition. Initial tests were performed to ascertain proper operation of the apparatus . During this phase several changes were made in the modulation and lock-in detection systems to improve sensitivity and remove artifacts in the lock-in output. The detector output appeared to be much smaller than expected; impure detector gas was believed to be the culprit. All other systems functioned normally.

The previous computer control configuration was abandoned in favor of a simpler version (written in "C") more suited for the current experimental protocol. The high performance and temperamental B-field flipping bridge met a similar fate, replaced by a reliable relay-based bridge incorporating a computer interface. The addition of an hourly worker has made it possible to perform maintenance and functional improvements without disrupting the experimental development.

Recently we have concentrated on trimming and understanding the B-field in the new solenoid. A set of highly efficient algorithms was developed to model the effects of varying B-fields on arbitrary resonances and increased greatly our ability to interpret and understand centroid scans which measure the B-field within the cavities. We had previously encountered some discrepancies between the data and the computer predictions. A possible cause for this was revealed when we noticed that the result was not symmetric under time reversal. A subtle mis-application of time dependent perturbation theory was found in the formulation of the algorithms, and a more appropriate formulation of the problem was found. The programs will be modified to reflect this "corrected" interpretation, and hopefully the B-field adjustment procedure will become self-consistent. The vastly improved field offered by this new solenoid should make subsequent investigations into stray fields more productive than previously possible.

1. Nuclear Physics Laboratory Annual Report, University of Washington (1987) p. 30.

4.7 Antiproton Mass Measurement

X. Fei,* G. Gabrielse,* J. Haas,† H. Kalinowsky,† W. Kells,+
L. A. Orozco, S. Rolston,* R. Tjoelker,* and T. A. Trainor

Since the successful trapping of antiprotons at LEAR in July, 1986[1], we have carried out a development program on several fronts to create apparatus for a precision inertial mass measurement of the antiproton to begin late this year.

At LEAR a new beam line has been constructed which includes two 45° magnets to bring the antiproton beam onto a vertical axis, and a tower and instrument shed have been constructed to house the vertical bore superconducting solenoid and associated apparatus.

At Harvard a precision trap system and associated electronics have been developed. The trap consists of seven co-linear cylindrical copper electrodes electrodeposited on the interior of a macor cylinder. The first and last electrodes form the endcaps of an anharmonic catcher trap for up to 3 keV antiprotons slowed in thin foils. These particles are slowed further in the anharmonic trap by collision with trapped electrons until they can be contained by the inner precision trap. This harmonic trap is formed by the inner five ring electrodes. Rings 2 and 6 form the endcaps of the harmonic trap. Rings 3 and 5 serve as compensation electrodes to eliminate anharmonic potential components, and the center ring 4 is split in order to drive and detect the cyclotron motion of the antiprotons in the trap. The antiprotons are further cooled in this trap by coupling to the resistive element of a resonant circuit at 4° K.

At the University of Washington a beam diagnostic system to operate in the bore of the superconducting solenoid at 6T has been developed (Sect. 11.6). This consists of two sandwiched parallel plate avalanche counters (PPAC) with segmented anodes to provide 5-segment beam position information in each of two dimensions perpendicular to the beam axis. The counters also provide timing information with a resolution of ~200ps. For slow extraction (10^4–10^5 antiprotons/sec) the discriminator signals for each segment are fed into a 10-channel rate meter with 0.1 sec time constant (Sect. 11.4). The 0–10V outputs for each channel are fed to ADCs for display as X and Y beam profile histograms.

For fast extraction (10^9 antiprotons in 200 ns) the PPACs are operated as ion chambers at reduced bias, and fast ADCs are able to profile the beam pulse in space and time.

* Department of Physics, Harvard University, Cambridge, MA, 02138
† University of Mainz, Federal Republic of Germany
+ Fermi National Accelerator Laboratory, Batavia, IL 60510

1. G. Gabrielse, X. Fei, K. Helmerson, S.L. Rolston, R. Tjoelker, T.A. Trainor, H. Kalinowsky, J. Haas, and W. Kells, Phys. Rev. Lett. 57, 2504 (1986).

4.8 γ-Yields from Time-Reversal Test Candidates

E.G. Adelberger, P.B. Fernandez, A. Garcia, C.A. Gossett, G. Loechelt, W.F. Rogers and H.E. Swanson.

The angular correlations of mixed γ-ray transitions can be used to test the Time Reversal Invariance (TRI) symmetry. The TRI-violating terms in the angular correlation are proportional to the relative phase shift η between the matrix elements of the operators corresponding to the different multipoles present in the transition. Two kinds of experiments have been performed[2], and the results show consistency with TRI down to $\eta \approx 10^{-4}$. Both of them use radioactive sources polarized by magnetic fields at low temperatures. One of them is a coincidence experiment in which the violation of TRI would manifest itself in the angular correlation W of two γ-rays in a cascade through a term of the form[3]

$$W_{T-odd} = B_1 U_1 (k_1 \cdot k_2)(J \cdot k_1 \times k_2)$$

where k_1, k_2 and J indicate the direction of the γ-rays and the initial angular momentum respectively. The other experiment requires the detection of the linear polarization of a single γ-ray. The T-odd term in this case is:

$$W_{T-odd} = (B_3 V_3)(J \cdot k)(J \cdot E)(J \cdot k \times E)$$

where E stands for the direction of linear polarization. We are studying the possibility of making a TRI test using a polarized beam to produce a polarized nucleus in a reaction and then study the deexcitation γ-rays. This method avoids the disadvantage of possible rotations of the intermediate state, due to interactions with an external magnetic field, in the case of a cascade experiment. Even more important, most of the tests done to date have been performed in nuclei with high Z which require corrections to account for final state interactions (additional phase shifts coming from interactions with atomic electrons). We have carried out a detailed search[3] of all known mixed transitions in light nuclei ($Z \leq 16$) to avoid the problem of final state interactions . As a result of the search we found that the 8.87 MeV(2^-) → 6.13 MeV(3^-) → g.s.(0^+) cascade in ^{16}O and the 1.27 MeV($3/2^+$) → g.s.($1/2^+$) transition in ^{31}P could be good candidates for a cascade-type experiment and a linear-polarization experiment respectively. Since the uncertainty $\Delta\eta$ is inversely proportional to the product of the the polarization times the square root of the counting rate, we have performed an excitation function for both candidates using the reactions $^{19}F(p,\alpha)^{16}O^*$ and $^{31}P(p,p')^{31}P^*$, the results of which we present in Figs. 4.8-1 and -2. We expect to measure the polarization of the emitting nuclei very soon.

1. K.S. Krane, Lawrence Berkeley Laboratory report LBL-1686.
2. F. Boehm, Comments Nucl. Part. Phys., 11, 251 (1983).
3. Section 4.1, this report.

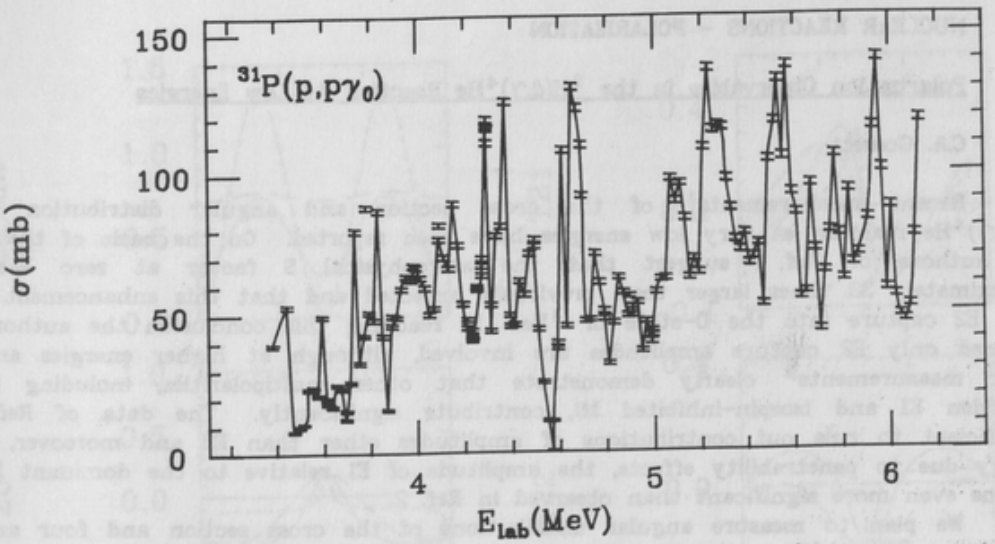

Fig. 4.8–1. Excitation function for the 1.27 MeV($3/2^+$) → g.s.($1/2^+$) transition in the $^{31}P(p,p')^{31}P$ reaction as a function of proton energy.

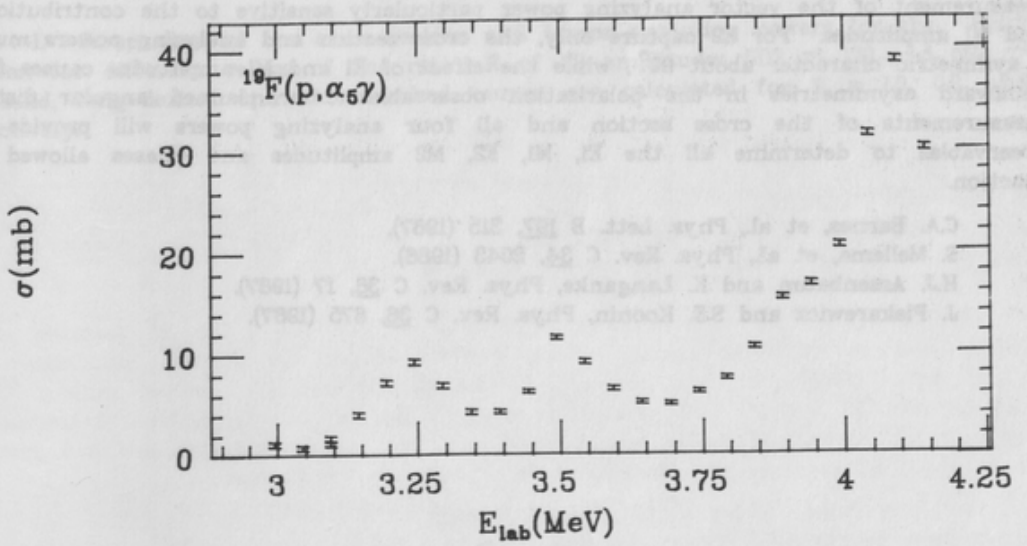

Fig. 4.8–2. Excitation function for the 8.87 MeV(2^-) → 6.13 MeV(3^-) transition in the $^{19}F(p,\alpha)^{16}O$ reaction as a function of proton energy.

5. NUCLEAR REACTIONS – POLARIZATION

5.1 Polarization Observables in the $^2H(d,\gamma)^4He$ Reaction At Low Energies

C.A. Gossett

Recent measurements[1] of the cross section and angular distribution of the $^2H(d,\gamma)^4He$ reaction at very low energies have been reported. On the basis of their work, the authors of Ref. 1 suggest that the astrophysical S factor at zero energy is approximately 32 times larger than previously expected and that this enhancement results from E2 capture into the D-state of ^4He. In reaching this conclusion the authors have assumed only E2 capture amplitudes are involved, although at higher energies analyzing power measurements[2] clearly demonstrate that other multipolarities, including isospin-forbidden E1 and isospin-inhibited M1, contribute significantly. The data of Ref. 1 are insufficient to rule out contributions of amplitudes other than E2 and moreover, at low energy due to penetrability effects, the amplitude of E1 relative to the dominant E2 may become even more significant than observed in Ref. 2.

We plan to measure angular distributions of the cross section and four analyzing powers for $^2H(d,\gamma)^4He$ at $E_d \approx 1$ MeV. At this energy predictions [1,3,4] for the ratio, R, of the E2 capture amplitudes, $\frac{5D2 \rightarrow 1S0}{5S2 \rightarrow 5D0}$, related to the amount of D-state in ^4He, vary from approximately 1 to 3. In Fig. 5.1-1 we illustrate our calculated sensitivities of the angular distributions of the cross section and tensor analyzing powers to R assuming the relative phases determined in Ref. 2. The vector analyzing power should be small and at 90° should be identically zero if only E2 amplitudes contribute, hence making measurement of the vector analyzing power particularly sensitive to the contribution of E1 and M1 amplitudes. For E2 capture only, the cross section and analyzing powers must have a symmetric character about 90°, while the effect of E1 and M1 amplitudes causes forward-backward asymmetries in the polarization observables. Our planned angular distribution measurements of the cross section and all four analyzing powers will provide enough observables to determine all the E1, M1, E2, M2 amplitudes and phases allowed in the reaction.

1. C.A. Barnes, et al., Phys. Lett. B 197, 315 (1987).
2. S. Mellema, et al., Phys. Rev. C 34, 2043 (1986).
3. H.J. Assenbaum and K. Langanke, Phys. Rev. C 36, 17 (1987).
4. J. Piekarewicz and S.E. Koonin, Phys. Rev. C 36, 875 (1987).

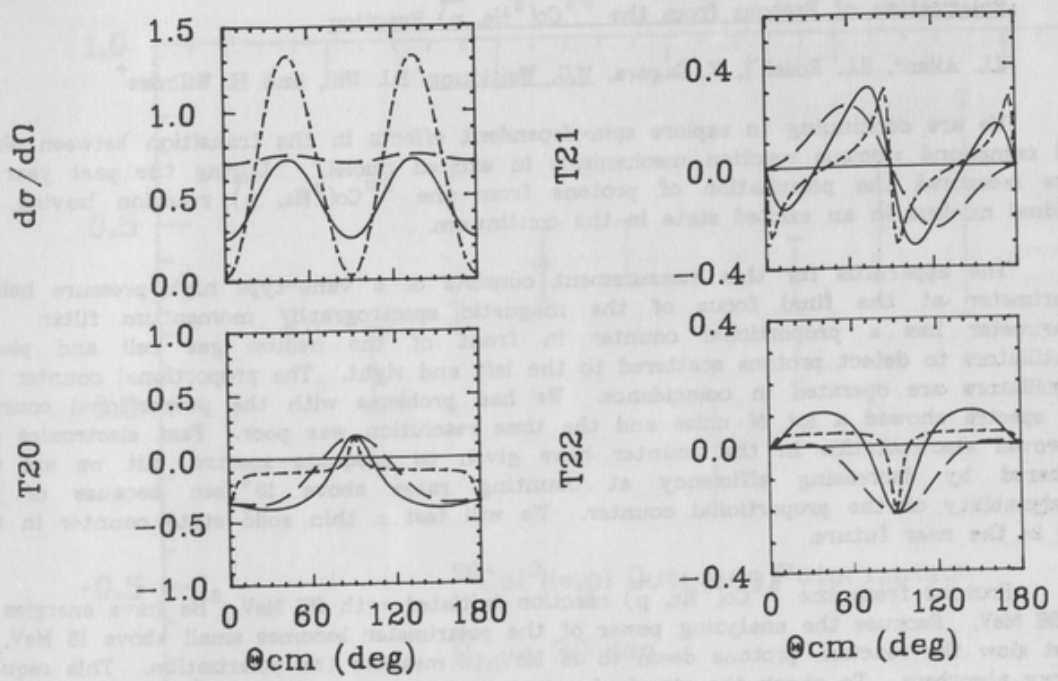

Fig. 5.1-1. Comparison of the cross section and tensor analyzing powers for the $^2H(d,\gamma)^4He$ reaction for different values of the ratio, R of E2 amplitudes 5D2 → 1S0 and 5S2 → 5D0. The solid, long-dashed and short-dashed curves are calculated for R = 1.0, 0.2, and 5.0, respectively.

5.2 Polarization of Protons from the $^{59}Co(^3He, \vec{p})$ Reaction

J.L. Allen*, S.L. Rosell †, K. Sagara, W.G. Weitkamp, D.I. Will, and H. Willmes+

We are continuing to explore spin-dependent effects in the transition between direct and compound nucleus reaction mechanisms in excited nuclei.[1] During the past year we have measured the polarization of protons from the $^{59}Co(^3He, \vec{p})$ reaction leaving the residual nucleus in an excited state in the continuum.

The apparatus for this measurement consists of a vane-type high pressure helium polarimeter at the final focus of the magnetic spectrograph/ momentum filter. The polarimeter has a proportional counter in front of the helium gas cell and plastic scintillators to detect protons scattered to the left and right. The proportional counter and scintillators are operated in coincidence. We had problems with the proportional counter: the spectra showed a lot of noise and the time resolution was poor. Fast electronics and improved electrostatics in the counter have given us adequate spectra, but we are still bothered by decreasing efficiency at counting rates above 10^4/sec because of the paralyzability of the proportional counter. We will test a thin solid state counter in this role in the near future.

Protons from the $^{59}Co(^3He, \vec{p})$ reaction initiated with 27 MeV ^3He have energies up to 36 MeV. Because the analyzing power of the polarimeter becomes small above 18 MeV, we must slow the reaction protons down to 18 MeV to measure the polarization. This requires energy absorbers. To check the standard calculations for stopping power[2], we measured the stopping power of both acetate and lucite for 18 MeV protons. We found the calculations for acetate to be correct to a precison of about 0.1 percent, but calculations for lucite are high by 1.7 percent.

Preliminary results taken at $\Theta_{lab} = 30^\circ$ and incident ^3He energy of 27 MeV are shown in Fig. 5.2-1. The data points represent averages over 1 MeV of proton energy. The error bars are statistical. We were limited to measurement of protons with energies less than 25.5 MeV by the maximum field of the momentum filter. The momentum filter control system is being modified to operate at higher fields.

The results at 30° are somewhat surprising. For the $(^3He, \vec{p})$ reaction at low excitation energies in light nuclei, where discrete states are excited, moderately large outgoing proton polarization is observed[4]. In the present case, the residual nucleus ^{61}Ni is left at between 10 and 20 MeV excitation energy. One would expect that averaging over energy, partial waves and states would wash out the polarization, yet a fairly persistent value of about 0.3 is observed. We intend to investigate this further.

* The John Fluke Company, Everett, WA 98206.
† Tacoma Community College, Tacoma, WA 98465.
+ The University of Idaho, Moscow, ID 83843.

1. W.G Weitkamp, I. Halpern, T.A. Trainor, S.K. Lamoreaux and Z.Y. Liu, Nucl. Phys. A417, 405 (1984).
2. H. Bichsel, Computer program DEDXR.
3. M. Irshad, C. Rioux, J. Asai, R. Pigeon and R.J. Slobodrian, Nucl. Phys. A286, 483 (1977).

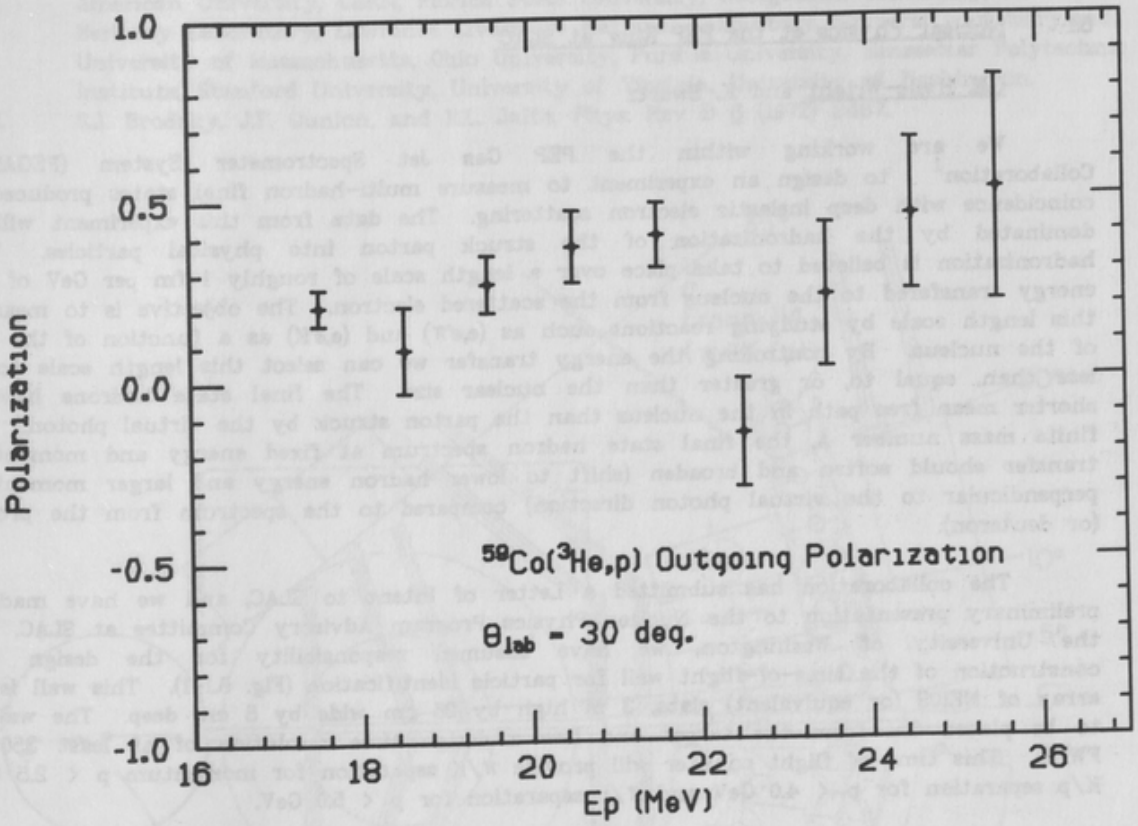

Fig. 5.2-1. Polarization of protons from the $^{59}Co(^3He, \vec{p})$ reaction initiated with 27 MeV ^3He.

6. MEDIUM ENERGY REACTIONS

6.1 Nuclear Physics at the PEP Ring at SLAC

C.E. Hyde-Wright and K. Swartz

We are working within the PEP Gas Jet Spectrometer System (PEGASYS) Collaboration[1] to design an experiment to measure multi-hadron final states produced in coincidence with deep inelastic electron scattering. The data from this experiment will be dominated by the hadronization of the struck parton into physical particles. This hadronization is believed to take place over a length scale of roughly 1 fm per GeV of the energy transfered to the nucleus from the scattered electron. The objective is to measure this length scale by studying reactions such as (e,e'π) and (e,e'K) as a function of the size of the nucleus. By controlling the energy transfer we can select this length scale to be less than, equal to, or greater than the nuclear size. The final state hadrons have a shorter mean free path in the nucleus than the parton struck by the virtual photon. For finite mass number A, the final state hadron spectrum at fixed energy and momentum transfer should soften and broaden (shift to lower hadron energy and larger momentum perpendicular to the virtual photon direction) compared to the spectrum from the proton (or deuteron).

The collaboration has submitted a Letter of Intent to SLAC, and we have made a preliminary presentation to the Nuclear Physics Program Advisory Committee at SLAC. At the University of Washington, we have assumed responsibility for the design and construction of the time-of-flight wall for particle identification (Fig. 6.1-1). This wall is an array of NE102 (or equivalent) slabs, 3 m high by 25 cm wide by 5 cm deep. The wall is to be placed 8m from the target and has a design time resolution of at least 350 ps FWHM. This time of flight counter will provide π/K separation for momentum $p < 2.5$ GeV, K/p separation for $p < 4.0$ GeV and π/p separation for $p < 5.0$ GeV.

At the University of Washington, we are also studying the acceptances and count rates for the (e,e'γ) and (e,e'K)Λ reactions. In the kinematics of quasi free Λ or Σ production on a nucleon, the (e,e'K) reaction probes the N(e,e'K)Λ and N(e,e'K)Σ vertex in the nuclear medium. For fixed final state, this reaction can be studied as a function of the photon invariant mass squared, q^2. The ratio of the (e,e'K) reaction on a nucleus to the elementary N(e,e'K) cross section will test the Impulse Approximation description of this reaction.

The PEGASYS project has a unique capability for measuring the exclusive (e,e'γ) cross section. For example, in He(e,e'γ), the elastic channel can be tagged by detecting a recoil α with a solid state telescope placed in the scattering chamber. The inclusive (e,e'γ) cross section is larger than the elastic (virtual compton) channel, however it is plagued by a large background from π^0 decay. Nonetheless, we are simulating the performance of the PEGASYS detector to find kinematic domains where the inclusive (e,e'γ) signal can be extracted. The optimum regions seem to be for large photon energy or large transverse momentum (relative to the virtual photon). The interference of bremsstrahlung with the compton process provides a particularly interesting observable in this reaction. In the x-scaling limit, this interference depends on the distribution of quarks weighted by the third power of the quark charge (one power from the bremsstrahlung amplitude, two powers from the compton amplitude)^2. Hence the reaction is sensitive primarily to the valence quarks, since the sea of quark anti-quark pairs will cancel out.

1. American University, CERN, Florida State University, Georgetown University, Lawrence Berkeley Laboratory, Lawrence Livermore National Laboratory, University of Maryland, University of Massachusetts, Ohio University, Purdue University, Rensselaer Polytechnic Institute, Stanford University, University of Virginia, University of Washington.
2. S.J. Brodsky, J.F. Gunion, and R.L. Jaffe, Phys. Rev D 6 (1972) 2487.

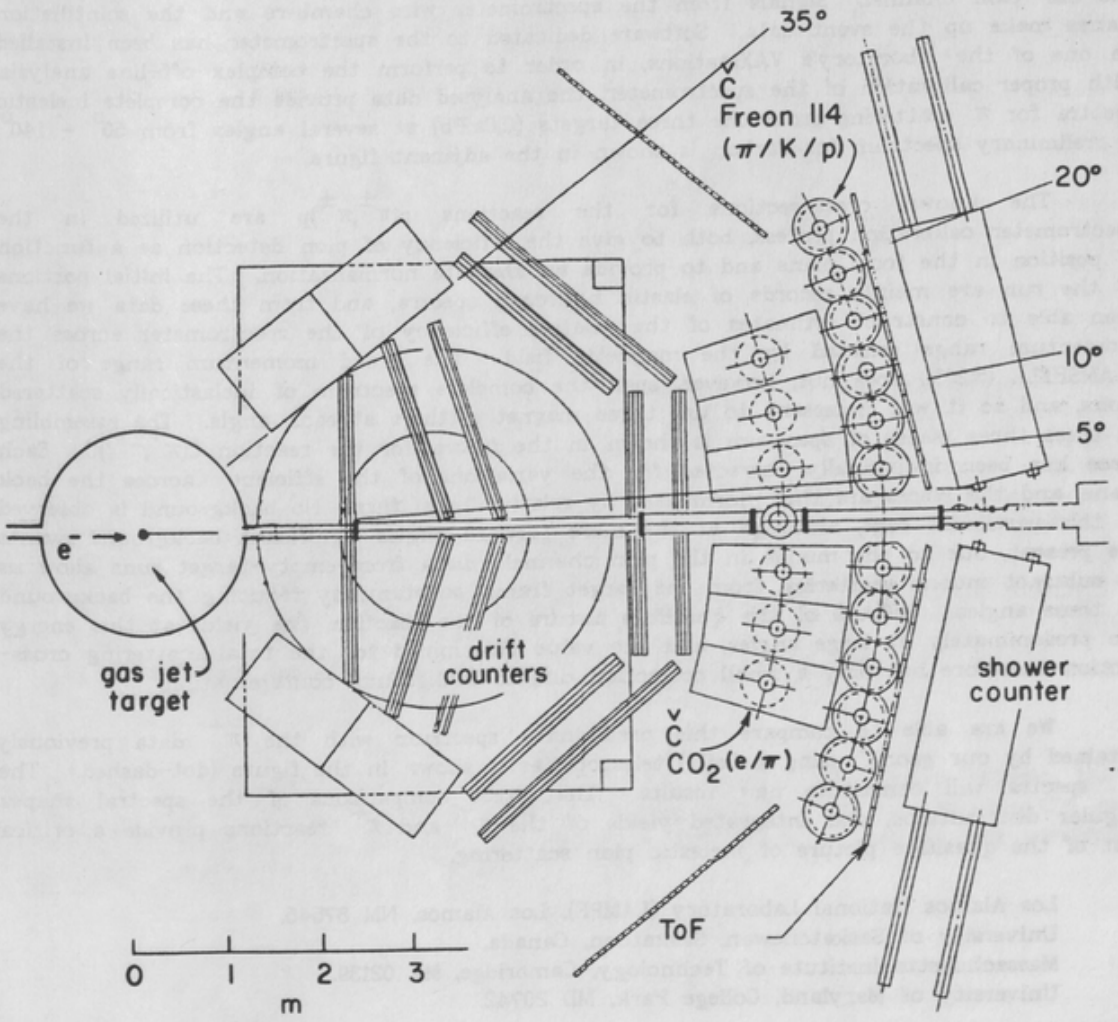

Fig. 6.1-1. Proposed PEGASYS layout.

6.2 Inclusive Inelastic Scattering Spectrum for π^- and π^+ from Nuclei at E_π = 100MeV

J.F. Amann*, R.L. Boudrie*, K.G.R. Doss †, D. Drake*, I. Halpern, J. Nelson#, M. Khandaker+, D.P. Rosenzweig, D.W. Storm, D.R. Tieger#, S.A. Wood#

We are in the process of analyzing the spectral data obtained during experiment #967 at LAMPF. The data were recorded using the CLAMSHELL magnetic spectrometer and the LEP pion channel. Signals from the spectrometer wire chambers and the scintillation planes make up the event data. Software dedicated to the spectrometer has been installed on one of the laboratory's VAXstations, in order to perform the complex off-line analysis. With proper calibration of the spectrometer, the analysed data provide the complete inelastic spectra for π scattering from the three targets (C,Ca,Pb) at several angles from 50^o - 140^o. A preliminary spectrum for Carbon is shown in the adjacent figure.

The known cross-sections for the reactions $p(\pi^\pm,\pi^\pm)p$ are utilized in the spectrometer calibration process, both to give the efficiency of pion detection as a function of position in the focal plane and to provide an absolute normalization. The initial portions of the run are mainly records of elastic hydrogen spectra, and from these data we have been able to construct estimates of the relative efficiency of the spectrometer across the momentum range selected by the magnetic field. The broad momentum range of the CLAMSHELL (±20%) does not, however, span the complete spectrum of inelastically scattered pions, and so it was necessary to use three magnet settings at each angle. The assembling of these three pieces of spectrum is shown in the figure, for the reaction $C(\pi^+,\pi^{+\prime})C$. Each piece has been individually corrected for the variations of the efficiency across the back plane, and the pieces are then normalized by relative beam flux. No background is observed in this particular case, although at the more forward angles significant background events are present, due to the muons in the pion channel. Data from empty-target runs allow us to subtract muons scattering from the target frame, substantially reducing the background at these angles. Because of the quasifree nature of the reaction, the yields at this energy are predominately at large angles, and the value determined for the total scattering cross-section therefore has only a small correction due to background contamination.

We are able to compare this preliminary spectrum with the π^+ data previously obtained by our group[1] using a Ge(Li) telescope, as is shown in the figure (dot-dashed.) The π^- spectra will constitute new results. The direct comparisons of the spectral shapes, angular distributions, and integrated yields of the π^- and π^+ reactions provide a critical test of the quasifree picture of inelastic pion scattering.

* Los Alamos National Laboratory (LAMPF), Los Alamos, NM 87545.
† University of Saskatchewan, Saskatoon, Canada.
# Massachusetts Institute of Technology, Cambridge, MA 02139.
+ University of Maryland, College Park, MD 20742.

1. K. Aniol et al, Phys. Rev. C 33, 208 (1986).

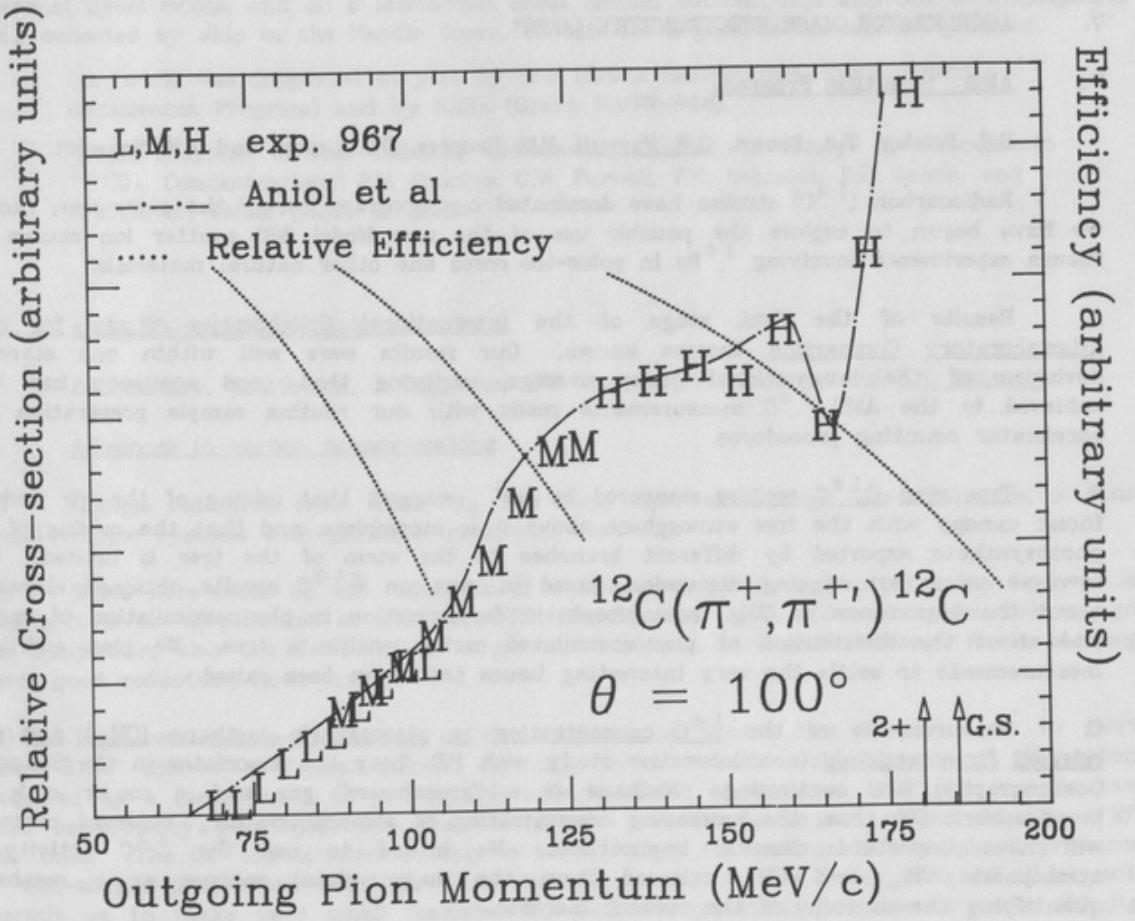

Fig. 6.2-1. Spectrum of scattered pion momentum, showing the overlap between the data from the Low, Medium, and High magnet setting (L,M,H). Also shown are the relative efficiency functions used for each of the settings (dotted), as well as the corresponding spectrum from Aniol et al. (dot-dashed).

7. ACCELERATOR MASS SPECTROMETRY (AMS)*

7.1 AMS: Scientific Program

D.R. Balsley, T.A. Brown, G.W. Farwell, P.M. Grootes, D.D. Leach, and F.H. Schmidt

Radiocarbon (^{14}C) studies have dominated our program during the past year, though we have begun to explore the possible use of the new Model 860 sputter ion source for future experiments involving ^{10}Be in polar ice cores and other natural materials.

A. Results of the first stage of the International Collaborative Study for ^{14}C Interlaboratory Comparison became known. Our results were well within one standard deviation of the international group average, verifying that good accuracy has been achieved in the AMS ^{14}C measurements made with our routine sample preparation and accelerator counting procedures.

B. Tree ring $\Delta^{14}C$ profiles measured by us[1] suggest that mixing of the air under a forest canopy with the free atmosphere above it is incomplete, and that the mixing of the photosynthate exported by different branches to the stem of the tree is limited. This involves us in an ongoing discussion, based in part on $\delta^{13}C$ results obtained elsewhere, about the importance of CO_2 from biospheric decomposition in photoassimilation of carbon, and about the distribution of photoassimilated carbon within a tree. We plan additional measurements to settle the very interesting issues that have been raised.

C. Measurements of the ^{14}C concentration in atmospheric methane (CH_4) and CH_4 released from wetlands (a collaborative study with P.D. Quay and associates in the School of Oceanography) are continuing. Methane is a "greenhouse" gas and a major sink for trophospheric OH; thus, the increasing concentration of atmospheric CH_4 observed currently will have important climatic implications. We intend to use the ^{14}C activity of atmospheric CH_4 and CH_4 released from the major global sources as a means of quantifying the source(s) of the current increase.

During the past year we measured the ^{14}C activity of CH_4 released from the Alaskan tundra and Minnesota peat bogs; these two wetland types are likely the major natural sources of CH_4 in the northern hemisphere. The results vary from 107 to 128 percent of modern carbon (pMC), indicating that a significant portion of the CH_4 flux from these sources is derived from organic material produced in the nuclear weapons era, i.e., post 1955. These results indicate a rapid cycling of carbon through the photosynthesis–methanogenesis cycle in wetlands.

We also obtained our first measurements of the ^{14}C activity of CH_4 in the atmosphere by extracting, purifying and combusting CH_4 from air collected on the Washington coast (48N, 124W). The preliminary results range from about 117 to 123pMC. These ^{14}C concentrations indicate that the input of CH_4 to the atmosphere is dominated by ^{14}C produced during the era of nuclear weapons testing, as they are higher than those observed by others for the southern hemisphere (about 108pMC). If a hemispheric gradient in atmospheric $^{14}CH_4$ indeed exists, then this might provide a means to distinguish northern vs. southern CH_4 inputs.

Our plans for the near future involve primarily the continued measurement of the ^{14}C activity on air samples collected on the Washington coast, in order to determine whether a

seasonal cycle exists, and on a latitudinal cross section between 50N and 30S of atmospheric CH_4 collected by ship in the Pacific Ocean, to test for a possible hemisphere gradient.

* Our work was supported in part by NSF (Grant EAR-8115994, Environmental Geosciences Program) and by NASA (Grant NAGW-844).

1. "Rapid Response of Tree Cellulose Radiocarbon Content to Change in Atmospheric $^{14}CO_2$ Concentration," P.M. Grootes, G.W. Farwell, F.H. Schmidt, D.D. Leach, and M. Stuiver, Tellus (1988), in press.

****

7.2 AMS: Technical Highlights

D.R. Balsley, T.A. Brown, J. Caggiano, G.W. Farwell, P.M. Grootes, and F.H. Schmidt

A. Advances in carbon sample-making.

(1) Sample reduction from from CO_2 has been improved through the completion of four small-volume systems with pressure-transducer read-out.

(2) Tests were made on the reduction of C directly into the well of the tiny Ta capsule where it is to be pelletized as graphite. The Ta capsules failed. (The reduction did not go to completion; also the Ta acted as a getter, and upon cooling it broke.) A Mo backing gave good reduction, however.

(3) Improved sample-positioning in the sputter ion source has permitted us to shift from 3/32" dia. to 1/16" dia. samples, resulting in a reduction of the amount of carbon required by a factor of 3 to 4. Very recently, we have shown that 1/32" dia. samples can also be properly positioned, and that they can give the same ion-output as the 1/16" dia. ones. (The Cs^+ ion sputtering beam is very sharply focussed on the sample; it produces a well-shaped hole about 0.020" in diameter.) Equipment is now being designed which will permit us to make very small diameter samples; we expect to be able to make 100 μg carbon samples which will give 25,000 or more useful ^{14}C counts. These samples are made by the graphitizing-scintering process described earlier.[1]

B. Achievement of 60-KV elevation potential for the ion source

A new electrostatic quadrupole and steering system was installed in the low-energy beam line. This, at long last, permitted the sputter ion source to be operated at its full design elevation potential of 60 K.V., up from 30 K.V. The most important result of increased elevation potential is improved beam emittance. The fraction of the negative ion beam which is transported through our 5/32" diameter entrance aperture is increased from 60 - 65% at 30 K.V. to 80 - 85% at 60 K.V. For the first time, we have demonstrated that we have essentially no beam loss between the 3/32" low-energy defining aperture and the stripper foil at the high-voltage terminal.

The secondary electron beam became so excessive at 60 K.V. elevation that the x-radiation produced by the electron beam was sufficient to present a health hazard to persons near the inflection magnet. A magnetic suppressor in the accelerator region and added Pb shielding in critical locations have almost completely removed the x-radiation.

C. Improved carbon beam intensity and stability

In September, we achieved a new high in ion source output efficiency; viz., 50 μA of $^{12}C^-$ ions (through the entrance aperture) at 1.0 mA extraction current. This beam produced a ^{14}C counting rate at the detector equivalent to 123 counts per second for contemporary carbon. The predicted rate for 100% ion transmission is 135 c/sec., based on the theoretical charge-state distribution. The small remaining loss is believed to occur in the high-energy beam tube due to beam spread at the stripper.

Several improvements in the Tandem system (a new stripper foil mechanism, electric horizontal steering at the terminal, improved beam scanners) have been of substantial benefit to AMS performance.

D. Durability of graphitized carbon samples

In September, we made two long marathon-type runs to determine how many counts we can really obtain from a single sample. Using a pair of identical samples of "1964 carbon" (tree ring material) we obtained >300,000 useful ^{14}C counts from each, with a measured ^{14}C ratio = 0.9981 $\pm$0.0057. We believe that the smaller diameter samples now being made will yield similar numbers of ^{14}C counts before deteriorating significantly.

1. Nuclear Physics Laboratory Annual Report, University of Washington (1987) p. 40.

8. RESEARCH BY OUTSIDE USERS

8.1 Thin Layer Activation Analysis for Application to the Study of Erosion-Corrosion in Feedwater Pipes

J.T. Stanley*

A study of erosion-corrosion of carbon steel feedwater piping is being carried out at Arizona State University under the sponsorship of the Electric Power Research Institute. A closed loop system has been set up in which water of controlled chemistry is pumped through test section carbon steel piping (2.5 inch diameter, Schedule 40). The system is constructed of stainless steel except for the test section. The test section actually consists of four sections joined together by flanges in order to test different materials and configurations, and to accommodate the requirements of the thin layer activation analysis technique which will be described. Two of the sections are straight pipes and the other two are 90° elbows. Erosion is observed by measuring the activity of a radioactive spot on the wall of the test section pipe.

For this type of experiment it is important that the radioactivity should only be present near the surface of the sample that is to be eroded. It is this configuration that gives the technique its high sensitivity to erosion rates. For example, consider a 1/4 inch wall thickness pipe. If it were irradiated in a nuclear reactor to produce a uniform distribution of radioactivity through the wall and then subsequently exposed to an environment that eroded one mil (0.001 inch) from the surface, the radioactivity would be decreased by 0.4% which is scarcely measurable. However, if the wall of the pipe were irradiated with protons that produce radioactivity to a depth of only 25 mils, then when one mil is eroded from the surface, the activity changes by 4%, which is easily measured.

In our case the radioactivity is created by irradiating with 13 MeV protons at the University of Washington accelerator facility. The proton beam is focused to a spot about 1/2 inch diameter and enters the pipe at one end in the case of the straight pipe sections or through a flanged port in the case of an elbow. For the straight pipe the beam strikes the surface of the pipe at an angle of 23° to the surface at four inches from the end of the pipe. After traveling a distance of about 12 mils in the pipe wall, the proton energy will have dropped to 6 MeV. The threshold energy for the $^{56}Fe(p,n)^{56}Co$ reaction is 6 MeV so that the radioactive ^{56}Co atoms are only created to a depth of (12sin 23 = 5 mils) below the surface.

The choice of ^{56}Co is a good one for this experiment since an 0.8 MeV gamma ray is emitted for each ^{56}Co atom that decays. A gamma ray of this energy is only slightly attenuated in traversing the wall of the pipe and thus we can monitor the activity of the radioactive material using scintillation counters located outside the pipe.

In order to convert from counting rate to erosion rate, it is necessary to know how the radioactive material is distributed below the surface of the sample. Consideration of the energy of the protons as a function of depth in the material and of the cross section for the (p,n) reaction as a function of proton energy will allow us to calculate the distribution of activity with depth.

* Arizona State University

8.2 Irradiation of Optical Materials

T.L. Criswell,* K.L. Ballou,* G. Bohnhoff-Hlavacek,* and V.S. Starkovich*

Reflection of light from transparencies (e.g., the inside of windshields, CRT screens, or instrument covers) is a chronic problem. Existing antireflective coatings, while reducing reflection, often work in too narrow a band of frequencies, are absorptive, or produce excessive diffuse scattering. The fundamental cause of reflection is the abrupt change in the index of refraction at the interface between the two media, air and the transparency. If the change in the index can be smoothed over distances of the order of the wavelength of light, the reflectivity will be reduced. Such smoothing can be achieved by producing a dendritic surface with an areal-average index. A method of producing such surfaces has been developed by adapting techniques used in nuclear track-etch detectors. Dielectric materials are irradiated with high fluences of heavy ions and the resulting damage tracks are chemically etched away. The remaining walls of the etch pits approximate the desired shape. The exact shape of the pit wall depends on the damage threshold of the material, the stopping power of the ion, and the etch process. The present study covers a wide selection of plastics and glasses, finding optimum ion-etch combinations to produce the desired antireflective surface for each material. Large-sample production will be emphasized this year.

* Boeing Aerospace Company, Seattle, WA 98124-2499.

8.3 Nondestructive Measurements of Power-MOSFET Single-Event Burnout Cross Sections

D.L. Oberg* and J.L. Wert*

Power MOSFETs can undergo catastrophic failure following exposure to a single energetic heavy ion (as found in cosmic rays). This failure is precipitated by the second breakdown of a parasitic bi-polar transistor. The likelihood of this failure is seen to be related to the device drain-source voltage as well as the energy deposited by the incident ion.

The nondestructive technique which was developed here last year[1] has now been applied to a wide variety of parts at several accelerators (including the 88" Cyclotron and the Bevalac at the Lawrence Berkeley Laboratory.) Data acquired at these facilities is shown in Fig. 8.3-1. It is seen that the voltage threshold for burnout is not simply a function of linear energy transfer.[2,3,4]

Tests have also been conducted on power MOSFETs which are from the same lot as those found in a still-functioning satellite power converter.[5] It was seen that the voltage threshold for burnout is just above the maximum operating voltage of the devices in the circuit.

* Boeing Aerospace Company, Seattle, WA 98124-2499.

1. Nuclear Physics Laboratory Annual Report, University of Washington (1987) p. 44.
2. "First Non-Destructive Measurements of Single Event Burnout Cross Sections for Power FETs", D.L. Oberg and J.L. Wert, Fifth Annual Symposium on Single Event Effects, April 7-8 1987.
3. "First Non-Destructive Measurements of Single Event Burnout Cross Sections for Power FETs", D.L. Oberg and J.L. Wert, 24th Annual Conference on Nuclear and Space Radiation Effects, July 28-31 1987.
4. D.L. Oberg and J.L. Wert, IEEE Trans. Nuc. Sci., NS-34, Dec. 87.
5. "SEU Sensitivity of Power Converters with MOSFETs in Space", G.L. Brucker, D.L. Oberg, J.L. Wert, P.R. Measel and T.L. Criswell, IEEE Trans. Nuc. Sci., NS-34, Dec 1987.

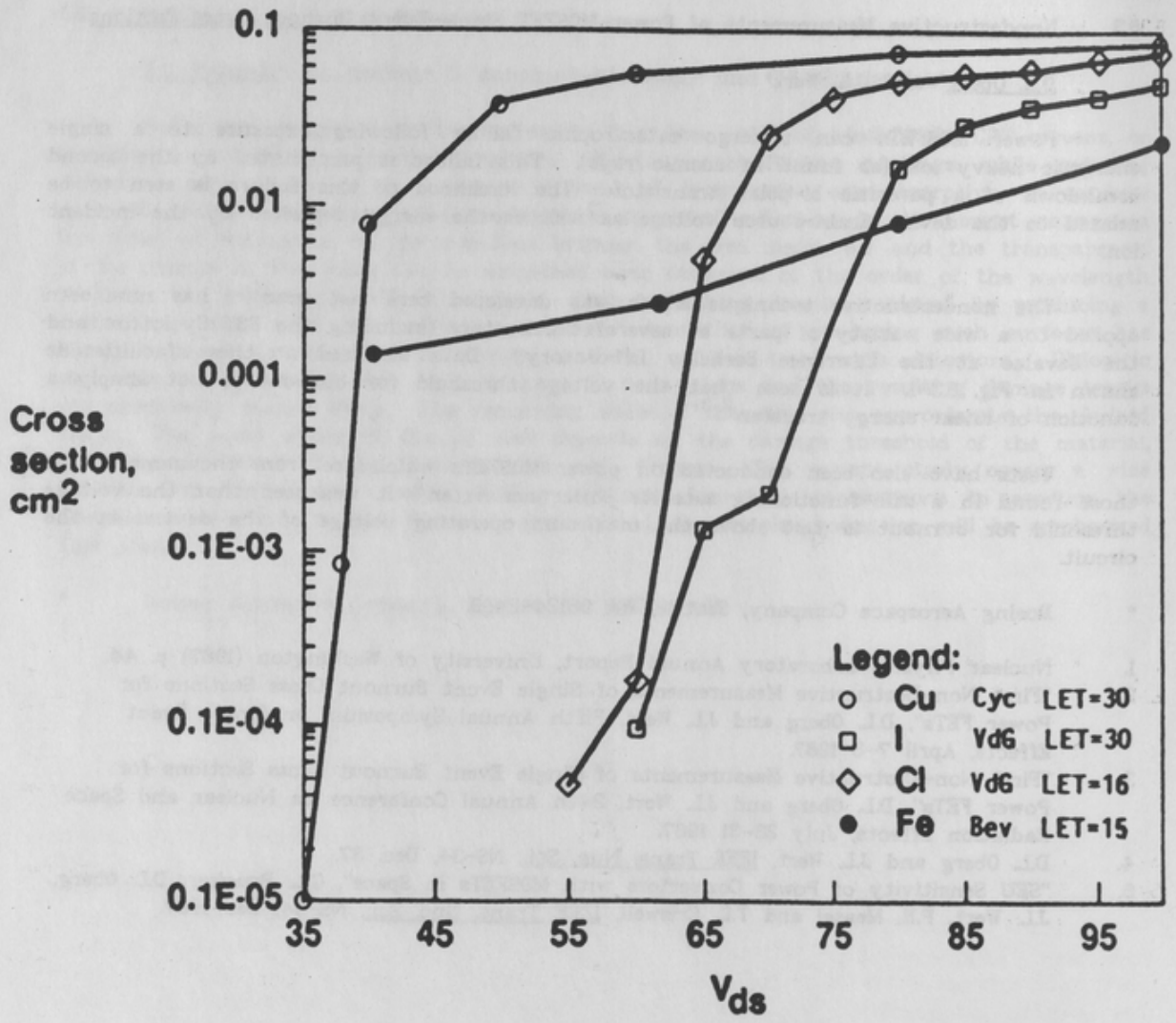

Fig. 8.3-1. Burnout Cross Sections for the IRF 130.

8.4 High LET Radioisotopes for Radioimmunotherapy

K.A. Krohn,* D.S. Wilbur,† and S. Hadley

A new joint effort involving the Department of Radiology and NeoRx Corporation has been initiated to investigate the value of alpha-emitting isotopes for tumor therapy. Alpha particles cause very intense radiation damage within a few microns of where they are emitted and thus one decay event within a cell is completely effective in destroying that cell. The NeoRx scientists are experts in attaching radioisotopes to monoclonal antibodies, large protein molecules that seek out and bind to cells that express complementary antigens. In this specific research we want to use ^{211}At which will be produced using the 27-28 MeV ^{4}He beam to irradiate bismuth targets. The reaction can be used to produce about 50 μCi of isotope in one hour, sufficient to develop the chemistry of attaching it to antibodies. ^{211}At labeled monoclonal antibodies could be very useful for therapy of many kinds of tumors, especially melanoma which is quite resistant to all current treatments.

* Department of Radiology, University of Washington.
† NeoRx Corporations, Seattle, WA 98119.

9. VAN DE GRAAFF AND ION SOURCES

9.1 Van de Graaff Accelerator Operations and Development

C.E. Linder, F.H. Schmidt, R.E. Stowell, T.A. Trainor, T.D. Van Wechel, W.G. Weitkamp, and J.A. Wootress

Emphasis has again been placed on completing the superconducting booster described in Chapter 10 of this report. Among the booster projects specific to the tandem accelerator was the installation of a 200-foil stripper mechanism. This device, which is described in Sect. 10.10, is now operating satisfactorily.

We experienced major problems with terminal voltage stability during the year. There have been a variety of symptoms. One rather puzzling one was an upward excursion of the terminal voltage either in response to a minor change in upcharge current, or spontaneously. The excursions, about 0.5 MV, exceeded the range of the terminal voltage regulator and occurred with a frequency of one every three or four minutes. The excursions were correlated with a rise in downcharge current. Since these excursions made reasonable operation impossible, we opened the tank and searched for possible causes. Nothing of significance was found, although we did change the collector screen in the terminal. Surprisingly, operation was fairly normal for a while after the tank opening.

Increasing instability of the terminal voltage (beside the excursions mentioned above) lead to the investigations described in Sec. 9.4. Since that analysis made it clear that the belt was somehow the cause of the instability, we changed the belt, beginning on April 4. The outer, charge-carrying surface of the old belt did not look bad, but the inner surface looked abraded, as though it had been rubbed with sandpaper. The cause of the abrasion was not apparent. We did find a bowed shield plate in the high energy midsection which showed signs of having rubbed the outside of the belt.

The new belt has only been operated a few days, but gives significantly improved performance. It may be among the best belts we've had in the machine.

The Accelerator Mass Spectroscopy group uses a signal from the generating voltmeter to stabilize the terminal voltage. One problem with this technique is that the voltmeter views the high energy column as well as the terminal. Because of belt ripple, the voltage distribution on the high energy column varies with time; this introduces noise into the terminal voltage stabilization loop. To reduce this noise, we tried moving the GVM to a port which is further away from the high energy column. Definitive tests have not yet been made, but this configuration appears to lead to better regulation.

During the year from April 16, 1987 to April 15, 1988 the tandem operated 3779 hours. Additional statistics of accelerator operations are given in Table 1.

Table 1
Tandem Accelerator Operations
April 16, 1987 to April 15, 1988

Activity	Days Scheduled	Percent
A. Nuclear Physics Research		
Light Ions	65	18
Polarized Ions	11	3
Heavy Ions	39	11
Booster Beams	26	7
Radiochronology	24	6
Subtotal	165	45
B. Outside Users		
Arizona State University	1	<1
The Boeing Company	3	1
NeoRx Corporation	1	<1
Subtotal	5	1
C. Other Operations		
Tandem Development	62	17
Tandem Maintenance	38	10
Booster Development	58	16
Unscheduled Time	38	10
Subtotal	196	54
Total	366	100

9.2 The Crossed Beams Polarized Ion Source

D.R. Balsley, A. Garcia, C.A. Gossett, G.C. Harper, R. Hobbs, J.R. Olson, and V.J. Zeps

Development of the crossed beams polarized ion source has been steadily progressing and the first nuclear physics experiment using the polarized beam was performed in December.

One of the most significant areas of progress in the last year has been that of increased longevity and stability of the beam. The Cs^+ beam formation section of the source has been quite reliable and has not required service in over five months of on and off operation. The Cs^+ neutralizer and H^- ionization regions are the most susceptible to breakdowns due to contamination by material sputtered by the Cs beam or by deposition of Cs metal on insulating surfaces. Failures of this type have been significantly reduced by redesign of the Cs neutralizer and replacement of the extremely unstable and unreliable temperature control and sensing systems. We now routinely operate at modest output currents, 200–300 nA for cumulated periods of several days without high voltage sparking or need for maintenance.

The problem of poor power coupling from the rf transition power generators to the strong field rf cavity reported last year[1] has been studied and solved. We now routinely measure proton polarizations of 0.90–0.92 with ~ 16 watts of power to the rf cavity. The rf cavities and drives for deuterium will be optimized in the near future. We are investigating the origin of a large unpolarized background of protons observed with the atomic beam isolated from the ionization region or with operation with deuterium.

We have continued to study the low output performance of the atomic beam source[2] and have designed and tested dissociator bottles with a nozzle design similar to that used at the University of Wisconsin. Atomic beam flux and H^-, D^- beam improvements of factors of 1.5–2 have been observed. Efforts to examine and optimize the atomic beam flux will continue. To date we have not had reliable measurements of the absolute Cs^0 flux. In the past several months a neutral beam calorimeter has been constructed. We plan to complete, install and calibrate the calorimeter soon. This device will enable us to determine the Cs^0 flux and with our knowledge of the atomic beam flux, we will be able to assess the performance of the crossed beam system.

Improvements have been made in the polarized source control system (see Sec. 9.3). Software control of the vacuum interlocks of the atomic beam source has been programmed, installed and tested. The experience gained with hardware and software development thus far will be extended to the software control of the Cs beam and spin precessor vacuum control systems as well as to control of high voltage and cooling interlock conditions. We have begun to remotely monitor and control portions of the polarized source from the tandem control room via a remote communications package connecting the polarized source to the linac microVAX control computer. A system of knob boxes which will be connected for control of the source in several locations through the microVAX and polarized source microprocessors is being designed.

1. Nuclear Physics Laboratory Annual Report, University of Washington (1987) p. 49.
2. Nuclear Physics Laboratory Annual Report, University of Washington (1987) p. 48.

9.3 Polarized Ion Source Computer Control System

C.A. Gossett, G.C. Harper, M.A. Howe, H.P. Readdy, R.J. Seymour, and H.E. Swanson

An effort has been launched to provide remote control of the polarized ion source through the linac touch screens. Until recently, only local control of most of the source parameters was possible by means of three microprocessor controllers provided by the source vendor, ANAC. Code for these controllers is written in the Motorola M6800 assembly language and burned into eproms, making coding changes somewhat more difficult than using a high level language. Recent acquisition of the assembler and source code listings has greatly facilitated this process.

The original controllers have a provision for remote communications with a host computer using a communication adapter made by ANAC which communicates with the controllers on a serial fiber optic link and with a satellite computer, a DEC Falcon microcomputer (soon to be upgraded to an LSI11/23) through a DEC DRV11 parallel interface. The DEC microcomputer then communicates with the linac host computer, a DEC MicroVAX, on another serial fiber optic link. The data acquisition computer will be able to control the spin precession and RF transitions via the DECNET connection to the MicroVAX.

Programming for the satellite computer is done in the MicroPower Pascal programming language which is the same used for all of the satellite computers in the linac control system. The host computer executive program, CSX, is written in the C language. The use of three different programming languages is justified in that the maximum use of existing software can be made. The polarized ion source differs from the rest of the linac control system in that the actual control rests mainly in the ANAC local controllers. The CSX program and the touch screens are used primarily as a monitor thus extending the capabilities of an already existing control system.

We found the original software inadequate for the following reasons. The software interlock features had not been implemented, requiring external hardwired interlocks to be provided. The processor for the spin precessor system had not yet been programmed, making operation of this part of the source incompatible with the rest of the control. The cesium system control was not workable in its original configuration and it was necessary to make external hardware changes to compensate for this. The remote communications package was incomplete and untested, making remote control questionable if software changes could not be made.

To date, three major milestones have been reached in this effort. Several modifications to the code for the vacuum system have been successfully implemented. Interlocks for the vacuum system in the atomic beam section of the source have been changed over from hardwired to software control. The remote communications package has been through its initial stages of hardware and software debugging and we have successfully displayed the atomic beam system parameters on and controlled them from the touch screens.

Future plans for the control system include conversion of the remaining atomic beam system interlocks, atomic beam system parameters, and the entire cesium system to remote control.This will be followed by the implementation of the controller for the spin precessor system. Sophistication of the touch screen capabilities should then parallel the advances of the controller software development.

9.4 Charging Belt Motion and Tandem Regulation

T.A. Trainor

Over the past year the tandem voltage stability deteriorated to the point that the voltage regulation system was driven to saturation for a significant fraction of the time. Among other things this made operation of the linac very difficult. Various components of the regulation system were checked and found to be working properly. The trouble was localized in the charging system.

A clear correlation was observed between large corona current fluctuations and fluctuations in the high energy column current (HECC), so attention was focussed on this parameter. A chart recording of the HECC showed no periodicity at the charging belt period (0.43 s) but did show occasional evidence of periods at 5.2 s, 3.9 s, 4.7 s and 2.15 s, among others. It was determined that this signal was the result of a contribution from the belt period at 0.43 s and an unknown source with a slowly varying period near 0.27s. At 8.5 MV the fluctuation in the HECC was ~ 30% of the average 120 μA.

A spectrum analyzer was used to look at the HECC further. The spectrum (Fig. 9.4-1) consisted of belt ripple at 2.34 Hz and harmonics and a broad peak at 3.7 Hz with tails that stretched down to 1 Hz and up beyond 5 Hz. The peak width was about 1Hz and the total area under this peak was much greater than that contributed by the belt harmonics, indicating that most of the HECC fluctuations, and perhaps terminal voltage fluctuations, were coming from this unknown source.

The vertical beam jitter observable at the high energy scanner was also spectrum analyzed. A photocell was fitted with a triangular window so that if the trace shifted on the scanner display the cell output would vary. The low side of the beam showed motion only at the new noise source frequency of ~ 3.7 Hz. The high side motion was mostly 3.7 Hz with ~ 20% contribution from belt harmonics at 2.34 Hz, 4.68 Hz, etc.

The nature of the spectra (absence of folding) indicated that the belt frequency and unknown source were linearly independent. This eliminated an initial hypothesis that the fluctuations were caused by the belt hitting the column mid-section and losing charge. This mechanism would have resulted in a modulation of one process by the other and consequent spectrum folding.

The hypothesis presently in favor is that the unknown noise source is currents induced in the high energy column by transverse motion of the belt due to interaction with the tank gas. The belt as a vibrator is a membrane moving at 60% of the speed of waves propagating on it past boundary conditions established by the free belt edges in one direction and the motor and alternator in the other. The vibrations are heavily damped by the 15 atmospheres of tank gas. There are a number of vibration modes in the 4 Hz to 50 Hz region.

Induced column currents and electrostatic force between belt and column increase with increasing belt curvature. The electrostatic force is destabilizing for transverse motion, so that increased charge on the belt favors shorter wave length, higher frequency modes of motion, as observed in the HECC noise spectra. At 8.5 MV and 320 μA belt current the belt is carrying about 70 μC of charge. The electrostatic forces are therefore comparable to the mechanical restoring force (~ 1-5 N).

The tank gas pressure was varied and it was found that below 165 psi this phenomenon was totally absent, and that above 185 psi it was fully developed and changed little with increasing pressure. The tandem operated at 7 MV and 165 psi ran very smoothly and with ideal regulation.

It is believed that a badly roughened inner belt surface increased the drag and general interaction of the belt with the tank gas, thereby making it prone to lateral motion driven by gas turbulence. A new belt was installed and the 3.7 Hz noise has not been observed at any tank pressure up to 215 psi. The HECC now has a 5% ripple at the belt frequency, the vertical jitter is negligible, and the regulation system again provides ideal regulation.

1. Nuclear Physics Laboratory Annual Report, University of Washington (1987) p. 46.

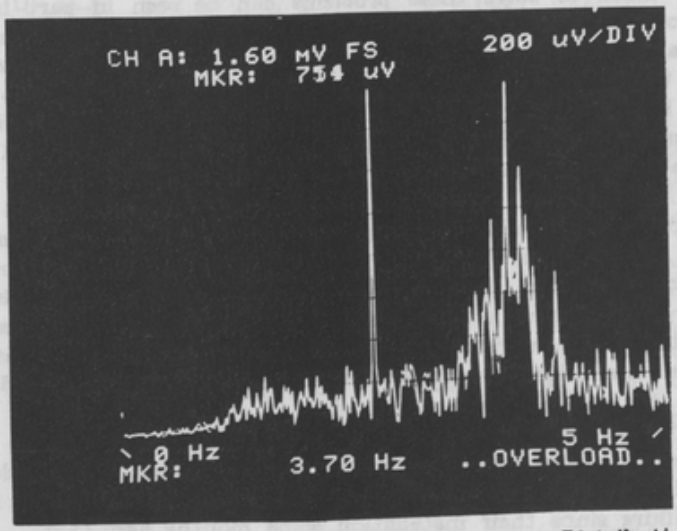

Fig. 9.4–1. High Energy Column Current 0–5 Hz Frequency Distribution.

9.5 Model 860 Sputter Source Modifications

D.J. Hodgkins and T.A. Trainor

The Model 860 is now fully commissioned and delivers intense beams of a variety of negative ions. Mass-analyzed beams include 400 μA $^{12}C^-$, 50 μA $^{28}Si^-$, 10 μA $^{7}Li^-$, 100 μA $^{63}Cu^-$, and 4μA $^{40}Ca^-$. These currents were observed through an acceptance of about 5 mrad-cm at 30 keV, corresponding to an emittance of 8 mm-mrad-MeV$^{1/2}$.

Early experience with the source indicated several problem areas. Supply of cesium vapor to the ionizer was unreliable, recovery from cesium oversupply was slow or not possible, the sputter target insulator was subject to frequent breakdown and failure by tracking, and the ionizer delivered a substantial amount of cesium beam to the target rod which was unproductive but loaded the cesium focus supply.

The measures taken to solve these problems can be seen in part in Fig. 9.5-1. The cesium feed tube (not shown) was extended, without coupling, through the source vacuum wall into an external coaxial vacuum jacket. A Cajon fitting at the end of the jacket couples the tube to the cesium reservoir. The heater was changed to two 150 W Rama rod heaters in a copper block clamped to the reservoir miniflange. Copper strips run from the block to the vacuum jacket and to the base of the reservoir, thus insuring uniform heating of the entire cesium system.

To improve recovery from cesium overshoot four large holes were milled in the cylinder surrounding the end of the target rod. This increases the pumping speed of cesium out of the ionizer region, but has not noticeably affected the relationship between cesium temperature and negative ion output. In the case of an oversupply of cesium (usually during startup) the reservoir is rapidly cooled for a short time with air. The source recovers in less than five minutes and bias voltages can be reapplied.

The original target insulator has been removed and support for the end of the target rod transferred to three macor rods located in a very well shielded region. The pathway from the ionizer region to these insulators now has a very low conductance. There has been no failure since their installation some months ago.

It was determined that cesium from the last two turns of the ionizer (nearest the target) was mainly sputtering the cone at the end of the target rod and the aluminum sample holder. These were first blocked and then removed with good result. With the target in the neutral position and a cesium current of 1-2 mA the cesium waist is located at the target and $\leq$1/2 mm diameter. With reduced cesium current this waist moves back toward the ionizer as one would expect from space charge effects.

Targets are aluminum cylinders with 3 mm dia. X 3 mm deep samples. A 1/4 mm thick lead washer is used to ensure good thermal contact with the cooled target rod.

For the 400 μA ^{12}C beam the cesium was incident at 10 keV with 1-2 mA true cesium current and ~ 10mA secondary electrons. The negative ions were accelerated across the 10 kV target potential and focussed at the final large diameter gap lens to a final energy of 30 keV. Focussing is optimum when there is little or no voltage drop across the small middle gap lens. Total source output was 1.2 mA. The 400 μA ^{12}C beam component

was ~ 1/2 the total analyzed beam, the rest being mostly higher carbon polymers. Thus, transmission through the analysis system was 67% assuming the entire source output was carbon.

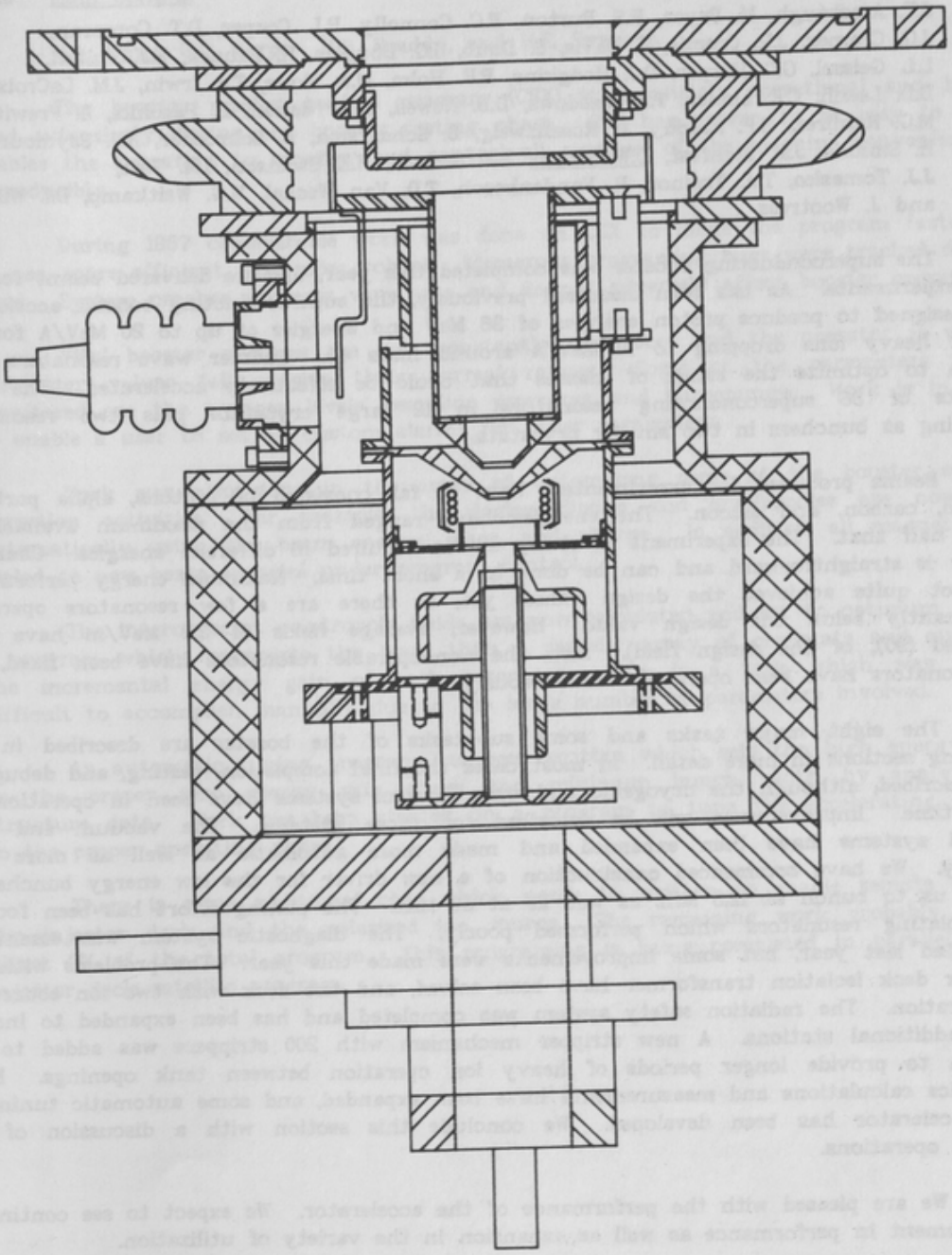

Fig. 9.5-1. Model 860 Sputter Source as modified.

10. BOOSTER LINAC PROJECT

10.1 Construction of the Superconducting Booster Accelerator

J.F. Amsbaugh, M. Bryce, R.S. Burton, R.C. Connolly, R.L. Cooper, D.T. Corcoran, J.G. Cramer, J.R. Cromie, J. Davis, S. Doub, J.G. Douglas, H. Fauska, B.J. Fulton, L.L. Geissel, G.C. Harper, D.J. Hodgkins, B.P. Holm, M.A. Howe, T.J. Irwin, J.M. LaCroix, D.D. Leach, C.E. Linder, T.A. Meadows, D.B. Newell, R.A. Nielsen, D. Paschke, L. Prewitt, M.G. Ramirez, H.P. Readdy, D. Rosenzweig, D. Schaafsma, A. Schroeder, R.J. Seymour, H. Simons, J.M. Stehfest, D.W. Storm, R.E. Stowell, H.E. Swanson, I.M. Tess, J.J. Tomasko, T.A. Trainor, R. Vandenbosch, T.D. Van Wechel, W.G. Weitkamp, D.I. Will, and J. Wootress

The superconducting booster was completed this year, and we delivered beams for the first experiments. As has been discussed previously, the superconducting booster accelerator was designed to produce proton energies of 36 MeV and energies of up to 20 MeV/A for the lighter heavy ions dropping to 10 MeV/A around mass 40. Quarter wave resonators were chosen to optimize the range of masses that could be effectively accelerated. The linac consists of 36 superconducting resonators in 12 large cryostats plus two resonators operating as bunchers in two smaller cryostats.

Beams produced for experimenters have so far consisted of protons, alpha particles, lithium, carbon, and silicon. The energies have ranged from the maximum available to about half that. The experiment involving silicon required 16 different energies. Changing energy is straightforward and can be done in a short time. Maximum energy performance has not quite achieved the design values yet, as there are a few resonators operating significantly below the design value. However, average fields of 2.8 MeV/m have been achieved (90% of the design field). Also, the non-operable resonators have been fixed, and all resonators have been operated simultaneously.

The eight major tasks and some sub-tasks of the booster are described in the following sections in more detail. In most cases the final completion, testing, and debugging are described, although the cryogenic and main control systems have been in operation for some time. Improvements will be described for those systems. The vacuum and cryo control systems have been expanded and made more automatic as well as more user friendly. We have commenced construction of a new driver for the low energy buncher to enable us to bunch at 12.5 MHz as well as at 50 MHz. The plating effort has been focused on replating resonators which performed poorly. The diagnostic system was essentially completed last year, but some improvements were made this year. The problems with the injector deck isolation transformer have been solved, and the deck with two ion sources is in operation. The radiation safety system was completed and has been expanded to include some additional stations. A new stripper mechanism with 200 strippers was added to the tandem to provide longer periods of heavy ion operation between tank openings. Beam dynamics calculations and measurements have been expanded, and some automatic tuning of the accelerator has been developed. We conclude this section with a discussion of the booster operations.

We are pleased with the performance of the accelerator. We expect to see continuing improvement in performance as well as expansion in the variety of utilization.

10.2 System Control

10.2a Main Control

M.A. Howe, G.C. Harper, H.P. Readdy, and H.E. Swanson

The booster master control program (CSX) is completely operational and has been used extensively during the booster testing phase. CSX has proven to be easy to use and enables the operators to monitor and control all systems of the machine conveniently and reproducibly.

During 1987 considerable work was done on CSX to make the program faster, easier to use, more efficient, and more robust. Numerous programing bugs were tracked down and fixed. System crashes are now very rare and do not adversely affect booster operation.

Vital booster systems are now constantly monitored and the operator is warned if parameter values fall outside their normal ranges. Some of the parameters that are monitored are the cryogen levels, beamline pressures, and turbopumps. Work is in progress to enable a user to set up custom alarms for other parameters.

Work was also done in the areas of automating some of the booster setup and operation activities. For example, the dogleg dipoles and quadrupoles are now set up automatically using the beam energy, mass, and charge. In addition all magnets can be scaled to new beam energies under program control.

The intercryostat quadrupole fields are now calculated and set to optimum values by a program which transports the beam thru a periodic array of cryostats and quads using the incremental energy gain of each resonator. This is a task which was extremely difficult to accomplish manually due to the large number of parameters involved.

An automatic tuning program has been written which sets the high energy buncher to the proper zero energy gain phase and minimum bunch width by analyzing time structure data. Work has been started on a program to tune the accelerating resonators to the proper operating phase.

There is some additional code which needs to written to enable remote control of the injector deck and the polarized ion source. The remaining work probably represents about 2% of the total program. This programing is being completed in parallel with the injector deck satellite program.

10.2b Control System for the Low Frequency Low Energy Buncher

T.D. Van Wechel

A control system has been designed and constructed for the low frequency low energy buncher (see Sec. 10.3). The new control system also replaces the present control system for the 50 MHz low energy buncher.[1] The buncher parameters are now under computer control. The system is currently being tested and will be on line soon.

Some of the concepts used in the design of the control system were based on the dual frequency buncher at Argonne.[2] The control system was divided into several functional modules installed in a modified NIM bin. A simplified explanation of each module follows.

In Fig. 10.2b–1 the outputs of the two cone probes are fed into a 180° RF signal combiner. The output of the 180° combiner is representative of the first derivative of the voltage across the grid gap. This signal contains the harmonic components f1, f2, f3 and f4. In the low frequency mode f1 is 12.5 MHz, f2 is 25 MHz, f3 is 37.5 MHz and there is no f4 component. In the 50 MHz mode f1 is 50 MHz, f2 is 100 MHz, f3 is 150 MHz and f4 is 200 MHz.

The function of the RF feedback module is to separate and provide variable attenuation, under computer control, of f1, f2, f3, and f4. The amplitude of the voltage across the grid of any frequency component fn is related to the amount of attenuation between the signal from the probe and the RF input of the fn RF control module. The master amplitude is set by a voltage controlled attenuator that provides attenuation to all of the harmonics. The signal is then amplified and split into four paths. The f1 path filters out the 12.5 MHz and 50 MHz components. The other three paths provide filtering and variable attenuation of f2, f3, and f4 with respect to f1.

A simplified schematic of an RF controller module is shown in Fig. 10.2b–2. Each controller has three inputs and an RF output. The RF input fn, from the RF feedback module, is hetrodyned with a local oscillator signal by a double balanced mixer, producing an intermediate frequency of 50 MHz. The 50 MHz signal is filtered and amplified with a portion being sampled and rectified to produce a d.c. voltage proportional to the amplitude of fn. This voltage is used in a control loop to set the amplitude at the input of the RF controller at −5 dBm. The amplitude of the voltage across the grid gap is changed by varying the attenuation in the RF feedback module as explained above. The phase of the intermediate frequency is compared to the phase reference signal by a double balanced mixer providing a feedback signal for the phase control loop.

A portion of the phase reference signal also goes through a complex phasor modulator(CPM), which serves as the regulating element for both the amplitude and phase control loops. The amplitude error voltage drives the I(in phase) control input, while the phase error voltage drives the Q(quadrature phase) control input of the CPM. The output of the CPM is hetrodyned with the local oscillator signal producing the sum and difference frequencies. One of these is fn which is filtered and amplified to drive the resonant structure of the buncher.

The Phase Reference module provides the 50 MHz phase reference signals to each RF control module. CPMs are used to provide computer settable phase shifts. The phase of the signal from the resonant phase detector is compared to the master phase reference to

provide phase lock of the buncher to the linac. The phases of the f2, f3, and f4 phase references are varied with respect to the master phase.

The local oscillator generator provides the local oscillator frequencies required by the RF control modules. The local oscillator frequencies are phase coherent with respect to the buncher clock. They are generated by hetrodyne and frequency division techniques.

1. Nuclear Physics Lab Annual Report, University of Washington (1985) p. 89.
2. K. Johnson, Dual Frequency Buncher, Argonne Bldg. 211 Design Note

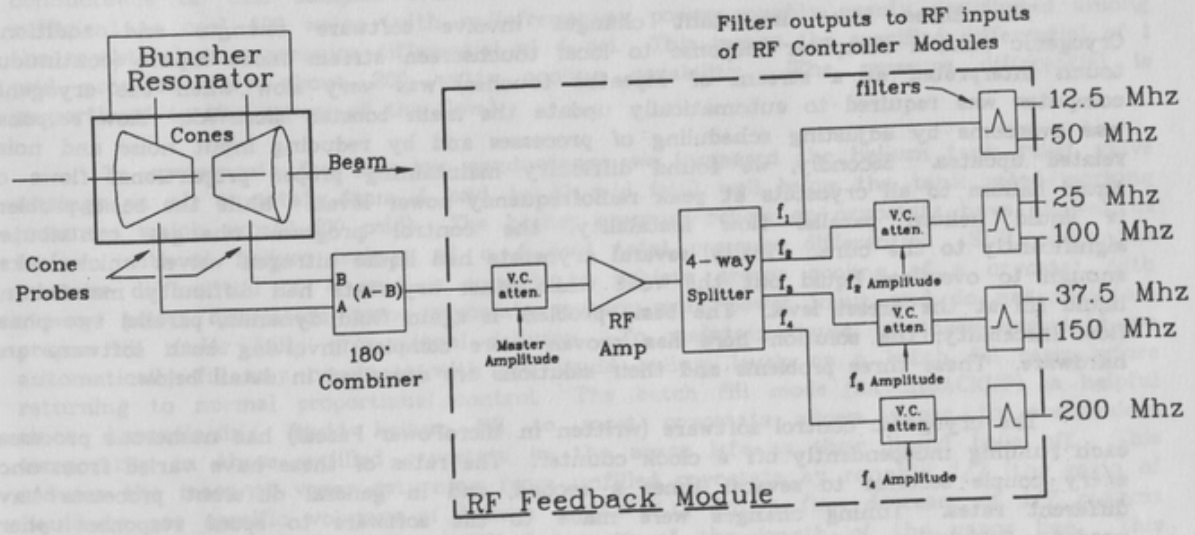

Fig. 10.2b-1.

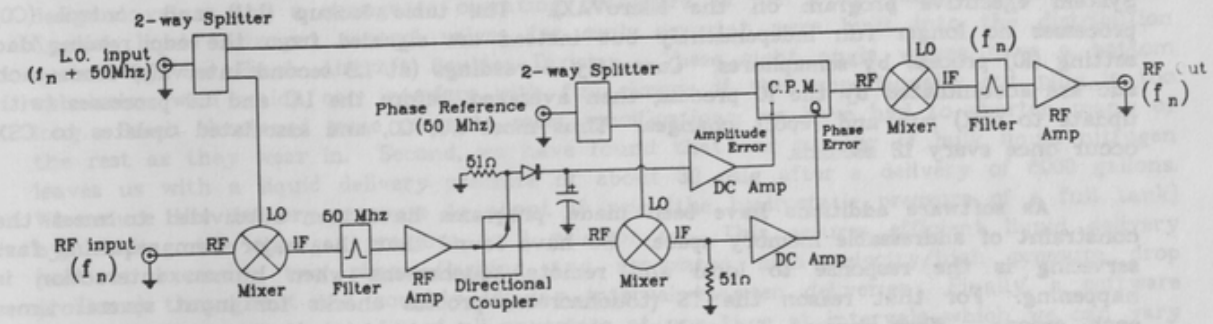

Fig. 10.2b-2. RF Controller Module.

10.2c Cryogenic Control

M.A. Howe, H.P. Readdy, D. Schaafsma, and D.I. Will

During the past year we have made several changes in the cryogenic control computer system. As reported last year[1], we installed an uninterruptible power supply on the control computer itself to minimize frequent crashes apparently caused by power line glitches. This addition has been highly successful; we have had only one unexplained computer crash in the last year.

The three most important changes involve software changes and additions. Cryogenic control computer response to local touchscreen stream mode inputs (continuous touch interpreted as a stream of repeated touches) was very slow when the cryogenic computer was required to automatically update the main booster MicroVAX. Slow response was overcome by adjusting scheduling of processes and by reducing input noise and noise related updates. Secondly, we found difficulty maintaining proper proportional flows of liquid helium to all cryostats at peak radiofrequency power levels. While the basic problem is liquid helium parallel flow instability, the control program changes contributed significantly to the cure. Finally, several cryostats had liquid nitrogen valves which leaked enough to overflow liquid out the vent while other cryostats had difficulty maintaining liquid fill at the preset level. The basic problem is again fluid dynamic, parallel two-phase flow instability; the solution here has proven more complex involving both software and hardware. These three problems and their solutions are described in detail below.

The cryogenic control software (written in MicroPower Pascal) has numerous processes each running independently off a clock counter. The rates of these have varied from once every couple seconds to several times a second, and in general different processes have different rates. Tuning changes were made to the software to speed responses where needed. Scheduling and priorities of the concurrently running processes were adjusted to minimize time taken in context switching and to minimize the possibility of stack overflows. Response to input from the local touchscreen and to input from the MicroVAX touchscreen, which had been slow whenever auto-update to the MicroVAX was switched on, was improved after reducing noise from some of the adc channels and averaging a number of readings from each channel before reporting a changed condition to CSX (the Control System eXecutive program on the MicroVAX). The table lookup (LU) and control (CO) processes no longer run independently but instead are signaled from the adc reading/dac setting (IO) process by semaphores. Currently 8 readings (at 1.5 second intervals) from each adc are accumulated by the IO process, then averaged, before the LU and CO processes (with update to CSX) run and report changes. Thus most LU, CO, and associated updates to CSX occur once every 12 seconds.

As software additions have been made, programs have been subdivided to meet the constraint of addressable memory space. We have found that the major item requiring fast servicing is the response to local and remote touchsreens when human interaction is happening. For that reason the TS (touchscreen) process checks for input several times each second. When human interaction occurs at the local touchscreen, TS signals the IO/LU/CO sequence. Any changes required are made immediately (using data from the past twelve seconds if needed) to provide rapid feedback to the operator. Similarly, when control setpoints are changed remotely at the MicroVAX touchscreen, the cryogenic computer MicroVAX (UV) process (which waits for input over the serial line) signals the IO/LU/CO

sequence immediately with a semaphore, thus providing rapid response to the remote operator.

The liquid helium parallel flow instability mentioned above occurs when the booster operates at full power, roughly 400–450 watts. We specified a distribution system capable of providing sufficient flow to cool 400 watts with 1 psi pressure differential. Preshipment acceptance testing of the system allowed us to insist on correction of the worst heat leaks and flow constrictions. Since testing was done on three separate sections we had only an estimate of helium mass conductance prior to installation at our facility. Helium flow conductance of this complex branched distribution system has been determined to be sufficient to cool 400 watts (with radiofrequency power roughly evenly distributed among the cryostats) at a pressure differential of 4 psi. This means the specified differential of 1 psid provides only about 200 watts cooling capability. (The pressure differential is proportional to the square of the flow.)

To compensate for this low conductance we increased the helium tank relief valve settings on all cryostats from 4 psid to 10 psid (still well below the tank rated working pressures which exceed 100 psid). The higher pressure reliefs on cryostats have allowed us to run without helium leakage at a 4 psid total pressure differential. Still, while the pressure differential of 4 psid is enough to achieve proper cooling of a cryostat with average power dissipation, some cryostats require more power input and do not maintain proper fill under fully proportional delivery. To maintain liquid in these cryostats we automatically fill any cryostats with low liquid helium levels on a batch fill basis before returning to normal proportional control. The batch fill mode (BATCHBACKUP) is helpful since discontinuing liquid helium fill to most cryostats allows vapor to accumulate temporarily in these unfilled cryostats in the space left as their liquid boils off. This reduces the mass of vapor returning from unfilled cryostats by roughly 1/7 (the ratio of liquid to gas specific volumes of helium at 4.3° K.) But a flow decrease of 1/7 reduces pressure drops by nearly 2/7 or 30% for most of the length of the vapor line. This pressure reduction in the vapor line is especially helpful since vapor line pressure differential dominates the total pressure drop. Together these two modifications have permitted us to operate rather comfortably despite the distribution system's high pressure drop.

Resolution of our liquid nitrogen fill difficulties has required repair of poorly designed valves and a change in operating procedure as well a software modification. Our Cryolab liquid nitrogen control valves for each cryostat were built into the distribution system by the Beech Aircraft Boulder Division. These right angle valves have a bottom tubulation weld which can interfere with full closure if the proportionally cut plug is too long. Beech shortened some plugs to meet specifications; we have had to shorten many of the rest as they wear in. Second, we have found that our supplier of bulk liquid nitrogen leaves us with a liquid delivery pressure of about 30 psig after a delivery of 6000 gallons. We reduce the delivery pressure to about 10 psig (the hydrostatic pressure of a full tank) by bleeding the top gas pressure to 1 psig or so. This assures efficient liquid delivery (without excessive two phase flashing and associated high velocity/high pressure drop problems) throughout the roughly 14 day interval between deliveries. Finally, a software modification permits batch fill of all cryostats at one time at intervals which we can vary from six to eighteen hours. High mass flow rates during batch fill assure high quality liquid delivery. Vanishingly small mass flow rates between batchfillings assure that largely gas is delivered to any leaky valve, reducing overflow problems further. We are now achieving good liquid delivery and only occasionally suffering liquid nitrogen overflow.

1. Nuclear Physics Laboratory Annual Report, University of Washington (1987) p. 64.

10.3 A 12.4 MHz Driver for the Low Energy Buncher

D. Rosenzweig and D.W. Storm

The present low energy buncher produces bunches for the linac at a 49.6 MHz repetition rate. The 20 nsec period is too short for many time of flight experiments. It is possible to chop the beam, but the existing chopper is sub-marginal for operation where one bunch is passed but neighboring bunches are completely suppressed. Also, if repetition periods in excess of 100 nsec are required, most of the beam must be thrown away by the chopper. Thus we are in the process of building a driver which will operate the same gridded buncher at a 12.4 MHz repetition rate. Then the pulse period will be 80 nsec, and multiples of this figure can be obtained satisfactorily with the present chopper.

We designed the driver following the work at Argonne National Laboratory.[1] For operation at 12.4 MHz, we will replace the present four-harmonic resonant line driver with a unit built with capacitors and coils. This unit will permit combination of three harmonics. We have built the box with connections to the buncher itself and have assembled and tuned the coils and capacitors to produce resonances at the desired frequencies of 12.4, 24.8, and 37.2 MHz.

We have also built a new electronic unit to permit computer control of either the 49.6 MHz or 12.4 MHz drivers. This unit was described in the previous section.

1. K. Johnson, Dual Frequency Buncher, Argonne Bldg. 211 Design Note.

****

10.4 Resonator Plating

M.R. Bryce, D.T. Corcoran, and T.A. Meadows

Early in 1987, as noted in last year's report,[1] the final resonators for completing the linac were plated. Also, four low-beta and two high-beta resonators were replated to upgrade their quality. The plating operation was put on hold while other linac systems were completed; however, there were a few experimental platings. Unfortunately, none has produced a consistently superior surface.

1. Nuclear Physics Laboratory Annual Report, University of Washington (1987) p. 66.

10.5 Beam Diagnostics

R.C. Connolly, H. Fauska, M.A. Howe, T.J. Irwin, D.D. Leach, H.P. Readdy, and W.G. Weitkamp

The diagnostic instrumentation of the booster provides the operator with information on the beam position, profile, energy, current, time structure and transverse emittance. The beam profile monitors, slits, apertures, solid state detector energy monitors, Faraday cups, microchannel-plate time structure monitors, emittance monitor and the diagnostics control system have been described previously[1]. The beam bunch phase detector[2] has not previously been described; a brief description follows.

The low energy buncher produces 0.8–1.0 ns bunches which are compressed to about 0.2 ns by the high energy buncher. The high energy buncher converts time spread into energy spread linearly for particles arriving within about 1 ns of the bunch center. Thus, phase walk can increase the energy–time phase space of the linac beam or, in the worst case, cause beam to be lost from the acceptance of the linac. Because of changes in the accelerating fields in the tandem (due, for example, to the terminal regulator compensating for the belt ripple), or because of small drifts in ion source energies, the time of flight of the bunches from the low energy buncher to the high energy buncher can vary by up to a few nanoseconds.

In order to eliminate this variation, the phase of the low energy buncher is controlled by comparing the signal from a phase detector near the high energy buncher to the clock signal. The phase detector is a helically loaded resonant (at 50 MHz) cavity. It has an amplifier with automatic gain control to produce a fixed amplitude signal for phase locking. When a cavity is driven by a fixed frequency there is a phase shift proportional to the difference between driving and resonant frequency (provided the difference is smaller than the resonator bandwidth). Therefore, it is important to avoid drift in the resonant frequency of the detector. In early runs, we found phase shifts of the signal from the detector of up to 20 degrees (at 150 MHz). The temperature coefficient of the system was measured to be 9° per $^{\circ}$C (at 150 MHz). Also, since most of the volume of the resonator contains air, we estimated the phase shift with relative humidity to be 6° per 10% (at 150 MHz). To eliminate these shifts, we stabilized the temperature of the cavity and the relative humidity of the gas in the cavity by flowing heated dry nitrogen through it and regulating the temperature of the exhaust gas.

After the regulation system was in place, we tested for drifts over a four day period and found that the beam phase stayed within 1° (150 MHz) of the set value.

All of the diagnostic instrumentation is being used routinely except for the emittance monitor. This device was purchased from Danphysik. The sensors have been installed on a beam line, all the software has been written and debugged, but use of the monitor has been delayed because of a wiring error in the control circuitry. We expect to solve this problem in the near future.

1. Nuclear Physics Laboratory Annual Report, University of Washington (1987) p. 68.
2. R.C. Connolly and D.D. Leach, paper in preparation.

10.6 Injector Platform Development

G.M. Harper, D.J. Hodgkins, and T.A. Trainor

The injector platform was completed in mid 1987 and delivered 10 μA of ^{7}Li at 200 keV for the first linac experimental run in September.

The second 300 kV isolation transformer supplied by Hipotronics failed twice, the first failure due to particulate matter in the oil, the second due to a broken shield wire. These problems were cured and the unit was tested extensively at 330 kV. The basic design seems to be satisfactory, but the quality assurance program was inadequate in our experience.

The model 860 sputter ion source integration was completed in August. Details of various modifications to this source to enhance performance are given in Sec. 9.4. The beam optics from source to platform image slits are a source gap lens, horizontal and vertical magnetic steerers, an einzel lens, an electrostatic quadrupole doublet, a 45° switch magnet, a 90° magnet and an einzel lens. The quadrupole lens compensates for the astigmatic effect of the two bending magnets.

Various tests of the platform performance with regard to producing well-bunched beams for the linac were performed. Details are described in Sec. 10.7. Beams of ^{1}H, ^{16}O and ^{63}Cu were accelerated and bunch widths measured for single-harmonic low-energy bunching as functions of the platform elevation potential as well as various source parameters. In each case the bunch width fell as the platform voltage increased until a lower width limit was reached. This lower limit occurred at ~ 280 ps and 50 keV for ^{1}H, 330 ps and 150 keV for ^{16}O and 800 ps and 230 keV for ^{63}Cu. The bunch widths were measured near the entrance to the linac by a multichannel plate detector time structure monitor.

10.7 Linac Beam Longitudinal Phase Space Measurements

G.C. Harper, D.D. Leach, D. Rosenzweig, and T. A. Trainor

The area required in longitudinal (energy–time) phase space to represent a particle beam sets limits on the achievable energy or time resolution. There are several contributions to this area and it is desirable to determine each one and minimize it to optimize linac performance. We are in the process of carrying out this program.

The low energy harmonic buncher was calibrated. Using beams from ^{1}H to ^{63}Cu at various injector energies, field amplitudes which minimized the bunch width at the linac entrance were determined for each of the 50, 100 and 150 MHz harmonics applied singly. A coefficient was then extracted for each harmonic which could be used to scale as $E^{3/2}/m^{1/2}$

In addition, optimum bunching with three harmonics superimposed was determined for a variety of ions and energies. It was determined that scaling the optimum single harmonic amplitudes by 1.6, 1.0 and 0.6 for 50, 100 and 150 MHz, respectively, results in optimum 3–harmonic bunching.

The quality of the injector platform beam was examined by correlating ion source energy homogeneities measured with the platform magnetic analyzer with bunch quality at the linac entrance, and determining bunch quality as a function of platform voltage. These results are discussed in Sec. 10.6. It was found that the beam energy spread was typically 10–20 eV, and that for all ions up to ^{63}Cu 200 kV on the platform was more than sufficient to reduce the bunch widths to minimum values determined by noise sources other than the platform.

Best bunch widths at the linac entrance produced by the low energy buncher using a single harmonic varied from 280 ps for ^{1}H to 800 ps for ^{63}Cu. However, there have been significant periods when the minimum widths are almost twice as high. The change from one mode to another is quite sharp, and intervals between changes may be minutes or days. The source of this fluctuation has not been determined. However, the quality of the tandem regulation, which has been quite poor (Sect. 9.4), was recently improved greatly by a charging belt change. This will provide more stable conditions under which to study buncher performance.

We have also begun development of a detector system to determine the linac correlated energy–time phase space in a target chamber. Various combinations of parallel plate avalanche counters, a multichannel plate and silicon detectors were tried. Time resolutions near 150 ps were achieved. This is good enough at present to pursue linac phase space measurements.

10.8 Cryogenic Supplies, Maintenance and Operating Experience

D.I. Will and J.A. Wootress

The major supplies used are bulk liquid nitrogen and bulk helium gas, both with impurities lower than 10 ppm. Our helium gas use was 79,430 scf total, used largely for purging and deriming. Our liquid nitrogen consumption averaged 1560 liters/day allotted as follows:

Item	Consumption
Quiescent	
All 14 cryostats	1000 liters/day
Distribution system	200 liters/day
Tank loss	50 liters/day
Exposed lines (improvements planned)	≈ 200 liters/day
Gas use, variable	≈ 100 liters/day
Subtotal	≈ 1550 liters/day
Active	
Power dissipated, 38 coupler intercepts	200 liters/day
Refrigerator precool (not normally used)	(≈ 700 liters/day)
Totals without refrigerator precool	≈ 1750 liters/day

Most routine maintenance is directed at rotating machinery on our helium refrigerator and its compressors. The distribution system also requires minor service.

Item	Hours ON	Major Service	Times Performed
Refrigerator Cold Box			
Top expander	≈ 6500 @	main seals/wristpin bearings	4
	≈ 130 rpm	crankpin bearings	2
		valve seals	1
Middle expander	≈ 7000 @	main seals	3
	≈ 130 rpm	wrist & crankpin bearings	1
Wet expander	≈ 2000 @	none, except lube	
	≈ 70 rpm		
RS Compressors:			
RS 1	8685	replace charcoal	
RS 2	8487	replace charcoal	1
RS 3	7844	replace charcoal	1
Distribution System		He into vacuum to warm and derime	4

The cold box was in use (with at least one expansion engine turning and at least one RS compressor on) 99% of 1987. Note that we change compressor charcoal less frequently than specified by Koch. In the future we plan to replace it once a year. This is in line with practice at Argonne's Atlas according to Jack Nixon. Our only major item of incidental maintenance was the replacement of the top expansion engine flywheel once in 1987 due to bad bearings. We have since rebuilt the one removed as a spare.

When we began purchasing this cryogenic system four years ago we were faced with three important choices. The first major unknown was our cooling power requirement. The second was between turbine and reciprocating expansion engines. Finally, we insisted on a distribution system of modular design with O-ring sealed warm joints and an active vacuum system despite outside advice to adopt an all-welded system. We are now quite pleased with the equipment we received and have found it to work well. In the following paragraphs, we describe the three choices and their consequences.

As described in more detail elsewhere in this report[1], we estimated our minimum cooling needs at 200 watts (from liquid helium vaporization at 4.3° K), we specified major equipment for 400 watts, we offered bid preference to any refrigerator capable of 600 watts, and we offered further bid preference for refrigerator expansion capability beyond 600 watts. The refrigerator we received from Koch Process Systems is rated at 500 watts without liquid nitrogen assist and at 600 watts with liquid nitrogen assist. It can be expanded to 1000 watts by adding two compressors and lengthening the top engine stroke. Excess cooling ability allows operation of the refrigerator in a region of high inherent process stability. Tests with heat input exceeding cooling capacity (during which dewar level drops) have demonstrated process instability empirically; the operator must intervene hourly to maintain constant heat exchanger temperatures and engine speeds. In sharp contrast, whenever cooling exceeds heating by even a small amount, we find the system very stable. It has run for a week at a time without intervention. Since our cooling requirements are 400-450 watts (roughly double the original estimate) and since we wish to run without liquid nitrogen assist, our refrigerator with 500 watts capability is ideal. The potential for expansion remains as a safety factor. Our distribution system, on the other hand proved to have somewhat low helium flow conductance (below specification) once it was assembled here (despite testing in sections at the manufacturer.) However, conservative specifications for pressure drop have permitted comfortable operations at 450 watts with increased pressure differential (4 psig) and active computer compensation for parallel flow instability.[1] Finally, excess refrigeration allows us to operate the accelerator for many experiments even with one engine or compressor under repair.

Our second choice, for piston rather than turbine expanders, has produced no surprises. We knew when we chose pistons that our maintenance personnel requirements would probably be higher. We believe that is so, though we have no turbine experience ourselves for good comparison. On the other hand we have found that a good reciprocating engine (aircraft) mechanic plus a cryogenics engineer can repair practically any part of a piston expander Koch machine, often at modest expense compared to new Koch parts and certainly much cheaper than the price of a new turbine. Again we are definitely pleased to know that this machine can be maintained in house with local parts if necessary.

Our final choice was for a modular distribution system with an active vacuum system using conflat seals for cold joints and O-ring seals for warm ones. This system has definite advantages for us over an all-welded system. Rapid vacuum pumpdown permits easy and reliable warmup for deriming. Modularity coupled with O-ring sealed valve pots makes leak tracing relatively straight forward; we can isolate modules to localize the leak and then remove the valve pot to pinpoint it. Modularity also allows expanding the distribution system module by module (though we would need to enlarge the vapor line in some existing modules to do so.) In summary, we feel that these three choices were, without doubt, the correct ones.

1. Section 10.2c, this report.

10.9 Radiation Safety System

H. Fauska, J.M. LaCroix, C.E. Linder, J.M. Stehfest, and W.G. Weitkamp

We have enlarged the radiation safety system at the accelerator to accommodate booster operations. The sensors for this system consist of Bonner spheres for neutrons and proportional counters for gamma rays. The sensors produce audible clicks at the rate of 1 click/sec = 1 mrem/hr to provide first level warning of radiation danger. The sensors also have relay contacts which close when the dose equivalent exceeds 100 mrem/hr, the "high radiation" level.

The accelerator area is divided into 8 zones, each of which can be isolated from the rest of the laboratory by shielding doors or barriers. A programmable controller monitors the "high radiation" contacts on all the sensors and the status of all the shielding doors and barriers. When a sensor in one of the zones shows high radiation, the programmable controller shuts off the beam entering the zone unless all doors and barriers allowing entry into the zone are closed. The linac resonators produce X rays regardless of the presence of beam so if a monitor in a resonator zone detects high radiation and the area is accessible, a loud whistle alerts the operator to the potential hazard.

We have also installed a Bonner sphere outside the building at the point where we expect the highest neutron field to be produced. If the dose equivalent exceeds 0.2 mrem/hr at this point, the beam will be turned off.

The status of all radiation sensors, shielding doors and barrier are displayed on a board in the control room. Radiation levels are displayed quantitatively by LED bar indicators which turn red when a high radiation level is present.

The system in the booster area is installed and functioning. We have had a few minor problems weatherproofing the outside monitor, calibrating the LED bar indicators and adjusting the volume on the clickers. We are now working on refurbishing the radiation safety system of the tandem, which dates back to 1968. We are installing new gamma monitors to replace aging home-built monitors and modifying the Bonner spheres in the vicinity of the tandem to be compatible with the new control system.

10.10 Tandem Foil Stripper

D.T. Corcoran, C.E. Linder, and W.G. Weitkamp

Use of the superconducting booster with high intensity heavy ion beams is expected to increase demand for stripper foils in the terminal of the tandem. Consequently, we have installed a 200-foil-capacity holder to replace the previous 38-foil-capacity holder. The new foil stripper has been in operation for about 3 months.

The design criteria for this installation were as follows: 1. Either a foil or the gas stripper tube may be inserted into the beam. 2. The foils will be biased up to 8 kV for the "terminal ripple remover."[1] 3. Transverse electric fields associated with biassing the foil must be minimized so the beam doesn't jitter sideways. 4. The beam may be steered both up-down and left-right.

We chose an NEC Model FS-6 foil changer as the basis of our design. This device holds 200 foils on inserts which are attached to a metal band by spring clips. The mechanism is mounted on an insulating bushing so the foils can be biased.

Figure 10.10-1 shows the position of the foil stripper with respect to the stripper box and the high energy beam tube. In order to fit the foil changer into the terminal without removing the gas stripper tube, it is necessary to mount it in the horizontal plane with the axis of the mechanism 60° to the axis of the beam. A system of shields insures that the beam encounters minimal transverse electric fields. The gas stripper tube is mounted on a hinge; a push rod moves it in and out of the beam. The gas stripper tube is connected electrically to the foil holder (and the terminal ripple remover) when the tube is in the beam. It is shorted to the terminal when the tube is out of the beam.

The foil stripper mechanism is driven by a lucite rod from the tank base. A proximity sensor counts rotations of the rod; a Veeder-Root 7910 up-down counter displays the foil number on the tandem control console.

In this installation, vertical steering is provided by 11 cm long plates 2.1 cm apart and horizontal steering by plates 5 cm long 1.7 cm apart. The plates are just downstream from the stripper foil. The plates have 10 kV power supplies connected so the plates are all at -5 kV when there is no steering.

To speed the floating of stripper foils, a semiautomatic stripper foil floater was built. A small motor drives a threaded rod which moves the glass slide holding the foils slowly and steadily into water, stopping at a preset point. This device minimizes foil breakage and greatly reduces the labor necessary to mount foils.

1. G.W. Roth and W.G. Weitkamp, Nucl. Instrum. Meth. 115, 501 (1974).

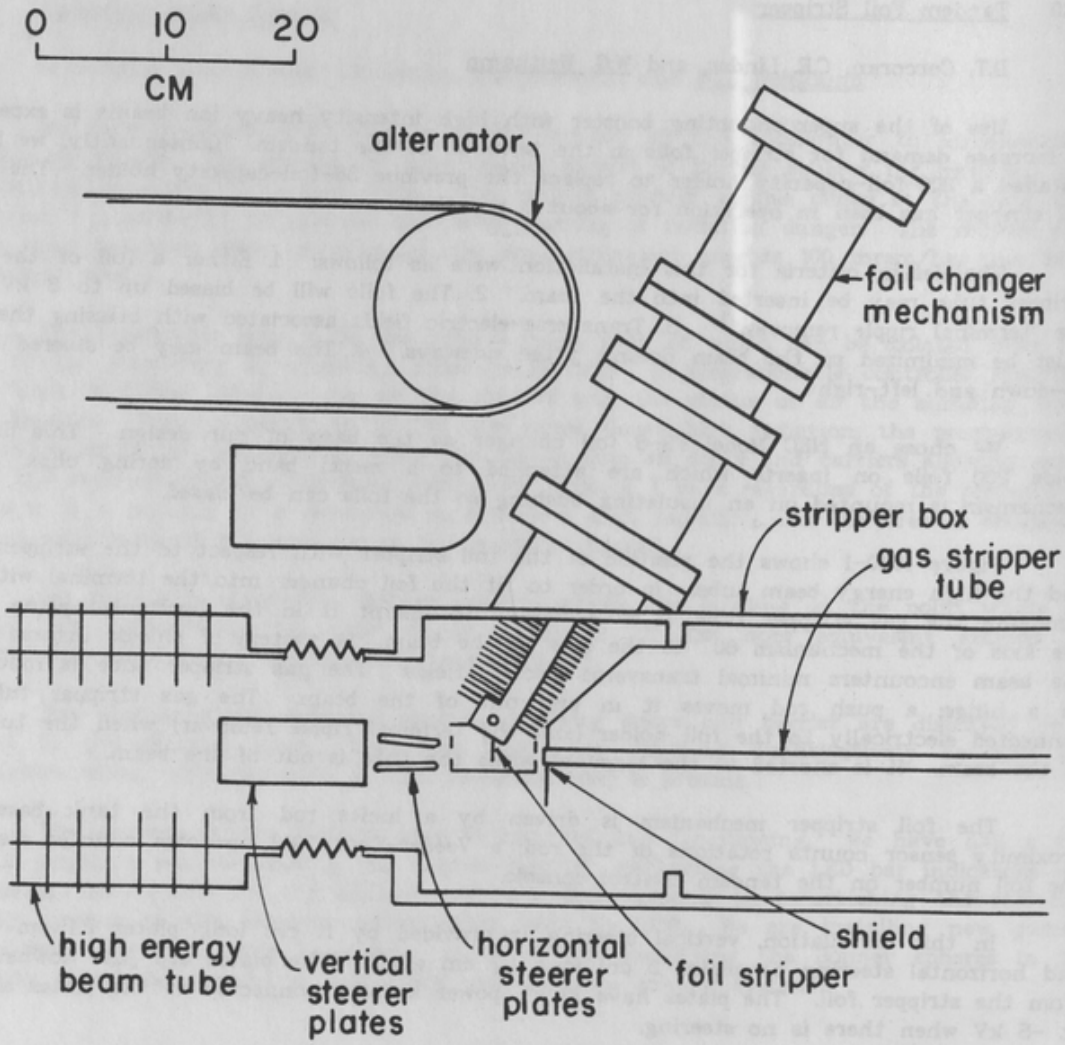

Fig. 10.10–1. Top view of the layout of the foil stripper installation in the tandem terminal. The beam travels from right to left. The gas stripper tube is shown in the beam; it can be remotely removed from the beam.

10.11 Completion of Vacuum System Installation

J.F. Amsbaugh

The vacuum system for the linac booster has been described elsewhere[1], and last year's report[2] described the last installations to be made. Early in the year we completed this upgrade of the high energy tandem beamlines, and we installed turbomolecular pump error status signals to the computer system. The turbomolecular pump controllers have an error LED which flashes at 4 different rates to indicate the error state. We modified the controller to send this signal to the computer over an optically isolated line. Software was written and added to display these error conditions.

The control system uses a flexible new method which facilitates runtime control changes and which is described in more detail in Sec. 12.7. Control system instructions are numbers read from data files into memory as linked lists organized into events and tasks with associated actions and their constraints. In adapting this method to the specific needs of the vacuum system, control sequences have been defined using this format. Much effort has been concentrated on the further development of the constraint files which control the system. The types of constraints available have been expanded as experience has demanded and now include: ADC level, difference, and rate of change, input and output status, timers and internal logic flags. These constraints are linked to outputs and the outputs are organized into events and tasks. Events control discrete sections of the vacuum system, e.g. the pumping station for cryostats #1 and #2. A task is a list of events running sequentially. Initially, rudimentary events were written to protect the vacuum system from simple failures, such as power failures, pumps overheating, and so forth, and these were combined into one of only two available tasks. The other original task simply bypassed all protection. Now we have a number of tasks. For example, vacuum station startup sequences have been defined as separate tasks, with automatic return to a main control task when complete.

In the last year, as more operational experience was gained, an important change was made to the program's operation. Previously, a key switch bypassed all constraints to handle special cases, e.g. pump down from atmospheric pressure. The key now runs a certain task depending upon which of the touch screen displays is being shown. This task runs a special event (bypass) for the displayed section and runs the normal events for the rest. This affords better interlock protection for the entire system.

1. John F. Amsbaugh, Twentieth Symposium of Northeastern Accelerator Personnel, edited by E.D. Berners, U. Garg, and C.P. Browne (University of Notre Dame, South Bend, IL, 1986), p. 349
2. Nuclear Physics Laboratory Annual Report, University of Washington (1987) p. 67.

10.12 Beam Dynamics

D.W. Storm

During the first tests of the linac last year, most of the adjusting of focusing elements was done empirically, even though fairly extensive beam dynamics calculations had been done. These calculations had been used successfully to produce an achromatic focus through the dogleg system, but for the linac itself the connection between the calculations and reality was fairly ephemeral. Since the resonators in each cryostat combined with the following quadrupole doublet form a repeating periodic structure (in the language of synchrotron structures[1], a cryostat and quadrupole can be considered a unit cell), it had always been planned that the beam should be focused in a periodic manner. That is, the combination of resonator defocusing and quadrupole focusing should produce a net focusing pattern which was approximately repeated from one cryostat–quadrupole combination to the next. The repetition can only be approximate, since the defocusing of the resonators is a consequence of the acceleration and phase focusing and depends on the resonator fields as well as on the beam energy. Thus it is not an independent parameter. However, for given resonator settings, the quadrupoles can be set to make the net focusing follow a similar pattern from one unit cell to the next.

We performed some rather detailed studies of this situation for the booster linac, and produced an internal report on the subject[2]. The conclusion of this work was that focusing such that each unit cell produces about a 90 degree rotation of the beam phase elipse will produce a beam of reasonable size everywhere throughout the straight section of the linac, provided that the beam is focused vertically and horizontally to a waist in an appropriate place in the first unit cell. The beam remains stable under variations in the focusing strength. The appropriate position of this waist is different for the horizontal and vertical focusing. The optimum relation between size and divergence (the eccentricity of the phase elipse) is determined by these calculations (and is quite similar for both horizontal and vertical focusing). The quadrupoles were designed to be able to produce this 90 degree rotation. Values for the focusing of the two quadrupole doublets between the dogleg and the first accelerating cryostat were found which will produce the desired waists in that cryostat while still producing a waist near the high energy buncher.

A computer program (QUADCALC) has been written which computes the quadrupole settings given the resonator fields. Furthermore, it can calculate the resonator fields from the settings of the bending magnet after the appropriate section of the linac. This program is used during the tune up phase of the linac when resonators are turned on and phased sequentially. The program is interfaced to the control system so that it actually sets the quadrupole currents to provide the desired fields. Modest adjustments to the two quadrupole doublets preceeding the linac are then made to optimize transmission through the south row. The final doublet in the south row is adjusted to optimize transmission through the north row.

Additional studies are being made of the focusing elements following the linac, in order to transport the beam around the last bending magnet, through the rebuncher, and into the switching magnet. At present we are experiencing some beam losses here and need to understand this system better.

1. E.D. Courant and H.S. Snyder, Annals of Physics 3, 1 (1958).
2. D.W. Storm, January 1988.

10.13 Linac Operation

J.F. Amsbaugh, R.C. Connolly, G.C. Harper, M.A. Howe, D.W. Storm, D.I. Will, and J.A. Wootress

This year saw the completion of the construction of the linac and the beginning of regular operation. We inaugurated the experimental program with a one week run in September, during which an 87 MeV Li beam was provided. The next run was in December, following a period when the new stripper was installed in the tandem. During this run proton and alpha particles of 32 and 59 MeV were provided. After December we repaired the three low beta resonators which had broken components (tuner, coupler, and rf sample cable). During March we provided a 120 MeV carbon beam (using the low beta and only 3 high beta resonators, as this gave the desired energy), followed by Si beams of 16 different energies from 145 to 109 MeV. In this case we used no high beta resonators and at most 18 low beta resonators to provide the desired energy. Also in March we provided a 60 MeV alpha particle beam. The three different experiments done during March involved continuous linac operation. The 16 energy changes made during the Si run supported our experience during practice runs that substantial energy changes can be made in times of order 30 min, while small changes can be made in a few minutes.

Each time we turn on the linac, we find that our previous experience helps with the tuning. At first turning on and phasing resonators was a tedious task. Now, using the computed values for the quadrupole magnets, we find that turning on and phasing the entire south row, for example, takes a little over an hour. The procedure involved starting with the beam centered on the slits of the 180 degree turn. Then the next resonator is turned on and the phase is found at which there is no energy gain, and at which the energy increases with increasing phase shift between the resonator and clock. The sign of this phase is defined such that this is the bunching phase. Then the phase is set to −70 degrees from the bunching phase, to give the 20 degree operating point. The magnet is reset to center the beam in the slits, and from the two magnet settings the energy gain in the resonator is determined.

Additional time is required for tuning for optimum transmission. This time depends critically on the stability of the tandem and of the ion sources, and when the beam going into the linac is stable, initial tuning requires a few hours. We are still not satisfied with the transmission of the beam through the linac. Some resonators are observed to steer the beam, indicating either misalignment or asymmetry in the resonator construction. This issue will be studied further.

During two of the March runs, the chopper was used to increase the time between beam bursts. As this chopper was designed to be used with the 30 keV beams bunched by the old 5 MHz buncher, it is somewhat surprising that it can select one bunch out of a group with a 50 MHz repetition rate. In fact, it cannot do this job perfectly, but we find that the neighboring bunches can be reduced to about 5% of the desired one, and the next ones essentially eliminated. When the 12.5 MHz buncher is completed, the present chopper should be able to further increase the period between beam bursts when this is necessary.

During our initial operations, we found that most of the linac components are reliable. The refrigeration system has performed well, although upon occasion it has gotten out of adjustment. Some quadrupole supplies and rf amplifiers have overheated, due to the high density of components in the satellite stations. Improved air flow has solved these

problems. Some of the resonator controllers have gotten noisy, and some cross-talk between resonators gave a problem. The latter problem was solved by replacing the RG-58 and RG-8 cables with double shielded cables. The former required repair or shielding of the offending units. The vacuum system has performed well.

Our present operating strategy involves having four of the most experienced linac physicists to tune and monitor the linac operation. Two people are involved in tuneup and one is present during routine operation. This is an expensive mode which we do not plan to perpetuate as operation becomes more routine. At present, however, tune-up is an opportunity for us to learn more about how the linac performs and to think of ways to improve the performance. Routine operation requires less attention, but still gives an opportunity to develop a better "feel" for running the machine.

11. INSTRUMENTATION

11.1 Electrostatic Deflector for Studying Spin Distributions at Near-Barrier Energies

A. Charlop, A. Garcia, S. Gil, D.D. Leach, S.J. Luke, and R. Vandenbosch.

The construction of an electrostatic deflector, discussed in last year's Annual Report,[1] has been completed and successfully tested. This deflector, when used in conjunction with several NaI detectors and a Breskin counter,[2] allows us to measure γ-ray multiplicities (M_γ). The Breskin counter, in conjunction with a time signal from the pulsed beam, provides us with the position and time of flight (TOF) of the particles; this information enables us to separate the fusion products from the elastic and other direct reaction products. The ratio of these residues in coincidence with the NaI detectors to the residues singles yields M_γ. Since fusion products are strongly peaked at 0^0 degree, a large detection efficiency can be achieved with this device if it is possible to separate the beam particles from the residues.

In a recent preliminary test we have been able to successfully separate the elastic particles from the fusion residues in the reactions $^{16}O+^{122}Sn$ and $^{16}O+^{154}Sm$ at bombarding energies near the Coulomb barrier. In Fig. 11.1-1 we present a time of flight (TOF) spectrum in singles and in coincidence with the NaI detectors. The larger peak in the singles spectrum is associated with the beam-like particles. The enhancement of the recoil peak in the coincidence spectra is due to the larger M_γ associated with the fusion processes as compared to the one associated with inelastic scattering, transfer, and other quasi-elastic processes. The lower-channel tail of the beam-like peak from beam-like particles seems to be mainly associated with slit scattering from the collimators. At bombarding energies close to the barrier, the magnitude of this tail under the recoil peak is the main source of ambiguity in the extraction of the area of this peak in the singles spectrum. Considerable improvement was achieved by carefully tuning the beam so as to minimize the amount of beam hitting the collimators.

1. Nuclear Physics Laboratory Annual Report, University of Washington (1987) p. 53
2. Section 11.2, this report.

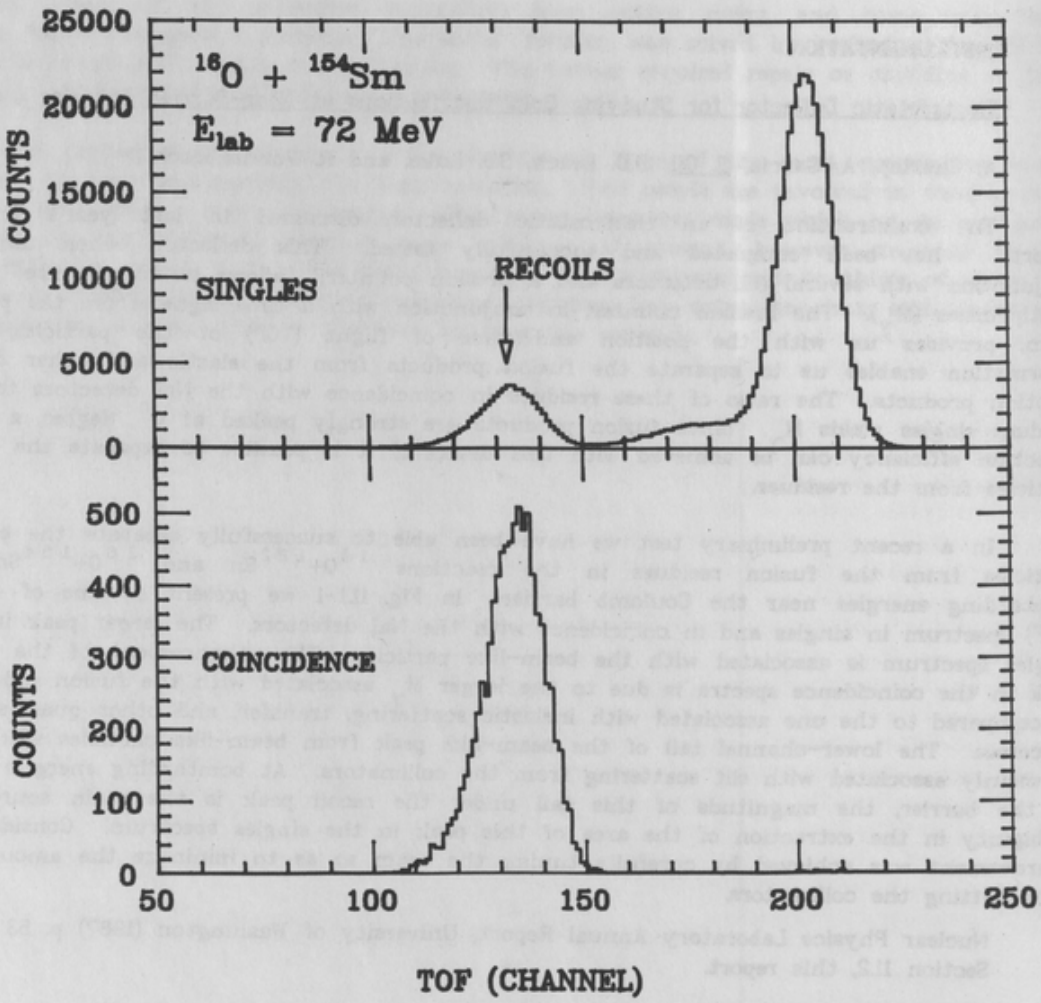

Fig. 11.1-1. TOF spectrum for the system $^{16}O+^{154}Sm$ at E_{Lab}=72 MeV, in singles and in coincidence with the NaI detectors.

11.2 Construction of a Large-Area Breskin-Type Recoil Detector

D.D. Leach

The electrostatic deflector for separation of heavy ion fusion recoils from beam particles has been discussed elsewhere in this report. A definitive identification of the recoils requires a time-of-flight measurement. We have constructed a large-area gas proportional counter of the Breskin type[1] to obtain a time signal and also to provide some position information. The large area is required because the recoils are dispersed due the evaporation of light particles, to multiple scattering in the target, and to varying deflections in the electrostatic field associated with the finite width of the ionic charge state distribution.

The detector has an active area of 7.6 cm by 7.6 cm. It is comprised of an 80 $\mu g/cm^2$ polypropylene entrance window and 7 electrodes. The timing signal is derived from a positively biased wire grid (10-micron diameter gold-plated tungsten wires at 0.127 mm separations) preceded by a negatively biased grid. Two of the grids have 2 nsec delay lines between each wire and hence enables position information to be obtained from the time difference between the anode signal and the delay-line signal. The detector is usually operated with isobutane at a gas pressure of 2-3 torr. The housing is designed so that a large-area surface barrier detector can be placed behind the last ground electrode.

In its most challenging application to date, this detector has been used to detect 6 MeV recoils from the $^{16}O+^{154}Sm$ reaction. The recoils produce somewhat larger signals than do the elastically scattered beam particles, allowing a first cut against beam particles by a discriminator before the time-to-digital converter.

1. A. Breskin et al., Nucl. Instrum. Methods 221, 363 (1984).

11.3 Design and Construction of Electronic Equipment

R. Barry, H. Fauska, J.M. Lacroix, D.B. Newell, L. Prewitt, J.M. Stehfest, R.E. Stowell, and T.D. Van Wechel.

The following major electronic projects were carried out and are described in detail in the indicated sections of this report.

a. A control system for a low-energy multiple-frequency buncher for the linac was designed and constructed (see Sec. 10.2d).

b. A 10-channel linear rate meter was designed and constructed (see Sec. 11.4).

c. Improvements, redesign, and upgrading of the laboratory scalers was undertaken (see Sec. 11.5).

d. A continuing effort was put into expanding and completing the radiation monitoring safety system (see Sec. 10.9).

Several additional electronics projects were undertaken.

a. Due to severe cross-talk between resonators on the linac, all control coax cables were replaced with the double shielded type.

b In-house telephones were added to the linac area.

c. Several minor modifications were made to the resonator control chassis described last year[1] including the addition of a flashing front panel LED to indicate a fast-out-of-lock condition on any of the r.f. resonator control boxes.

d. The purchase of additional NMR's for the linac required modification of range switching and dynamic range to match all existing units.

e. Considerable additional effort was put into CAD documentation of various electronic systems on the linac.

f. The forward and reflected power measuring circuits for the linac r.f. amplifiers that are read by the computer were calibrated to within 5%.

g. A logic control box was designed and built for the vacuum system on the linac that makes all three fast-acting valves close if any one closes. Control circuitry for the cryo pump vacuum compressor was added to allow computer control.

h. A circuit was designed and built to provide an analog output from the commercial Lakeshore Cryogenic temperature readouts on the linac to allow reading by the satellite computers.

i. A control chassis was built for the injector deck 45° and 90° magnets to allow either manual or computer control as well as a tracking mode of operation.

1. Nuclear Physics Laboratory Annual Report, University of Washington (1987) p. 69.

11.4 A Ten Channel Linear Rate Meter

R.E. Stowell

A 10-channel linear count rate meter was designed and constructed in a standard single width NIM module. The inputs were designed to accommodate fast negative going pulses such as those that come from generic fast discriminator NIM modules. The outputs are dc levels of 0 to 10 volts amplitude, proportional to count rate. Input connectors are of the lemo type and output connectors consist of front panel pin jacks and a multi-pin rear panel connector. A front panel switch allows selection of $3X10^3$, $1X10^4$, $3X10^4$ or $1X10^5$ counts full scale, with all 10 channels switched simultaneously.

The heart of each ratemeter is a LM331 I.C. operating in the frequency -to-voltage conversion mode. This is followed by a filter circuit with a 0.1 second time constant that sets the overall response time of the ratemeter. The output circuits are buffered with an op amp and can be internally set for any full-scale voltage between 0 and 10 volts. A block diagram of one of the identical 10 channels appears in Fig. 11.4-1.

Range switching of appropriate rc time constants to accommodate the four ranges of maximum counts full scale was accomplished by mounting all components on the pc board and using micro miniatures relays for the actual switching. This avoids cross-talk between channels and reduces the front panel switch requirements to a simple one-pole four-position type that is small enough to fit on the front panel.

Originally this instrument was intended to drive ten external analog meters. Since then a program has been written for our data collection system that lets the ratemeter feed its outputs to our standard ADC's and presents the output as a 10 vertical bar graph display on a VAX station monitor.

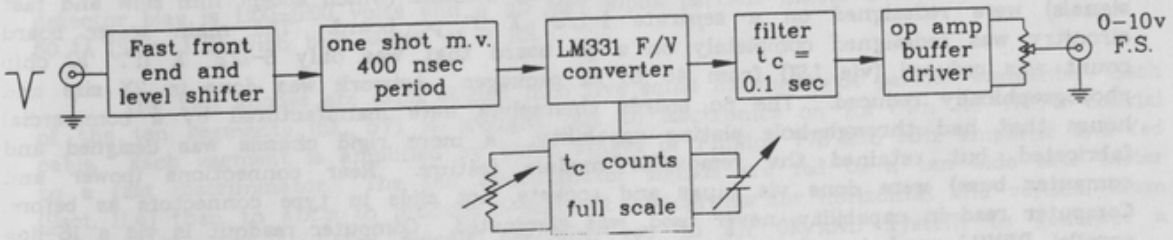

Fig. 11-4.1

11.5 Improvements and Upgrading of the Laboratory Scalers

J.M. Lacroix, L. Prewitt, R.E. Stowell, and T.D. Van Wechel.

Because of continuing deterioration and increasing problems with reliability, the laboratory scalers built in 1978[1] were redesigned and rebuilt.

After those scalers had been in use for some months, reliability problems began to appear. Tracking these problems for several months revealed two basic types of failures: broken traces on the printed circuit (pc) boards and poor solder joints.

The pc boards were quite large (11" X 17') and had been made in-house. Flow soldering of components to the boards had been done by an outside commercial firm. The pc cards were double sided with many through-the-board connections. Since the lab does not have the capability to do through-hole plating, jumper wires were used for these connections and flow soldered on both sides of the board before adding any components. There was strong evidence that proper flux preparation of copper surfaces was not done prior to the flow soldering.

In addition, close examination of the in-house artwork used for the negatives for the pc boards revealed several flaws. Because of the board complexity, some traces had inadequate line width and, because of the large size of the boards, were subject to hairline breaks when the boards were flexed even slightly.

Physically, these scalers consisted of 16, ten-digit units that were mounted in a mother bin and could be individually removed. Because we had built 32 actual scalers (2 bins, 16 scalers each) we were able to keep one bank of 16 more or less working. However, because of progressive long term deterioration and the need for additional scalers by some experimenters, the decision was made to redesign and rebuild the scalers.

The ten-digit readouts and some mechanical parts (mother bin and front panels) were judged faultless and retained. The front end modules (which accept nim slow and fast signals) were redesigned on a separate 1-1/2" X 3" pc board. The main scaler board circuitry was redesigned completely on a pc board that was only 6-1/2" X 11". IC chip count was reduced (via LSI) from 40 to 21 packages. Artwork was done in 2X size and photographically reduced. The pc boards themselves were manufactured by a commercial house that had through-hole plating capability. A more rigid chassis was designed and fabricated, but retained the removable module feature. Rear connections (power and computer buss) were done via plugs and sockets, not slide in type connectors as before. Computer read-in capability, never used, was eliminated. Computer readout is via a 16-line parallel DRV11J card transfer instead of the former IEEE interface. Original specifications were retained; i.e., 75 MHz count rate, fast or slow NIM inputs, manual or computer reset and start/stop switches.

The first bank of 16 scalers were installed nine months ago in the counting room and have performed flawlessly. The second bank has been completed and tested and will be installed as needed.

1. Nuclear Physics Laboratory Annual Report, University of Washington (1987) p. 126.

11.6 Position-Sensitive Parallel Plate Avalanche Counter for Light Ion Beam Diagnostics

D.D. Leach, H. Simons, and T.A. Trainor

The antiproton mass measurement scheduled later this year (Sect. 4.7) will use 5 MeV antiprotons from the LEAR facility at CERN. The lower beam energy is expected to yield substantially more trappable antiprotons than the 21 MeV beam used in 1986 for feasibility tests, but the range has been reduced by a factor of 13 to 225 μm Be equivalent, putting stringent thickness limitations on any in-beam diagnostics. In particular, with the more complicated beam transport to the trap system a thin beam-profiling device near the trap is very desirable.

We decided to attempt to develop a parallel plate avalanche counter (PPAC) system which would meet our requirements for thinness ($\leq$25μm Be equivalent), time resolution (< 500ps), beam profiling, and ambient conditions (6 T B-field and 1 atm SF_6). This program was successful.

The whole assembly is 5 cm diam. by 3.5 cm long. The active area is 1.8 cm diam. Two PPAC's, each 0.75 cm thick, are mounted on a lucite header which provides a mount for gas lines and coaxial cables.

Each PPAC is two PC board disks separated by a lucite ring. The electrodes are two-sided 250 $\mu g/cm^2$ aluminized mylar. The anode is stretched and epoxied directly to one disk. The cathode is stretched over a lucite boss contoured to minimize breakdown at the edge of the active region and epoxied to the other disk. The gap between electrodes is 1.25 mm. Two vacuum windows, consisting of 9 μm mylar supported by 125 μm thick 90% transparent molybdenum grids seal the detector assembly at either end from the 1 atmosphere ambient consisting of a variable mixture of Ar and SF_6 used to fine tune the antiproton energy loss.

Isobutane gas at 50 - 75 Torr and 100 atm-cc/sec flows through the assembly. The detector bias is 1100-1200 volts and a 5.5 MeV alpha particle makes a 10-30 mV pulse across 50 Ω, (Sect. 11.7) with base width of 4 nS.

The two anodes are each etched into five equal 2.5 mm wide parallel segments. Each of the ten segments (5X, 5Y) is brought out to electronics on its own RG 174/U coaxial cable. Each segment is amplified by three stages of Phillips 776 275 MHz amplifier and fed to a fast discriminator. The ten discriminator signals are fed to a ten-wide rate meter (Sect. 11.4) then to ADC's to produce 5-segment histograms for horizontal and vertical beam profiles. The discriminator signals are also fed to an OR/AND system to generate a coincidence pulse for timing purposes.

The detectors were tested in a 6 T magnetic field perpendicular to the electrodes with ^{241}Am alphas. It was found that the field reduced the pulse height by ~ 13%. The detectors were tested with 5 MeV protons and provided good beam profile information updated at ~ 10Hz. The event rate/segment was ~ 10^4 Hz.

11.7 Energy Loss in Thin Gas Detectors

T.A. Trainor

The performance of the parallel plate avalanche counter (PPAC) described in Sec. 11.6 provides an opportunity to look at energy loss of lightly ionizing particles in thin gas layers where only a few primary charges are created.

The PPAC developed here is 1.25 mm thick, with 250 $\mu g/cm^2$ aluminized mylar electrodes, an active area 1.25 cm in diameter, and uses isobutane gas at ~ 1/10 atmosphere. The operating voltage is 1150 – 1200 volts, and the gain is $\sim 5 \times 10^4$.

The mean energy losses for 5 MeV protons and alpha particles in this PPAC are 2 keV and 26 keV respectively . However, due to the nature of charge multiplication in the avalanche counter only a fraction of the gas volume near the cathode produces all of the observed signal. This fraction, 1/n, is related to the gain G by $G = e^n/n$. Under the conditions described above n = 12–14. Therefore, the mean energy loss responsible for the detector output should be about 150 eV and 2 keV for protons and alpha, respectively. The ionization yield in isobutane is about 30 ion pairs/keV, so the mean yield for protons should be 4.5e and that for alphas about 60e.

Pulse height spectra for 5 MeV protons and 5.5 MeV alpha particles from a collimated ^{241}Am source were obtained simultaneously. A typical spectrum is shown in Fig. 11.7–1. The detector output across 50 Ω was amplified 100X by two stages of a Phillips 776 broadband amplifier and digitized by a LeCroy 2249A charge–sensitive ADC. The spectrum zero is at channel 30, and the scale is 0.128 pC/channel. The alpha peak corresponds to 36pC, and is consistent with a primary charge of 60e and a detector gain of 3.7×10^4.

Using a mean alpha primary charge of 60e to establish scale, we find that the proton peak is at 9e, not 4.5e as expected from the mean energy loss value. There are two phenomena contributing to this discrepancy. The first has to do with the statistical nature of the energy–loss process. The 5 MeV proton can transfer up to 10 keV to an electron in the gas in a single collision. Because this is much greater than the mean energy loss (150eV in this case), the proper energy loss distribution is highly skewed, with a long tail at higher energy loss and most probable value much less than the mean. In some cases this situation is described by the Vavilov family of distributions which extends from the normal distribution in the limit of large total loss/single transfer ratio to the Landau distribution at the other extreme (e.g., for fast electrons).

On the basis of the very small total loss/single transfer ratio the present proton spectrum should be described by a Landau distribution. Such a distribution is included in the figure, along with a Poisson distribution for 9e and a Poisson distribution for 60e corresponding to the alpha peak.

The Landau distribution overestimates the high energy tail considerably. This is because the detector signal is not strictly the energy lost in the thin gas layer. For example, the high energy transfer events represented by the Landau tail produce high energy delta electrons which do not range out in the active gas volume. These events register as much lower pulse heights in the spectrum.

The second effect, having to do with the shift in apparent mean energy loss, has to do with delta electrons produced by the proton in material upstream of the counter gas. The proton enters the gas through a mylar window accompanied by some number of these forward-peaked electrons, and the charge produced by a proton in the gas volume comes from the combined action of several charged particles. Therefore, the signal produced in the PPAC does not reflect an equilibrium energy loss process characterized by a mean energy loss because of the sudden change of density at the foil-gas boundary. Monte-Carlo calculations are required to properly describe the PPAC plus height spectrum.[1,2]

1. H. Bichsel, Radiation Protection Dosimetry, 13, 91 (1985).
2. H. Bichsel and R.P. Saxon, Phys. Rev. A, 11, 1286 (1975).

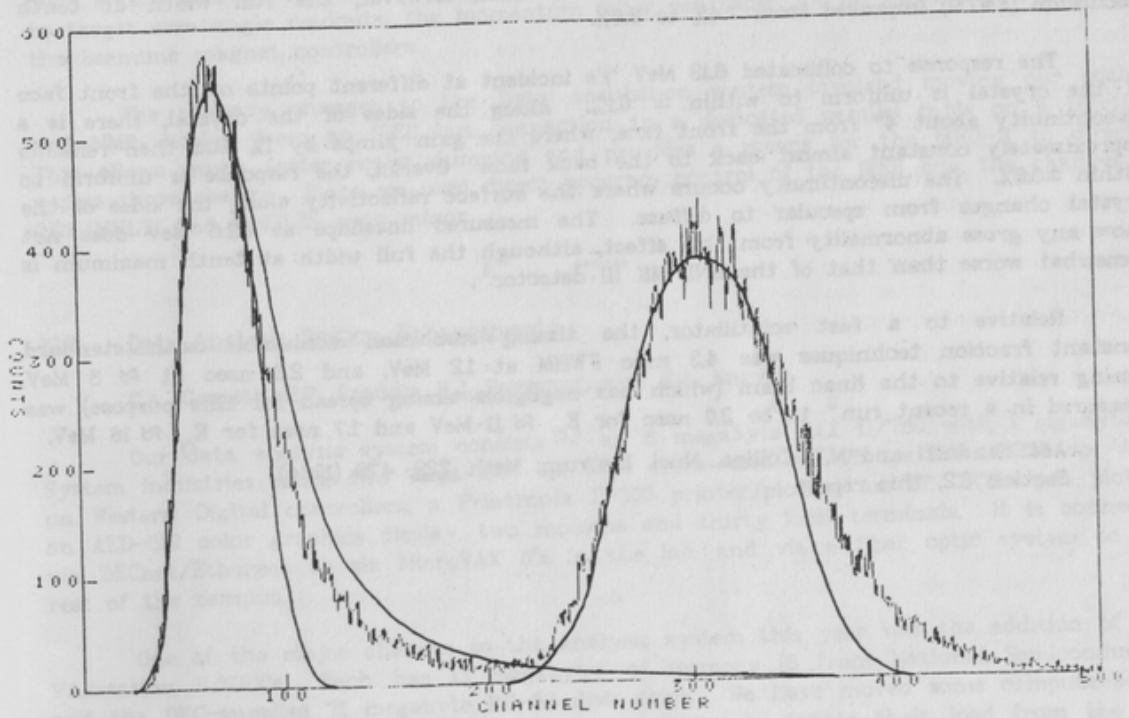

Fig. 11.7-1. PPAC Pulse Height Spectrum.

11.8 10"x15" NaI (Tl) Detector

J.A. Behr, J.H. Gundlach, and K.A. Snover

We have installed a new 10" diameter by 15" deep NaI(Tl) detector produced by Bicron Co. in place of our old 10"x10" NaI(Tl), with the purpose of improving the resolution of our high energy γ-ray spectrometer.

We have measured the energy resolution (FWHM/E) to be 7.3% at the 662 keV line from ^{137}Cs, 3.1% at the 6.13 MeV line from a Pu^{13}C source (the 3$^-$ to ground state transition in ^{16}O), and 2.2% (for events not rejected by the plastic anticoincidence shield) at 22.6 MeV from ^{11}B(p,γ_0) at E(p)=7.25 MeV. In the latter case the γ's were collimated by Pb to illuminate the entire crystal diameter at 10" from the front face. The FWHM resolution for accepted events was not improved by using a tighter collimation geometry illuminating a circle 4" diameter at the back face; however, the full width at tenth maximum (FWTM) improved from 7.4% to 6.6%.

The response to collimated 6.13 MeV γ's incident at different points on the front face of the crystal is uniform to within $\pm$ 0.1%. Along the sides of the crystal, there is a discontinuity about 4" from the front face, where the gain jumps by 1% and then remains approximately constant almost back to the back face. Overall, the response is uniform to within $\pm$0.6%. The discontinuity occurs where the surface reflectivity along the sides of the crystal changes from specular to diffuse. The measured lineshape at 22.6 MeV does not show any gross abnormality from this effect, although the full width at tenth maximum is somewhat worse than that of the BNL MK III detector[1].

Relative to a fast scintillator, the timing resolution achievable with standard constant fraction techniques was 4.3 nsec FWHM at 1.2 MeV, and 2.6 nsec at $\approx$ 6 MeV. Timing relative to the linac beam (which has negligible timing spread for this purpose) was measured in a recent run[2] to be 2.0 nsec for $E_\gamma \approx$ 11 MeV and 1.7 nsec for $E_\gamma \approx$ 16 MeV.

1. A.M. Sandorfi and M.T. Collins, Nucl. Instrum. Meth. 222, 479 (1984).
2. Section 3.2, this report.

12. COMPUTER SYSTEMS

12.1 Data Acquisition System Enhancements

C.A. Gossett, H.P. Readdy, R.J. Seymour, and K.A. Snover

The principal data acquisition system is a DEC PDP 11/60 with a CAMAC-based experiment interface controlled by a BiRa MBD-11 microcomputer. The 11/60 uses the RSX-11M operating system, an RL-01 and RL-02 disk drive, a 1600 bpi 75ips tape drive, a Printronix P-300 printer/plotter with a Trilog Tektronix hardcopy board, a DEC VT-11 graphics display and Northwest Digital Systems terminal. The NDS terminal has a C. Itoh printer attached to copy the screen. The CAMAC crate connects to twelve Tracor Northern TN-1213 ADCs, plus occasional LeCroy 2249As, 2251s and 2256As. We have 15 NPL-built 10 digit scalers and an NMR slave display connected to the system. An IEEE-488 bus connects to target arm angle readouts, the momentum filter controller, an HP spectrum analyzer and the beamline magnet controllers.

The primary changes to the Data Acquisition system involved moving our scalers and NMR display from an IEEE bus connection to a dedicated parallel cable on a DRv11-J. This allows much faster scaler dumping and provides a means for the MBD-11 to directly access those scalers. Since we used direct program control of the IEEE bus, the changes to QDA/MULTI and SINGLES were minor.

******

12.2 Data Analysis System Enhancements

C.A. Gossett, H.P. Readdy, R.J. Seymour, and K.A. Snover

Our data analysis system consists of an 8 megabyte VAX 11/780 with 1 gigabyte of System Industries disks, two 75ips 1600 bpi tape drives and one 75 ips Telex 6250 bpi drive on Western Digital controllers, a Printronix P-300 printer/plotter, an HP 7475a pen plotter, an AED-512 color graphics display, two modems and thirty local terminals. It is connected via DECnet/Ethernet to six MicroVAX II's in the lab, and via a fiber optic system to the rest of the campus.

One of the major changes to the analysis system this year was the addition of five VAXstation II/GPX's. Each has 13 megabytes of memory (8 from National Semiconductor) and the DEC-supplied 71 megabyte RD-53 disk drive. We have moved some compute-bound or out-of-the-norm processes to individual MicroVAXes to isolate their load from the 780. Three of these are owned by the Nuclear Theory group of the Physics Department. Another system-wide change was our connection to a campus-wide fiber optic ethernet system. This allows direct E-mail and file exchange with the other campus computers. We have been able to offload CASCADE calculations to our local VAXstations or to a campus VAX 8700 with greater speed and disk resources.

There have been the usual enhancements to programs such as HP (spectra manipulation, math and display), HEEWEE (kinematics) and TopDrawer (Stanford's graphics package). We installed PC TEX on our laserprinter's AT-clone in preparation for moving away from our current SuperScript word processing package.

12.3 Nuclear Theory System

C.A. Gossett, W.C. Haxton, H.P. Readdy, R.J. Seymour, and K.A. Snover

As mentioned above, the Nuclear Theory group has acquired three VAXstation GPX's. Their people work in conjunction with many of ours and the common installation in our building provides them with a lower operating cost and provides us with additional computer resources. In exchange for providing system management services, we have access to the VAXstations' console screens. We also share usage of their 6250 bpi tape drive and occasional scratch disk space. They access their machines over the campus DECnet/Ethernet system. We have a Micom terminal multiplexor, but its installation has been plagued by the long cables required by the campus steam tunnel routing. The principal two GPX's each has a DEC RA-81 445 megabyte disk and 13 megabytes of memory. The third has the DEC RD-53 drive. An Aviv/Telex 6250 bpi tape system moves among the machines as needs dictate.

The theory MicroVAXes are being used to handle the interactive computing needs of the theory group, and also permit the theoreticians to treat certain problems requiring large-scale computing. Among the latter are resonant oscillations of solar neutrinos, the neutrino physics of supernova collapse, parity violation in the NN system, final-state effects in beta decay measurements of the neutrino mass, and nuclear parity violation in the vicinity of A=16. In addition, an extensive library of shell model and associated density matrix codes are now operating on these machines. In some cases the machines have helped foster collaborative projects between the NPL and the theory group. An example is the recent work on parity violation that grew out of the NPL ^{14}N experimental results. Both NPL and Theory Group students and staff are working on the theoretical interpretation of these results, using the MicroVAXes (and the Livermore Crays) in the associated shell model calculations.

******

12.4 Campus Network

C.A. Gossett, H.P. Readdy, R.J. Seymour, and K.A. Snover

The campus connection is via FiberCom G-1 modems. The campus fiber "ring" is over six miles long. It connects 230 DECnet nodes, with an equal number of TCP/IP, XNS and Novell nodes. The system gives us access to the central campus computers for such services as BITNET and ARPAnet connections. We are on a "sub-ring", isolated by a "bridge" from most of the campus traffic we don't care about.

12.5 New Data Acquisition System Trials

C.A. Gossett, H.P. Readdy, R.J. Seymour, K.A. Snover, and T.A. Trainor

We are starting the process of converting from the PDP 11/60 to a MicroVAX-based acquisition system. We are running LAMPF's Q system as an off-line analysis package on one of the VAXstations. (See also Sec. 6.2 of this report.) We have a copy of FermiLab's VAX Multi and ONLINE system. We have installed and taken data with TUNL's XSYS. XSYS was chosen for the actual runs due to the minimal effort required to install it in a test configuration and to modify it for our purposes. For use with the ratemeter testing we gave it a "moving spectrum analyzer" display as an integral part of its event sorting section (EVOP). (See also Sec. 11.4 of this report.) For another run we modified it to support four-way routed 1024 by 512 two-D histograms in both acquisition and display. (See also Sec. 3.2 of this report.)
Current effort is centered on controlling our lab-specific hardware and integrating an IEEE-bus capability. Items such as our lab scalers' greater storage requirements (10 digits do not fit in XSYS's 32-bit fields) will undoubtedly generate a number of problems. Planned future work includes integration of our faster SINGLES system, a VAXstation-specific display package in place of its Tektronix-based system, a MULTI interface to ease the transition of existing experiments and analysis of the effect on livetime of having a fixed percentage real-time analysis package sharing the same computer as acquisition.

******

12.6 Installation of SINGLES and MULTI at TANDAR

E. Achterberg,* K.C. Green,† and R.J. Seymour

Our PDP-11 based system was "ported" to Argentina's TANDAR vertical tandem laboratory in Buenos Aires. It was installed on a PDP-11/34 under RSX-11 v4.1. Dr. Eberhard Achterberg did the extensive work required to make the system work under the newer operating system. This included changing a number of the system services calls and completely reorganizing the package's overlay trees. We assisted by modifying the MBD-11 code for their installation and by the redesign and construction of a new 4 megabyte version of our "dataspace memory" system.[1] This new dataspace uses a private section of Unibus backplane arranged to the DEC "extended" Unibus specification. This provides a 22-bit address bus and allows the use of unmodified DEC memory boards that TANDAR had on site. The 11/34's Unibus data lines are passed directly to the private bus, whereas the private address information is provided by a bank of static RAM registers written as needed by the 11/34.

* Physics Department, TANDAR laboratory, CENA, Buenos Aires, Argentina.
† Digital Equipment Corporation, Palo Alto, CA

1. Nuclear Physics Laboratory Annual Report, University of Washington (1981) p. 216.

12.7 A Flexible Linked List Software Control System

J.F. Amsbaugh, H.P. Readdy, R.J. Seymour, D.W. Storm, and H.E. Swanson

The vacuum system of the linac is monitored and controlled by a PDP 11/23+ programmed in MicroPower Pascal. Since the system cannot be conveniently shut down for programming changes, control system software was developed with a goal of making runtime changes quickly and easily. Also desirable was flexible expansion of any part of the control sequence with as few predetermined limits as possible.

Instructions for changing outputs such as valves, timers, or logical flags are contained in data files, with selected sequences loaded into memory. "Events" are output changes, or "actions", grouped as linked lists of descriptive records dynamically allocated at runtime. A linked list of events and/or preprogrammed "procedures" comprise the "task" which is run by the list processor in the control computer. The list processor makes decisions about each action specification in an event based on the action's linked list of "constraints". Constraints include any of the system status parameters and user directions from the local touchscreen or the MicroVAX. Each action can have multiple sets of constraints, and the action will be taken if all the elements in any one set of conditions is true. A report is made to the operator about which constraint has prevented him from making an intended change, and an operator with privilege can redefine the event or run a different task. All of the list types can be expanded with only physical memory as a limit, and new list types may be added to the "main" list. Runtime changes are facilitated by menus presented by a linked list control program, Vaccmd, which runs on the MicroVAX.

Because the linked list is a list of numbers read from data files, another program, Vactpu, was developed to make using these files simpler. An event's actions and their constraints as described in a text file can be translated by Vactpu into a data file loadable into the PDP 11/23+. Vactpu utilizes the VAX text processing utility (TPU) with procedures and keys defined to do translations between text and data files. The file called up by Vactpu is shown in a lower window. The translation appears in an upper window. As editing is done to either the text or data file the translated change appears in the other window after the return key is pushed. Vactpu refers to a system definition file containing a unique number and full name for each parameter, text describing high/low bit states, and hardware information. A prompt feature which can be toggled with a defined key allows selection from a group of parameters if the search string is present in multiple name fields. Dictionaries of abbreviations make construction of a text file easier.

Our experience has shown that most of the necessary control functions can be adapted to this linked list definition. Programmed procedures have been used for those which can not be adapted efficiently. The program logic used in evaluating combinations of conditional action definitions for a given output has evolved to deal with conflicts, and new constraint types have been added. Multiple list-processor programs are used to allow lists larger than addressable memory. Adaptations made to the general purpose list processor and development of event files specifically for the vacuum system are described in Sec. 10.11.

13. APPENDIX

13.1 Nuclear Physics Laboratory Personnel

Faculty

Eric G. Adelberger, Professor
John G. Cramer, Professor; Director, Nuclear Physics Laboratory
George W. Farwell, Professor Emeritus
Cynthia A. Gossett, Research Assistant Professor
Pieter M. Grootes, Joint Senior Research Associate, Geological Sciences
Isaac Halpern, Professor
Charles E. Hyde-Wright, Assistant Professor
Fred H. Schmidt, Professor Emeritus
Kurt A. Snover, Research Professor
Derek W. Storm, Senior Research Scientist; Director, Superconducting Booster Project
Thomas A. Trainor, Research Associate Professor
Robert Vandenbosch, Professor
William G. Weitkamp, Research Professor; Technical Director, Nuclear Physics Laboratory

Research Staff

Salvador Gil, Research Associate
Marta Kicinska-Habior, Research Associate[1]
Warren F. Rogers, Research Associate
Christopher W. Stubbs, Research Associate

Predoctoral Research Associates

John A. Behr
Thomas A. Brown
Aaron Charlop
Patricia B. Fernandez
Alejandro Garcia
Jens H. Gundlach
S. John Luke
Brian McLain
Douglas P. Rosenzweig
Kenneth Swartz
Ryoji Watanabe
Peter Wong
Valdis J. Zeps

Professional Staff

John F. Amsbaugh, Research Engineer
David Balsley, Research Engineer
Roger C. Connolly, Research Engineer[2]
Jim Davis, Research Engineer[3]
J. Greg Douglas, Visiting Controls Engineer[3]
Harold Fauska, Senior Research Scientist[4]
Gregory C. Harper, Research Engineer
Gervas M. Hinn, Research Scientist/Target Maker[5]
Robert D. Hobbs, Research Engineer[3]
David J. Hodgkins, Research Engineer
Mark A. Howe, Research Engineer
Donald D. Leach, Research Scientist[6]
Thomas A. Meadows, Research Scientist[3]
L. Thomas Nirider, Research Engineer[7]
Joseph R. Olson, Research Engineer[8]
H. Pamela Readdy, Computer System Engineer
Richard J. Seymour, Computer System Manager
Rod E. Stowell, Electronics Engineer/Electronic Shop Supervisor
H. Erik Swanson, Research Physicist
Timothy D. Van Wechel, Electronics Engineer
Douglas I. Will, Research Engineer

Technical Staff

Robert L. Cooper, Instrument Maker
Dean T. Corcoran, Engineering Technician
James R. Cromie, Accelerator Technician[3]
Louis L. Geissel, Instrument Maker, Student Shop Leadman
Brian P. Holm, Instrument Maker[9]
John M. LaCroix, Electronics Technician
Carl E. Linder, Engineering Technician
George E. Saling, Accelerator Technician[4]
Kenneth Schuh, Drafting Technician[3]
Hendrik Simons, Instrument Maker, Shop Supervisor
John M. Stehfest, Electronics Technician
Jay J. Tomasko, Accelerator Technician[3]
John A. Wootress, Accelerator Technician

Administrative Staff

Barbara J. Fulton, Administrative Secretary[9]
Rebecca Nielsen, Office Assistant[3]
Maria G. Ramirez, Administrative Assistant
Ida M. Tess, Technical Secretary

1. Permanent Address: Institute of Experimental Physics, University of Warsaw, Poland.
2. Now at: Grumman Aerospace Corporation, Los Alamos, NM 87545.
3. No longer associated with the Nuclear Physics Laboratory.
4. Retired – part time employee.
5. Now at: Department of Geology, University of Washington, Seattle, WA 98195.
6. Now at: John Fluke Mfg Co Inc, Everett, WA 98206.
7. Now at: Boeing Aerospace Company, Seattle, WA 98124-2499.
8. Now at: Science Applications International Corp, Bellevue, WA 98005.
9. Now at: Department of Chemistry, University of Washington, Seattle, WA 98195

Part Time Staff

Richard Barry
Melanie Bryce
Richard Burton
Joseph Caggiano
Kelly Caviezel*
Celia Champagne
Brian Christman
David Cohanim
Steven P. Doub
David Hamann
Mark Lemmon
Robert McClement
Kevin McMurry
Leane Nakamoto
Darren Paschke
Lee Prewitt
John Rogers
Alan Schroeder

* No longer associated with the Nuclear Physics Laboratory.

13.2 Degrees Granted, Academic Year 1987–1988

Ph.D. Degrees:

"A Search for an Intermediate–Range Interaction: An Experimental Test of the Fifth Force Hypothesis," Christopher W. Stubbs, Ph. D. Thesis, University of Washington, (1988).

Master's Degrees:

"Preparation of the Momentum Filter for Use in Polarization Experiments," John L. Allen, Master's Thesis, University of Washington (1988).

"Polarization Measurements for the $^{59}Co(^{3}He,p)^{61}Ni$ Reaction, Sharon L. Rosell, Master's Thesis, University of Washington (1988).

FRONT ROW: WATANABE, BEHR, STUBBS, ZEPS, LUKE, GUNDLACH, CHARLOP, VANDENBOSCH, SIMONS, MCLAIN, COOPER, NAKAMOTO
STEHFEST, LACROIX, TRAINOR, SWANSON, CRAMER, HYDE-WRIGHT, WEITKAMP

BACK ROW: ROGERS, HALPERN, GARCIA, WOOTRESS, TESS, SNOVER, SAGARA, CAGGIANO, SCHROEDER, READDY, SEYMOUR, CORCORAN, AMSBAUGH, RAMIREZ, VAN WECHEL, WILL, HARPER, STOWELL, HOWE, GEISSEL, WONG, BRYCE, FERNANDEZ, LINDER, GOSSETT, ROGERS, BALSLEY, STORM, GROOTES, ROSENZWEIG, FARWELL, GIL

NOT PHOTOGRAPHED: ADELBERGER, BROWN, CHRISTMAN, HAMANN, HODGKINS, LEMMON, MCCLEMENT, MCMURRY, PASCHKE, SALING, SCHMIDT, SWARTZ

13.3 List of Publications

Published Papers:

"Statistical Giant Dipole Resonance Decay of Highly Excited States of ^{63}Cu," M. Kicinska-Habior, K.A. Snover, C.A. Gossett, J.A. Behr, G. Feldman, H.K. Glatzel, J.H. Gundlach, and E.F. Garman, Phys. Rev. C 36, 612 (1987).

"(γ,n) Studies of the Giant Isovector E2 Resonance in Lead, Cadmium, and Calcium," D.W. Storm, I. Halpern, C.A. Gossett, T. Murakami, D.P. Rosenzweig, D.R. Tieger, P.T. Debevec, A. Freytag, L.J. Morford, S.A. Wender, and D.H. Dowell, Canadian J. of Phys. 65, 677 (1987).

"Systematic Behavior of the Giant Dipole Resonance in Highly Excited Nuclei", C.A. Gossett, J.A. Behr, G. Feldman, J.H. Gundlach, M. Kicinska-Habior, and K.A. Snover, J. Phys. G: Nucl. Phys. 14 Suppl. S267 (1988).

"New Constraints on Composition-Dependent Forces Weaker than Gravity," E.G. Adelberger, C.W. Stubbs, W. Rogers, F.J. Raab, R. Watanabe, H.E. Swanson, B.R. Heckel, J.G. Gundlach, Phys. Rev. Lett., 59, 849 and 59, 1790 (1987).

"Statistical Giant Dipole Resonance Decay of Highly Excited States of ^{67}Cu," M. Kicinska-Habior, K.A. Snover, C.A. Gossett, J.H. Behr, G. Feldman, H.K. Glatzel, J.H. Gundlach, E.F. Garman, Phys. Rev. C36, 612 (1987).

"^{37}Cl Solar Neutrino Capture Cross Section," E.G. Adelberger and W.C. Haxton, Phys. Rev. C., 36, 879 (1987).

"Light-Particle Multiplicity Accompanying Projectile Breakup at 20 MeV/A," R. Vandenbosch, R.C. Connolly, S. Gil and D.D. Leach, T.C. Awes, S. Sorenson and C.Y. Wu, Phys. Rev. C 37(3), 1301 (1988).

"Overview of the Transactional Interpretation of Quantum Mechanics," J.G. Cramer, Intl. J. Theor. Phys. 27(2), 227 (1988).

"Angular Momentum Limitation of Cluster Emission from the Compound Nucleus: ^{16}O(^{16}O,α)^{28}Si and ^{16}O(^{16}O, ^{8}Be)^{24}Mg," J. Czakanski, W. Zipper, W. Dümmweber, W. Hering, D. Konnerth, W. Trombik, K.G. Bernhardt, H. Bohn, K.A. Eberhard and R. Vandenbosch, Phys. Lett. B 199, 166 (1987).

"Organic Carbon in Surface Deep-Sea Sediments: C-14 Concentrations," S. Emerson, C. Stump, P.M. Grootes, M. Stuiver, G.W. Farwell, and F.H. Schmidt, Nature, 329, 51 (1987).

"Ion Source Sample Preparation Techniques for Carbon-14 AMS Measurements," D.R. Balsley, G.W. Farwell, P.M. Grootes, and F.H. Schmidt, Nucl. Instrum. Methods, B29 37 (1987).

"Early Expectations of AMS: Greater Ages and Tiny Fractions. One Failure? - One Success," F.H. Schmidt, D.R. Balsley, and D.D. Leach, Nucl. Instrum. Methods, B29 97 (1987).

"Pre-equilibrium neutron emission in the nucleon exchange transport model," J. Randrup and R. Vandenbosch, Nucl. Phys. A 474, 219 (1987).

"(γ,n) Studies of the Giant Isovector E2 Resonance in Lead, Cadmium, and Calcium," D.W. Storm, I. Halpern, C.A. Gossett, T. Murakami, D.P. Rosenzweig, D.R. Tieger, P.T. Debevec, A. Freytag, and L.J. Morford, S.A. Wender, and D.H. Dowell. Can J. Physics, 65, 677 (1987).

Papers to be Published or Submitted:

"Giant Nuclear Resonances," K.A. Snover, Yearbook of Science and Technology, 1989, McGraw-Hill, in press.

"Fundamental Interactions" , E.G. Adelberger, Yearbook of Science and Technology, 1989, McGraw-Hill, in press.

"Velocity Reversal and the Arrow of Time," J.G. Cramer, to be published in Foundations of Physics.

"Rapid Response of Tree Cellulose Radiocarbon Content to Changes in Atmospheric $^{14}CO_2$ Concentration," P.M. Grootes, G.W. Farwell, F.H. Schmidt, D.D. Leach, and M. Stuiver, to be published in Tellus.

"Excited-State Giant Resonances in Proton Capture," G. Feldman, J.A. Behr, D.H. Dowell, C.A. Gossett, J.H. Gundlach, M. Kicinska-Habior and K.A. Snover, Proceedings of the Sixth International Symposium on Capture Gamma Ray Spectroscopy, Aug. 1987, Leuven, Belgium, J. Phys. G, to be published.

Conference Presentations, Proceedings, and Invited Talks:

"The Giant Dipole Resonance at Moderate Temperature and Spin," K.A. Snover, Proceedings of the First Topical Meeting on Giant Resonances in Heavy Ion Collisions, Sept. 1987, Legnaro, Italy, Nucl. Phys. A482, in press.

"Giant Dipole Resonances in Hot Nuclei," K.A. Snover, Texas A&M Symposium on Hot Nuclei, Dec. 1987, College Station, TX, World Scientific, to be published.

"Status Report on the University of Washington Superconducting Booster Accelerator Project," D.W. Storm, Symposium of North Eastern Accelerator Personnel, Sept. 1987, Tallahassee, FL, to be published.

"Status Report on the University of Washington Superconducting Booster Accelerator Project," D.W. Storm, Proceedings of the Third Workshop on RF Superconductivity, 1987, Argonne, IL, ANL-PHY-88-1, p. 367, 1988.

"The Giant Dipole Resonance in Highly Excited ^{92}Mo and ^{100}Mo," M. Kicinska-Habior, First Topical Meeting on Giant Resonance Excitations in Heavy Ion Reactions, Sept. 1987, Padova, Italy, conference proceedings (contributed papers).

"Spin Dependence of the Giant Dipole Resonance Strength Function in Highly Excited Nuclei in the Mass Region A=39–45," M. Kicinska–Habior, First Topical Meeting on Giant Resonance Excitations in Heavy Ion Reactions, Sept. 1987, Padova, Italy, conference proceedings (contributed papers).

"GDR Decays and the Shape of $^{90}Zr^{*}$ at Moderate Temperature and Spin," J.H. Gundlach, First Topical Meeting on Giant Resonance Excitations in Heavy Ion Reactions, Sept. 1987, Padova, Italy, conference proceedings (contributed papers).

"Constraints on Composition–Dependent Interactions from the Eöt–Wash Experiment," E.G. Adelberger, VIIth Moriond Workshop on Neutrinos and Exotic Phenomena in Particle Physics and Astrophysics, January 1988, Les Arc, France, to be published.

"Search for a Fifth Force: Results from the Eöt–Wash Experiment," APS Division of Nuclear Physics Meeting, October 1987, New Brunswick, New Jersey, to be published.

"Recent Results from the Eöt–Wash Experiment," C.W. Stubbs, Meeting of the Royal Astronomical Society, February 1988, London, UK, to be published.

"Statistical Decay of the Giant Dipole Resonance" C. A. Gossett, Gordon Conference on Nuclear Structure Physics, Tilton, New Hampshire, August, 1987 (invited talk).

"Systematic Behavior of the Giant Dipole Resonance in Highly Excited Nuclei," C.A. Gossett, J.H. Behr, G. Feldman, J.H. Gundlach, M. Kicinska–Habior, and K.A. Snover, Proceedings of the Sixth Capture Gamma–Ray Symposium, Leuven, Belgium, August, 1987 (invited talk).

"High Energy Gamma Emission Following Heavy Ion Collisions," C.A. Gossett, 26th International Winter Meeting on Nuclear Physics, Bormio, Italy, January, 1988, to be published (invited talk).

"The Giant Dipole Resonance and the Deformation of Heated Nuclei," K.A. Snover, American Physical Society, Baltimore, MD, October 18–21, 1988 (invited talk).

"Spin Distributions in Heavy Ion Subbarier Fusion," R. Vandenbosch, American Physical Society, Baltimore, MD, October 18–21, 1988 (invited talk).

Summary Talk, K.A. Snover, Third Workshop on Radiative Capture, Sigtuna, Sweden, August 27–30, 1987.

"Excited–State Giant Dipole Resonances in Proton Capture," G. Feldman, Fast Nucleon Capture Workshop, Sigtuna, Sweden, August, 1987 (contributed paper).

Abstracts:

"Importance of Biospheric CO_2 in a Subcanopy Atmosphere Deduced from ^{14}C AMS Measurements", P.M. Grootes, G.W. Farwell, F.H. Schmidt, D.D. Leach, and M. Stuiver, 13th International Radiocarbon Conference, Dubrovnik, Yugoslavia, June 20–25, 1987.

"A Search for Composition–Dependent Forces Weaker than Gravity," C.W. Stubbs, Proceedings of the International Symposium on Experimental Gravitation, August 1987, Guangzhou, PRC, to be published.